University of Alberta

Electrografted Thick Diazonium Derived Films for Biosensing Applications

by

John Thomas Toman

A thesis submitted to the Faculty of Graduate Studies and Research
in partial fulfillment of the requirements for the degree of

Master of Science

Chemistry

Spring 2013
Edmonton, Alberta

To my mother, Libby

Abstract

Electrografting permits bonding of an organic film to a conductive substrate. It is therefore important to control the formation of organic films as best as possible and to understand the linkage between the organic film and the substrate as best as possible. This work explores electrografting of diazonium salts using high reduction potentials to prepare thick aryl films as substrates for SPR immunoassays. Film thickness was linear with respect to applied reduction potential for the modification of gold electrodes with phenylacetic acid and nitroazobenzene diazonium salts. Further, the presence of redox active functional groups was determined to be unnecessary due to the large driving force of the reaction. Phenylacetic acid films were shown to provide a suitable platform for antibody immobilization and antigen binding, with LOD's comparable to other SPR based biosensors. The immobilization of antibodies and subsequent antigen binding was shown to be highly dependent on surface morphology.

Contents

List of Tables

List of Figures

List of Abbreviations

T	Absolute Temperature
K_{ADS}	Adsorption Constant
ϑ	Angle of Incidence
ω	Angular Frequency
a-rIgG	Anti-Rabbit ImmunoglobulinG
A	Area
AFM	Atomic Force Microscopy
BSA	Bovine Serum Albumin
C_o	Bulk Concentration
C	Celsius
cm	Centimeter
ΔR	Change in Reflectivity
CA	Chronoamperometry
CDR	Complimentary Determining Region
[C]	Concentration
i	Current
CV	Cyclic Voltammetry
ε_d	Dielectric constant of dielectric
ε_m	Dielectric constant of metal
ε_p	Dielectric constant of prism
D_o	Diffusion Coefficient
i_d	Diffusion Current
K_d	Dissociation Constant
E_p	Electrolysis Peak
eV	Electron Volt
F	Faraday Constant
HBF_4	Fluoroboric Acid
FT	Fourier Transform
F_{ab}	Fragment Antigen Binding
Fc	Fragment Crystallizable
F_v	Fragment Variable

θ	Fractional Coverage
R	Ideal Gas Constant
Ig	Immunoglobulin
IR	Infrared
IRRAS	Infrared Reflection Absorption Spectroscopy
K	Kelvin
kcal	Kilocalorie
kDa	Kilodalton
LOD	Limit of Detection
MΩ	MegaOhm
i_m	Migration Current
mA	Milliamp
mM	Millimolar
mV	Millivolt
M	Molar
nm	Nanometer
N/m	Newton Meter
z	Number of Moles of Electrons Transferred
EDC	N-(3-dimethylaminopropyl)-N'-ethylcarbodiimide Hydrochloride
NHS	N-hydroxysuccinimide
rIgG	Rabbit ImmunoglobulinG
Pa	Pascal
PBS	Phosphate Buffer Saline
PEG	Poly-Ethylene Glycol
ϕ	Potential Gradient
SAM	Self-Assembled Monolayer
$NaNO_2$	Sodium Nitrite
c	Speed of Light in a Vacuum
σ_{blank}	Standard Deviation of Blank
SPR	Surface Plasmon Resonance
v	Sweep Rate

NBu_4BF_4	Tetrabutylammonium Tetrafluoroborate
ToF-SIMS	Time of Flight Secondary Ion Mass Spectrometry
V	Volt
k_{ATR}	Wave Vector of a Totally Internally Reflected Photon of Light
k_{photon}	Wave Vector of a Photon of Light
k_{SP}	Wave Vector of a Surface Plasmon
XPS	X-ray Photoelectron Spectroscopy

1 Introduction

1.1 Organic Coatings

Improvements in materials can be closely linked to human development, with entire stages of history being named after the critical materials of use. From the stone age to the bronze and iron ages; advances in material science have coincided with great leaps in civilization. Now, it seems to be the age of polymers with over 126 million metric tons of polymer materials consumed a year.[1] Polymers can have unique combinations of characteristics that cannot be met by traditional materials such as metals or ceramics. Many applications of polymetric materials require them to be deposited on a surface to efficiently impart desirable features to a substrate. Coatings are generally used for one or more of three reasons: for decoration, for protection, and/or for functional purposes. The paint on the exterior of a car is meant to look good, but it also provides protection against corrosion. Electronic coatings protect against moisture and corrosion but can also increase dielectric strength between conductors. Biomedical implant coatings can reduce platelet adhesion within biological matrixes. In all applications coatings need to be stable under adverse conditions, provide the required physical properties, and be safe for the users.[1] Therefore it is important to control the formation of the coating on the substrate as best as possible and to understand the linkage between the organic film and the substrate as best as possible.

Many different methods are commonly employed to form organic coatings on surfaces. One of the most common methods being spin coating, used to prepare organic coatings based on polymer solutions with thicknesses ranging from ten's of nanometers to hundreds of micrometers.[2] Spin coated films are ideal for temporary coatings, such as lithographic resins, since the organic film is only physisorbed to the surface.[3] Another commonly used method is plasma deposition in which strong chemical linkages are formed between the reactive species produced and the substrate. This results in robust films generally thicker than 1 μm that are routinely used for corrosion protection or anti-scratch coatings.[4, 5, 6] Self-assembly is used to spontaneously form highly ordered films on oxides, metals, or silicon and is the method of choice for forming films of molecular thicknesses. Self-assembly is generally used under moderate conditions as it forms weak bonds between the coating and substrate that can easily be broken under harsh conditions.[7, 8, 9] Electrodeposition is used to deposit coatings on conductive surfaces by applying a potential, usually anodic, to fuel a redox process that initials polymerization of a monomer. The polymer then de-

posits on the surface via non-covalent interactions. Electrodeposition has been traditionally used to coat surfaces with metals in the auto, petrochemical, and aerospace industries. More recently electrodeposition has been used to form films of conducting organic polymers with potential applications in solar cells, light-emitting diodes, and sensors.[10, 11, 12, 13] Another technique to form organic coatings using an applied potential is electrografting. Contrary to other deposition techniques electrografting allows the formation of thin organic films (1-100 nm) with very strong film-substrate links, typically a covalent bond. Recently electrografted films have been used to prepare functionalized surfaces for use in sensors, electronics, corrosion protection, composite materials, and energy conversion.[13, 14]

1.2 Electrografting

Electrografting is a relatively new technique originally shown by Lecayon et al.[15] In this work they demonstrated the formation of a thin homogeneous polyacrylonitrile films on a metal cathode. Further work on this reaction showed that the polymer is not only deposited but, more importantly, forms a bond between the polymer and the conductive surface.[16, 17, 18, 19, 20] Since then the term electrografting has been used to characterize any electrochemical reaction that permits bonding of an organic layer to a conductive substrate. Both oxidation and reduction reactions can be performed electrochemically and used to prepare electrografted films. Previously, oxidative electrografting has been demonstrated for a variety of molecules, including amines,[21] alcohols,[22] and carboxylates.[23, 24] However, for these reactions to be effective a substrate not readily oxidized needs to be used. This limits their applications as very few substrates (not metals) can be used. On the other hand reductive electrografting has been demonstrated on a variety of different substrates using various electroactive molecules.

Vinylic monomers were the first molecules to be electrografted on conductive surfaces and have been the subject of extensive experimental work. A variety of vinylic monomers have been deposited on a many different oxidiazble and non-oxidiazble materials: iron,[15] nickel,[25] copper,[26] gold,[27] platinum,[28] stainless steel,[29] carbon,[30] silicon,[31] and Teflon.[32] The resulting polymetric films have been characterized and the mechanism of formation is well understood. The electrografting of vinylic molecules takes place through a radical to radical coupling polymerization. Charge transfer from the electrode to an adsorbed monomer molecule gives rise to a radical anion that binds to the surface, resulting

in a bonded anion. The bonded anion is stabilized by attack of a new monomer which results in a dimer anion. The polymerization reaction continues along this anionic mechanism.[14] Note that only the initial step is electrochemical, the growth of the films is a result of chemical reactions. This makes it difficult to control the thickness of these polymetric fims.

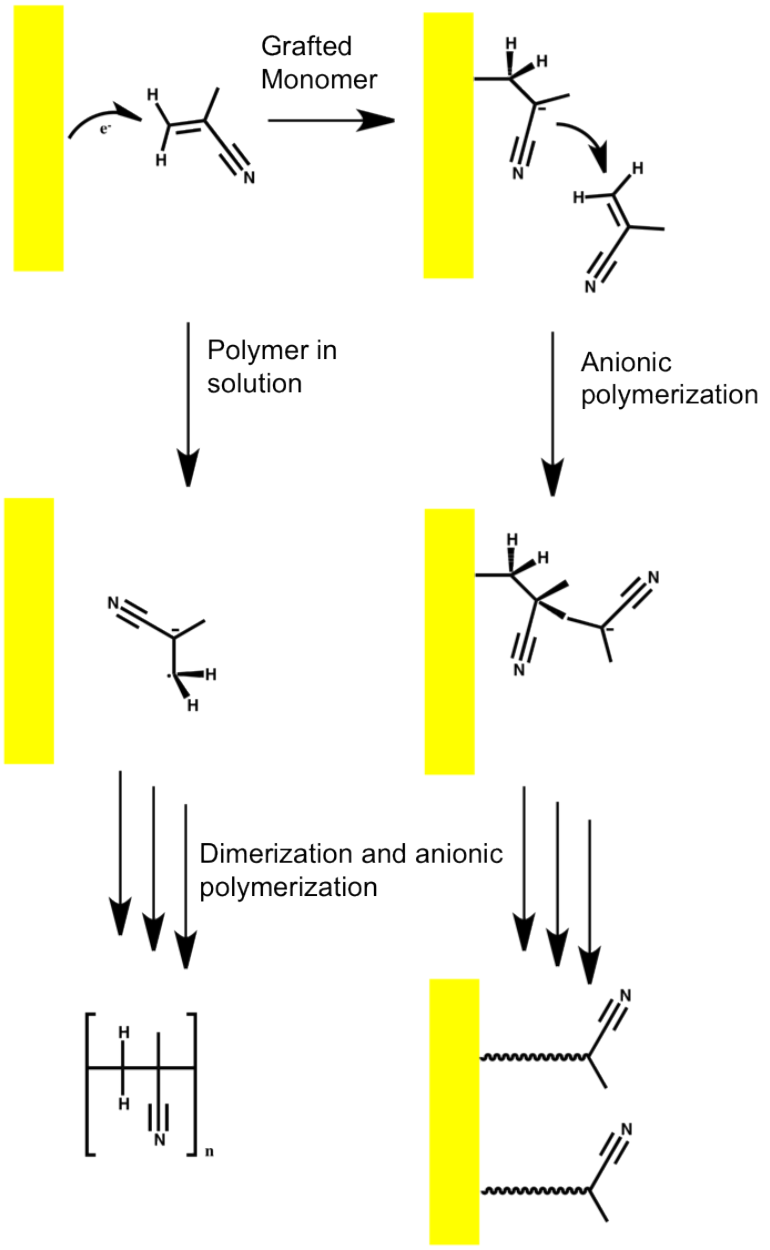

Figure 1.1: Mechanism of the electroreductive grafting of vinylic compounds. Figure adapted from Belanger et al.[14]

The choice of solvent during the electrografing of vinylic molecules is crucial. During the electroreduction of the monomers a second route is possible where the bonded anion desorbs

from the surface and polymerizes in solution, if the polymer is not soluble in solution it can deposit on the electrode non-covaltenly.[33] This results in a thick unbonded layer covering the electrode surface. Additionally, the anionic reduction must be carried out in a glove box without oxygen or water, limiting its use. Although, recently some specially designed monomers have been electrografted in aqueous solutions.[34]

The electroreductive grafting of many other molecules has been extensively studied: alkyl halides,[35] ammoniums,[36] sulfoniums,[37] iodoniums,[38] and diazoniums.[39, 40, 41, 42, 43] In recent years diazonium salts have attracted a lot of attention, with nearly 50% of the work reported on electrografting involving diazonium salts.[14] This is likely due to there relative ease of preparation and use, formation of stable films, and great degree of control over film thickness and functionality.

1.3 Diazonium Salts

Aryl daizonium salts have been known for a long time and are often used in organic chemistry for the production of dyes.[44] Commonly, diazonium salts are used in dediazonation reactions to form aryl radicals or cations. In the mid-20th century the reaction of diazonium salts with mercury electrodes was shown to result in phenylmercuric chloride and diphenylmercury.[45] Also, diazonium salts were proposed as coupling agents for the labeling of enzymes.[46] However, it wasn't until more recently that the electrochemical dediazonation of aryl diazonium salts to form aryl radicals was used to graft aryl films on conductive surfaces. The first report of electrochemical reduction to form a blocking layer come from Parker *et al.* in 1980.[47] It was determined that radicals generated blocked the surface of the electrode; however, the nature of the blocking layer was not investigated. In 1992 Pinson and co-workers reported the mechanism of attachment of aryl diazonium salts to glassy carbon electrodes.[48] Since then interest in diazonium derived layers has increased significantly.

One reason aromatic diazonium salts are so attractive is there ease of preparation. Synthesized in an acidic aqueous medium, usually HBF_4, starting from an aromatic amine in the presence of $NaNO_2$ the primary amine undergoes nitrosation to form a diazonium. As many aromatic amines are commercially available, the preparation of a large number of diazonium compounds can be easily carried out. Diazonium synthesis has also been carried out in aprotic solvents with tert-butyl nitrite.[49] Aliphatic diazonium salts are extremely

unstable, with only a few example of their grafting being demonstrated.[50]

Diazonium salts can be grafted to surfaces using various methods, on many substrates, through a variety of experimental conditions. The most common method being electrografting, which takes place through the electrochemical reduction of the diazonium cation to form an aryl radical. The aryl radical then binds to the surface. Through simulations this reaction has been shown to be concerted, which means there are no intermediates between the diazonium cation and the radical; this also means the radical is formed near the surface, which is favorable for grafting. If the reduction potential is pushed too negative the radical can be reduced to the aryl anion, which should be unfavorable for grafting. The radicals produced either react to the surface or react with other grafted aryl groups, causing the film to grow. The mechanism of diazonium cation electrochemical grafting can be seen in Figure 1.2. Diazonium salts have been grafted to many different substrates, including carbon,[48] semiconductors,[51] metals,[52, 53] oxides,[54] nitrides,[55] carbides,[55] and polymers.[56] They have also been grafted to surfaces spontaneously[40] or through the use of reducing agents,[57] ultrasonication,[55] heating,[58] mechanical grafting,[59] and photochemistry. [60]

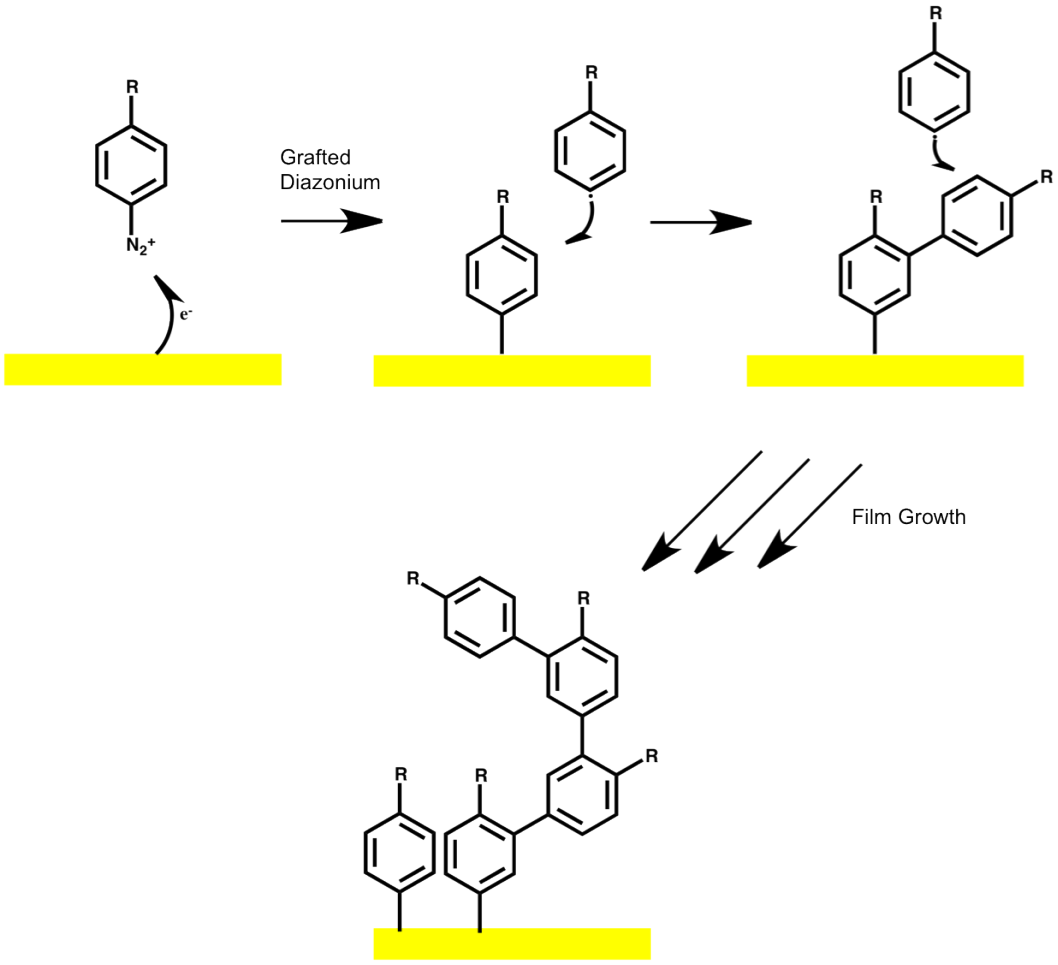

Figure 1.2: Mechanism of the electroreductive grafting of aryl diazonium cations.

Unlike vinylic compounds, the reductive potential must be applied throughout the reaction for film growth to occur; therefore, diazonium derived layers offer a high level of control over film thickness. Films can range anywhere from sub-monolayer[61] to hundreds of nanometers[52] depending on the deposition conditions. Due to the formation of a bond between the organic layer and the surface diazonium derived layers show high stability under various adverse conditions. Diazonium derived layers on carbon have shown stability under ambient conditions for up to six months and under ultrasonic treatment in many different organic solvents.[48] Additionally, 4-nitrobenzene layers have been shown to be stable on carbon up to 200 °C,[62] with cleavage occurring between 300-500 °C, and during potential cycling of 5.6 V. [63]

Diazonium salts provide a versatile and efficient starting material to functionalize a variety of substrates. The layers are robust and the thicknesses can be varied from monolayers

to hundreds of nanometers. This is why they are now used to modify surfaces for a variety of applications, including energy conversion, molecular electronics, and biosensors.

1.4 Surface-Based Biosensors

Any chemical sensor has two functional units. The receptor, which interacts with the analyte and gives the sensor its selectivity. The transducer, which determines the amount of interactions between the receptor and the analyte and converts it into a measurable signal.[64] In biosensors the receptor is some biological molecule, such as an enzyme,[65] peptide,[66] antibody,[67] or DNA sequence.[68] In most cases the receptor and transducer are integrated into a surface-based device and exposed to a sample in either a liquid or gas phase. Therefore, the reactions that take place in most sensors are interfacial and how the interface is designed will play a huge role in the performance of the sensor.

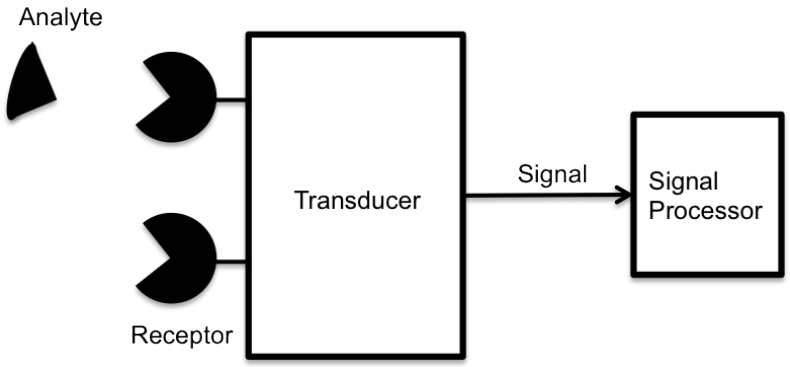

Figure 1.3: Schematic diagram of a basic sensor.

The receptor molecule must be immobilized on the surface of the transducer. The immobilization must be able to be performed reproducibly, allow the receptor able to interact with the anaylte, and not change the activity of the receptor. Additionally, undesirable non-specific interactions must be limited. These requirements become more difficult to fulfill when the analyte is a large biological molecule, like a protein. Because of the large size ensuring that the receptor is accessible to the analyte is more difficult. Protein analytes can also bind to interfaces in many different ways; specifically to the receptor molecule or non-specifically to other parts of the interface.[69] Additionally, there can be cross-reactivity between similar types of molecules.

Immunoassays involve the use of an antibody as a receptor to quantitate the presence of an antigen. An antibody, a class of protein called immunoglobulin (Ig), is a Y-shaped blood

plasma protein produced by B-cells in the immune system and consist of IgA, IgD, IgE, IgG, and IgM. Of these IgG is the most common and provides the majority of antibody-based immunity against pathogens. It is composed of two 50 kDa heavy chains consisting of four homologous domains and two 25 kDa light chains consisting of two homologous domains. The base of the antibody, known as the fragment crystallizable (F_c), is constant for all antibodies of a given class. The arms of the antibody, called the fragment antigen binding (F_{ab}), are composed of one constant and one variable domain for each heavy and light chain of the antibody. The variable fragments (F_v) are the most important as they determine antigenic specificity with antigen binding occurring at complementary determining regions (CDR's). More specifically, CDR's are formed by three hypervariable loops on both the variable heavy and light chains that form a single surface at the terminus of each arm.[70, 71]

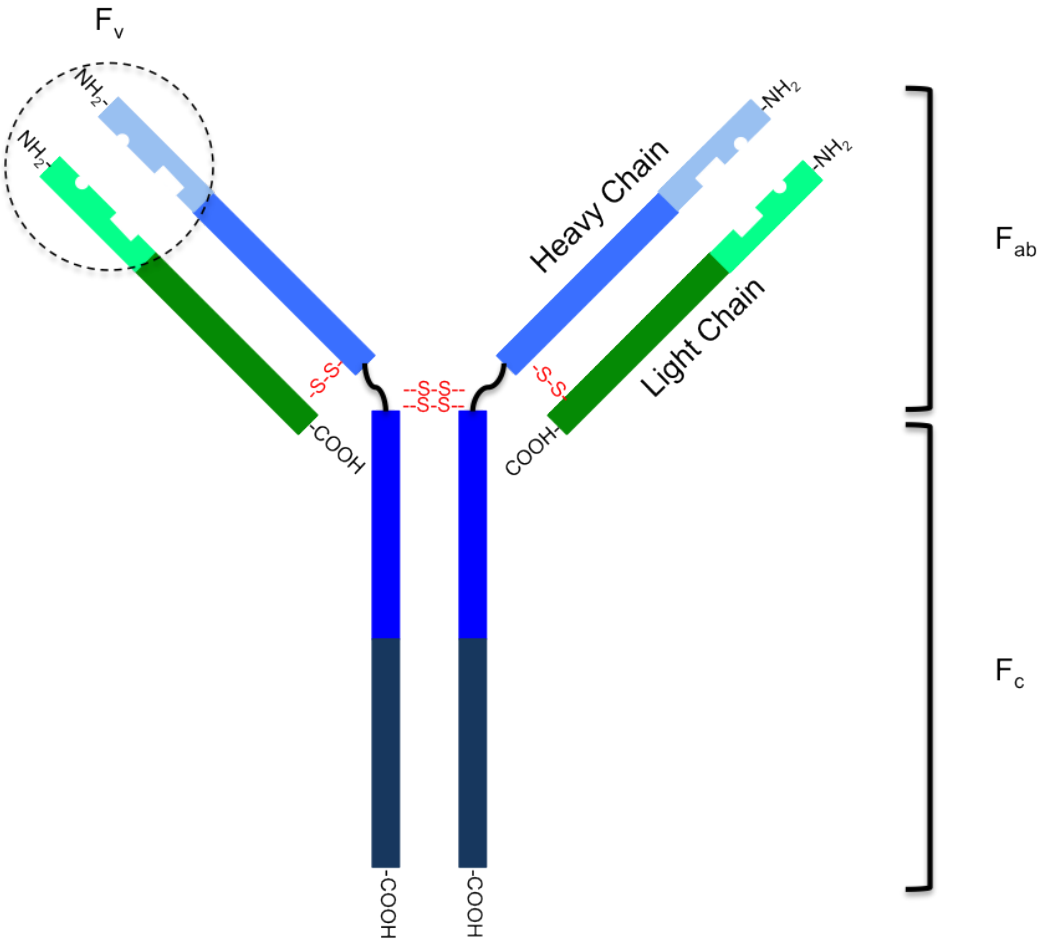

Figure 1.4: Structure of Immunoglobulin G.

Strategies have been developed by scientists to produce reliable surface chemistry for

sensors that can monitor complex biological systems, like protein-protein interactions. Self-assembled monolayers (SAM's) are a common method, as they provide a high degree of control over the sensing surface. More recently diazonium derived surfaces have been used to control immobilization of bio-recognition moleclues.

Self-assembly on metal surfaces, more specifically the spontaneous adsorption of co-terminated alkanethiols, has been the dominant method of surface modification for sensing devices. SAM's are commonly used in electrochemical and optical sensing devices, such as surface plasmon resonance or surface enhanced Raman spectroscopy. Alkane thiol chemistry has also seen increased applications in modification of nanoparticle systems. Since their discovery in the early 1980's by Nuzzo and Allara,[72] thiol and dithiol SAM's have been the preeminent method for modifying metal surfaces. Due to the ease of preparation and controllability of surface functionality SAM's have been used extensively in molecular electronics, biocompatible surfaces, chemical wettability, system fabrication, and biorecognition sensors.[73, 74, 9] This wide ranging usage is largely due to their ability to form tightly packed highly ordered monolayers, which is largely due to the nature of the Au-S bond as well as the interactions between the molecules themselves. The Au-S bond is semi-covalent at $\sim$50 kcal mol^{-1},[9] strong enough to produced a stable film but still with the lability necessary to move on the surface and tightly pack together. Additionally, in alkanethiols the van der Waals interactions between the hydrocarbon chains provide 1-2 kcal mol^{-1}per methylene unit further promoting a densely packed film. However, the nature of the bonding is also the root of many of the problems associated with SAM's. The lability of the Au-S bond results in low thermal stability,[75] a narrow electrochemical window,[76] and is susceptible to oxidation.[77]

The far greater stability of diazonium derived layers was the initial draw that led to their increased usage in fabrication of sensing interfaces. Recently, there have been many advances in diazonium chemistry that has broadened their utility for sensing applications. Diazonium salts have been used to modify almost all types of conductive surfaces, including carbon, metals, silicon, and indium tin oxide. It should be noted that the surface chemistry is not the same on all surfaces. For example the rates of electron transfer through the film have been shown to be much higher on metal surfaces, while the stability is much higher on carbon surfaces.[69] The *in situ* formation of aryl diazonium cations allows more complex head groups to be integrated into interfaces, as diazotization and purification steps can be difficult with complicated molecule used in sensing.[78] The spontaneous adsorption of diazonium

salts is much more compatible with bulk manufacturing and allows for simple patterning of sensing substrates.[79] Additionally, mixed diazonium layers have been prepared, allowing for the integration of multiple molecular components into the sensing layer.[80]

Aryl diazonium salts have been used to fabricate a wide range of sensor interfaces. Many of these sensing interfaces involve the development of chemical sensors. Hall et al. synthesized a hydroquinone derivative diazonium salt for electrochemical pH sensing. In which the quinone/hydroquinone couple was used to monitor pH. Similar systems have been used to prepare pH microelectrode for *in vivo* electrochemistry.[81] Diazonium derived chemical sensors have also been developed for a range of metal ions and chemical species, such as Cu^{2+}, Cd^{2+}, Pb^{2+}, and NADH.[82, 83] Furthermore, diazonium salts have been employed in a number of biosensing applications with the immobilization of enzymes,[84] antibodies,[85] DNA,[86] and whole cells. [87]

1.5 Low-Fouling Films

Another critical aspect for the development and performance of bioassays is the ability to suppress non-specific adsorption of biomolecules. In diagnostic testing for biological samples analytes are usually present in complex biological matrixes such as blood, plasma, or urine. These samples contain many other molecules that can potentially interfere with the assay. It is possible to perform pre-analysis clean up steps; however, with each step you add time, cost, and the possibility of changing the activity of the analyte. In order to reduce the possibility of non-specific interactions, many biosensors employ some type of low-fouling surface chemistry. The development of low-fouling surfaces is also of critical importance for medical implants,[88] drug delivery carriers,[89] and marine coating.[90]

It has been hypothesized that the ability to resist non-specific adsorption is tightly correlated to the hydration of the surface.[77] The the first step of any protein adsorption is expulsion of water reducing the free energy barrier for forming an interaction between the surface and the protein. In low-fouling materials the strength of surface hydration is what mainly determines its low-fouling abilities by providing a physical and energetic barrier to resist non-specific adsorption. Additionally, surface flexibility has been shown to contribute to low-fouling properties.[91] There are two main classes of low-fouling materials, polyzwitterionic[92] and polyhydrophilic.[93] Both of these materials obtain their low-fouling abilities through the strength of surface hydration. Hydrophilic materials bind water to the

surface through hydrogen bonding, whereas, zwitterionic materials use ionic solvation. For both materials functional group distribution, film thickness, packing density, and molecular chain conformation are of the utmost importance.[77]

The most commonly used material today for reducing non-specific interactions in biosensors are hydrophilic polyethylene glycol (PEG) SAM's. This system provides excellent resistance to protein adsorption, however, they are also extremely susceptible to oxidation in biochemically relevant solutions.[94] More recently, zwitterionic materials have seen growing use as potential low-fouling materials. They have been shown to be highly resistant to non-specific interactions and be very biocompatible.[95] Although, work still needs to be done to optimize synthesis and surface coating of these types of films.

1.6 Surface Plasmon Resonance

The first immunoassays involved the use of radio-labeled antibodies[96], however, the hazardous nature of these labels resulted in a shift to the use of enzymes,[97] fluorescent tags,[98] or nanoparticles.[99] Still, the incorporation of labels is less convenient due to synthetic challenges, multiple label issues, and potential of changing the activity. The label-free format of surface plasmon resonance (SPR) has enjoyed significant growth as a monitoring tool for biomolecular interactions occurring at a metal-dielectric interfaces.[100, 101, 102, 103] A surface plasmon is a quasi-free longitudinal electromagnetic wave the propagates along a metal dielectric interface and decays exponentially into the adjacent medium. The penetration depth of a surface plasmon into the dielectric is typically 100-500 nm.[100] In SPR sensors a surface plasmon wave is excited by a photon of light and the effect of this interaction on the characteristics of light is measured. This requires the photon of light to satisfy the momentum-matching conditions. This can be achieved through prism coupling, waveguide coupling, or grating coupling. Figure 1.5 shows the most common technique, prism coupling. In which a thin metal film is placed in contact with a prism and p-polarized light is directed through the prism an attenuated total reflection occurs at the prism-metal interface. The wave vector for a photon of light (k_{photon}), a surface plasmon wave (k_{SP}), and a photon of light totally internally reflected at a prism metal interface (k_{ATR}) can be expressed as:[104]

$$k_{photon} = \frac{\omega}{c} \tag{1.1}$$

$$k_{SP} = \frac{\omega}{c}\left(\frac{\varepsilon_m \varepsilon_d}{\varepsilon_m + \varepsilon_d}\right)^{1/2} \tag{1.2}$$

$$k_{ATR} = \frac{\omega}{c}\sin\theta\,(\varepsilon_p)^{1/2} \tag{1.3}$$

where ω is the angular frequency, c is the speed of light in a vacuum, θ is the angle of incidence and ε_m, ε_d, and ε_p are dielectric constants of the metal, dielectric, and prism, respectively.

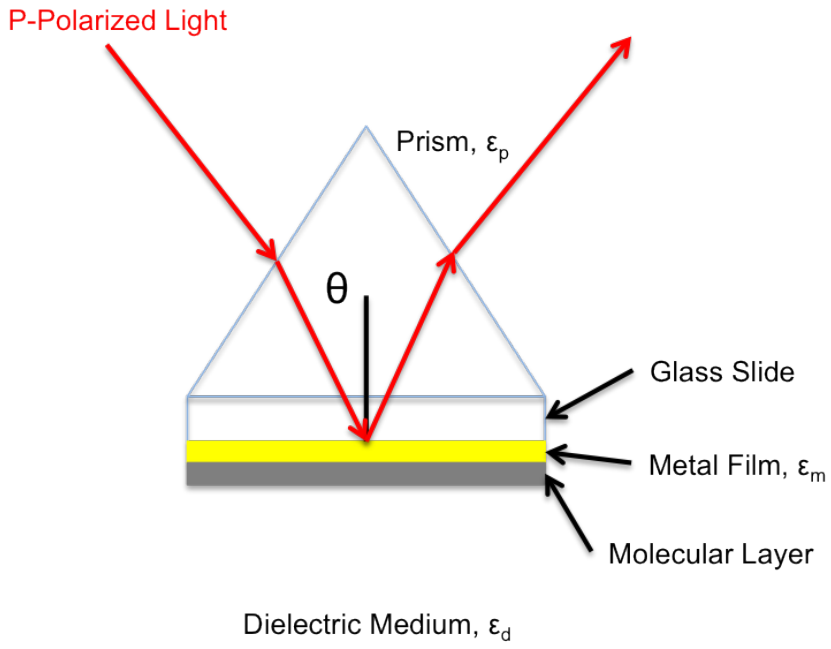

Figure 1.5: Excitation of surface plamon by a light beam via prism coupling.

The wave vector equation of the totally internally reflected photon (k_{ATR}) may be tuned to match that of the surface plamon (k_{SP}) by adjusting the wavelength or incident angle of light. When $k_{ATR} = k_{SP}$ they are in resonance, which may be observed as a minimum in reflected intensity, known as the SPR angle. As mentioned above, the surface plasmons are evanescent waves that decay exponentially into the dielectric. The surface plasmon waves are extremely sensitive to changes in the refractive index of the dielectric which will alter k_{SP} and the conditions for resonance. Monitoring these changes in resonance is the basis of SPR sensors. Numerous SPR biosensors have been developed to detect a host of different analytes. Ranging from small molecules to bacterial pathogens. However, all SPR sensors still suffer from two inherent limitations: specificity of detection and sensitivity to interfering effects.[100] With this in mind it is critical to optimize the sensing surface to specifically

bind the analyte of interest and to minimize non-specific interactions.

SAM's are commonly used to control the interfacial surface chemistry in SPR bioassays. Due to their ease of preparation and controllability of surface functionality.[105] Additionally, Dextran layers have been used to control interfacial chemistry. Dextran is a hydrophilic linear polymer based on a 1, 6-glucose unit. Each chain polymer has several binding points to the surface. The flexible chain extends ∼100 nm into solution forming a highly hydrophilic surface with little tendancy for non-specific adsorption.[106, 107]

1.7 Objectives

Within the field of biosensors, diazonium derived layers have seen increasing use as substrates for biomolecule immobilization. Their ease of preparation, surface stability, and plethora of available functional groups makes them ideal for tailoring interfacial surface chemistry. With this in mind, the main objective of this work was to study diazonium derived layers for use as biosensing substrates. To further extend the applicability of diazonium derived layers, Chapter 2 focused on control and understanding of diazonium electrografting on gold. Using high reduction potentials various diazonium cations were grafted to gold surfaces. The structure and stability of these films was then studied. To better understand the effect of diazonium derived film structure on immunoassay performance, Chapter 3 concentrated on SPR immunoassay studies on various diazonium derived layers. Diazonium derived films of varying thickness and surface roughness were used to immobilize antibodies and monitor surface binding capacity of the antigen. Additionally, the use of diazonium derived films as potential low-fouling materials was examined.

References

[1] Babinec, S. J.; Berta, D. A.; Cornell, M. C.; Eller, R.; Christian, G. H.; Kakarala, N.; Nordstrom, J. D.; Pickett, T.; Reinhart, K.-W.; Ryntz, R. A.; Schoff, C. K.; Stretch, S. D.; Yaneff, P. V. *Coatings of Polymers and Plastics*; Marcel Dekker, Inc: New York, 2003.

[2] Scriven, L. E. *MRS Proceedings* **1988**, *121*, 717–729.

[3] Napoli, L.; Russell, J.; *Process for formain a lithographic mask*; 1988.

[4] Kwon, O.-K.; Kwon, S.-H.; Park, H.-S.; Kang, S.-W. *Electrochemical and Solid-State Letters* **2004**, *7*, C46.

[5] Wicks, Z.; Jones, F.; Pappas, S.; Wicks, D. *Organic Coatings. Science and Technology*, 3rd ed.; Wiley: New York, 1992.

[6] Knouma, M. *Film Deposition by Plasma Techniques*; Springer Verlag: Berlin, 1992.

[7] Fischer, D.; Curioni, A.; Andreoni, W. *Langmuir* **2003**, *19*, 3567–3571.

[8] Yee, C. K.; Ulman, A.; Ruiz, J. D.; Parikh, A.; White, H.; Rafailovich, M. *Langmuir* **2003**, *19*, 9450–9458.

[9] Vericat, C.; Vela, M. E.; Benitez, G.; Carro, P.; Salvarezza, R. C. *Chemical Society reviews* **2010**, *39*, 1805–34.

[10] Cui, C. Q. *Journal of The Electrochemical Society* **1990**, *137*, 3418.

[11] Fink, C. G.; Jones, F. L. *Transactions of The Electrochemical Society* **1931**, *59*, 461.

[12] Seim, H. J.; Holt, M. L. *Journal of The Electrochemical Society* **1949**, *96*, 205.

[13] Palacin, S.; Bureau, C.; Charlier, J.; Deniau, G.; Mouanda, B.; Viel, P. *Chemphyschem : a European journal of chemical physics and physical chemistry* **2004**, *5*, 1468–81.

[14] Bélanger, D.; Pinson, J. *Chemical Society reviews* **2011**, *40*, 3995–4048.

[15] Lécayon, G.; Bouizem, Y.; Gressus, C. L. *Chemical physics letters* **1982**, *91*, 506–510.

[16] Leroy, S.; Boiziau, C.; Perreau, J.; Reynaud, C.; Zalczer, G.; Lécayon, G.; Le Gressus, C. *Journal of Molecular Structure* **1985**, *128*, 269–281.

[17] Perreau, J.; Reynaud, C.; Boiziau, C.; Lécayon, G.; Makram, C.; Le Gressus, C. *Surface Science* **1985**, *162*, 776–781.

[18] Reynaud, C.; Boiziau, C.; Juret, C.; Leroy, S.; Perreau, J.; Lecayon, G. *Synthetic Metals* **1985**, *11*, 159–165.

[19] Boiziau, C.; Lécayon, G. *International Journal of Adhesion and Adhesives* **1986**, *6*, 207–214.

[20] Tanguy, J.; Viel, P.; Deniau, G.; Lécayon, G. *Electrochimica Acta* **1993**, *38*, 1501–1512.

[21] Adenier, A.; Chehimi, M. M.; Gallardo, I.; Pinson, J.; Vilà, N. *Langmuir : the ACS journal of surfaces and colloids* **2004**, *20*, 8243–53.

[22] Aeda, H. M.; Itano, T. K.; Uang, C. Z. H.; Atayama, K. K. **1999**, *15*, 531–536.

[23] Brooksby, P. a.; Downard, A. J.; Yu, S. S. C. *Langmuir : the ACS journal of surfaces and colloids* **2005**, *21*, 11304–11.

[24] Andrieux, C. P.; Gonzalez, F.; Save, J.-m. **2004**, *7863*, 4292–4300.

[25] Tanguy, J.; Deniau, G.; Augé, C.; Zalczer, G.; Lécayon, G. *Journal of Electroanalytical Chemistry* **1994**, *377*, 115–123.

[26] Charlier, J.; Detalle, V.; Bureau, C.; Valin, F.; Lécayon, G. *The Journal of Adhesion* **1998**, *66*, 275–287.

[27] Cuenot, S.; Gabriel, S.; Jérôme, C.; Jérôme, R.; Duwez, A.-S. *Macromolecular Chemistry and Physics* **2005**, *206*, 1216–1220.

[28] Bureau, C.; Deniau, G.; Valin, F.; Guittet, M.-J.; Lécayon, G.; Delhalle, J. *Surface Science* **1996**, *355*, 177–202.

[29] Ignatova, M.; Voccia, S.; Gilbert, B.; Markova, N.; Cossement, D.; Gouttebaron, R.; Jérôme, R.; Jérôme, C. *Langmuir : the ACS journal of surfaces and colloids* **2006**, *22*, 255–62.

[30] Petrov, P.; Lou, X.; Pagnoulle, C.; Jérôme, C.; Calberg, C.; Jérôme, R. *Macromolecular Rapid Communications* **2004**, *25*, 987–990.

[31] Charlier, J.; Ameur, S.; Bourgoin, J.; Bureau, C.; Palacin, S. *Advanced Functional Materials* **2004**, *14*, 125–132.

[32] Combellas, C.; Kanoufi, F.; Nunige, S. *Chemistry of materials* **2007**, 3830–3839.

[33] Cuenot, S.; Gabriel, S.; Jérôme, R.; Jérôme, C.; Fustin, C.-A.; Jonas, A. M.; Duwez, A.-S. *Macromolecules* **2006**, *39*, 8428–8433.

[34] Cécius, M.; Jérôme, R.; Jérôme, C. *Macromolecular Rapid Communications* **2007**, *28*, 948–954.

[35] Andrieux, C. P.; Gallardo, I.; Savaent, J. M.; Su, K. B. *Journal of the American Chemical Society* **1986**, *108*, 638–647.

[36] Wang, D.; Buriak, J. M. *Surface Science* **2005**, *590*, 154–161.

[37] Love, D.; Colichman, E. *Journal of Organic Chemistry* **1962**, *18*, 40–46.

[38] Vase, K. H. j.; Holm, A. H.; Pedersen, S. U.; Daasbjerg, K. *Langmuir : the ACS journal of surfaces and colloids* **2005**, *21*, 8085–9.

[39] Laurentius, L.; Stoyanov, S. R.; Gusarov, S.; Kovalenko, A.; Du, R.; Lopinski, G. P.; McDermott, M. T. *ACS nano* **2011**, *5*, 4219–27.

[40] Adenier, a.; Barre, N.; Cabetdeliry, E.; Chausse, a.; Griveau, S.; Mercier, F.; Pinson, J.; Vautrinul, C. *Surface Science* **2006**, *600*, 4801–4812.

[41] Polsky, R.; Harper, J. C.; Wheeler, D. R.; Dirk, S. M.; Arango, D. C.; Brozik, S. M. *Biosensors & bioelectronics* **2008**, *23*, 757–64.

[42] Harper, J. C.; Polsky, R.; Wheeler, D. R.; Lopez, D. M.; Arango, D. C.; Brozik, S. M. *Langmuir : the ACS journal of surfaces and colloids* **2009**, *25*, 3282–8.

[43] Shewchuk, D. M.; McDermott, M. T. *Langmuir : the ACS journal of surfaces and colloids* **2009**, *25*, 4556–63.

[44] Galli, C. *Chemical Reviews* **1988**, *88*, 765–792.

[45] Elofson, R. M. *Canadian Journal of Chemistry* **1958**, *36*, 1207–1210.

[46] Burstone, M. S.; Weisburger, E. K. *Journal of Histochemistry & Cytochemistry* **1961**, *9*, 301–303.

[47] Ahlberg, E.; Helgée, B.; Parker, V. D.; Halonen, P.; Glaumann, H. *Acta Chemica Scandinavica* **1980**, *34b*, 181–186.

[48] Delamar, M.; Hitmi, R.; Pinson, J.; Saveant, J. M. *Journal of the American Chemical Society* **1992**, *114*, 5883–5884.

[49] Mahouche-Chergui, S.; Gam-Derouich, S.; Mangeney, C.; Chehimi, M. M. *Chemical Society reviews* **2011**, *40*, 4143–66.

[50] Xu, Z.; Qi, Z.; Kaufman, A. *Electrochemical and Solid-State Letters* **2003**, *6*, A171.

[51] Allongue, P.; Henry de Villeneuve, C.; Cherouvrier, G.; Cortès, R.; Bernard, M. C. *Journal of Electroanalytical Chemistry* **2003**, *550-551*, 161–174.

[52] Ceccato, M.; Bousquet, A.; Hinge, M.; Pedersen, S. U.; Daasbjerg, K. *Chemistry of Materials* **2011**, *23*, 1551–1557.

[53] Boukerma, K.; Chehimi, M. M.; Pinson, J.; Blomfield, C. *Langmuir* **2003**, *19*, 6333–6335.

[54] Mesnage, A.; Abdel Magied, M.; Simon, P.; Herlin-Boime, N.; Jégou, P.; Deniau, G.; Palacin, S. *Journal of Materials Science* **2011**, *46*, 6332–6338.

[55] Bureau, C.; Pinson, J.; *No Title*; 2008.

[56] Combellas, C.; Kanoufi, F.; Mazouzi, D.; Thiébault, A.; Bertrand, P.; Médard, N. *Polymer* **2003**, *44*, 19–24.

[57] Pandurangappa, M.; Ramakrishnappa, T. *Journal of Solid State Electrochemistry* **2008**, *12*, 1411–1419.

[58] Bahr, J. L.; Tour, J. M. *Chemistry of Materials* **2001**, *13*, 3823–3824.

[59] Pandurangappa, M.; Ramakrishnappa, T.; Compton, R. G. *Carbon* **2009**, *47*, 2186–2193.

[60] Busson, M.; Berisha, A.; Combellas, C.; Kanoufi, F.; Pinson, J. *Chemical communications (Cambridge, England)* **2011**, *47*, 12631–3.

[61] Anariba, F.; DuVall, S. H.; McCreery, R. L. *Analytical chemistry* **2003**, *75*, 3837–44.

[62] Toupin, M.; Belanger, D. *Journal of Physical Chemistry C* **2007**, *111*, 5394–5401.

[63] D'Amour, M.; Bélanger, D. *The Journal of Physical Chemistry B* **2003**, *107*, 4811–4817.

[64] Lindsay, S.; Ratner, M. *Advanced Materials* **2007**, *19*, 23–31.

[65] Alonso-Lomillo, M. A.; Domínguez-Renedo, O.; Matos, P.; Arcos-Martínez, M. J. *Analytica chimica acta* **2010**, *665*, 26–31.

[66] Bolduc, O. R.; Clouthier, C. M.; Pelletier, J. N. *Peptides* **2009**, *81*, 6779–6788.

[67] Kanda, V.; Kariuki, J. K.; Harrison, D. J.; McDermott, M. T. *Analytical chemistry* **2004**, *76*, 7257–62.

[68] Nelson, B. P.; Grimsrud, T. E.; Liles, M. R.; Goodman, R. M.; Corn, R. M. *Analytical chemistry* **2001**, *73*, 1–7.

[69] Chehimi, M. M. *Aryl Diazonium Salts. New Coupling Agents in Polymer and Surface Science*; Wiley-VCH Verlag: Weinheim, 2012.

[70] Huber, R.; Deisenhofer, J.; Colman, P. M.; Matsushima, M.; Palm, W. *Nature* **1976**, *264*, 415–420.

[71] Amzel, L. M.; Poljak, R. J. *Annual review of biochemistry* **1979**, *48*, 961–97.

[72] Nuzzo, R. G.; Allara, D. L. *Journal of the American Chemical Society* **1983**, *105*, 4481–4483.

[73] Holmlin, R.; Chen, X.; Chapman, R.; Takayama, S. *Langmuir* **2001**, 2841–2850.

[74] Akkerman, H. B.; Blom, P. W. M.; de Leeuw, D. M.; de Boer, B. *Nature* **2006**, *441*, 69–72.

[75] Kawaguchi, T.; Yasuda, H.; Shimazu, K.; Porter, M. D. *Langmuir* **2000**, *19*, 9830–9840.

[76] Monolayers, S.-A.; Delamarche, B. E.; Michel, B.; Biebuyck, H. A.; Gerber, C. *Advanced Materials* **1996**, *8*, 719–729.

[77] Chen, S.; Li, L.; Zhao, C.; Zheng, J. *Polymer* **2010**, *51*, 5283–5293.

[78] Baranton, S.; Bélanger, D. *The journal of physical chemistry. B* **2005**, *109*, 24401–10.

[79] Gooding, J. *Electroanalysis* **2008**, *20*, 573–582.

[80] Liu, G.; Liu, J.; Böcking, T.; Eggers, P. K.; Gooding, J. J. *Chemical Physics* **2005**, *319*, 136–146.

[81] Yang, X.; Hall, S.; Burrell, A.; Officer, D. *Chemical Communications* **2001**, 2628–2629.

[82] Liu, G.; Böcking, T.; Gooding, J. J. *Journal of Electroanalytical Chemistry* **2007**, *600*, 335–344.

[83] Ghanem, M. a.; Chrétien, J.-M.; Kilburn, J. D.; Bartlett, P. N. *Bioelectrochemistry (Amsterdam, Netherlands)* **2009**, *76*, 115–25.

[84] Polsky, R.; Harper, J. C.; Dirk, S. M.; Arango, D. C.; Wheeler, D. R.; Brozik, S. M. *Langmuir : the ACS journal of surfaces and colloids* **2007**, *23*, 364–6.

[85] Corgier, B. P.; Bellon, S.; Anger-Leroy, M.; Blum, L. J.; Marquette, C. a. *Langmuir : the ACS journal of surfaces and colloids* **2009**, *25*, 9619–23.

[86] Hansen, M. N.; Farjami, E.; Kristiansen, M.; Clima, L.; Pedersen, S. U.; Daasbjerg, K.; Ferapontova, E. E.; Gothelf, K. V. *The Journal of organic chemistry* **2010**, *75*, 2474–81.

[87] Polsky, R.; Harper, J. C.; Wheeler, D. R.; Arango, D. C.; Brozik, S. M. *Angewandte Chemie (International ed. in English)* **2008**, *47*, 2631–4.

[88] Guo, J.; Feng, Y.; Ye, Y.; Zhao, H. *Journal of Applied Polymer ...* **2011**.

[89] Portney, N. G.; Ozkan, M. *Analytical and bioanalytical chemistry* **2006**, *384*, 620–30.

[90] Yebra, D. *Progress in Organic Coatings* **2004**, *50*, 75–104.

[91] Jeon, S.; Lee, J.; Andrade, J.; De Gennes, P. *Journal of Colloid and Interface Science* **1991**, *142*, 149–158.

[92] Jiang, S.; Cao, Z. *Advanced materials (Deerfield Beach, Fla.)* **2010**, *22*, 920–32.

[93] Xiu, K. M.; Cai, Q.; Li, J. S.; Yang, X. P.; Yang, W. T.; Xu, F. J. *Colloids and surfaces. B, Biointerfaces* **2011**, *90*, 177– 183.

[94] Ostuni, E.; Chapman, R. G.; Liang, M. N.; Meluleni, G.; Pier, G.; Ingber, D. E.; Whitesides, G. M. *Langmuir* **2001**, *17*, 6336–6343.

[95] Lee, B. S.; Shin, H.-S.; Park, K.; Han, D. K. *Journal of materials science. Materials in medicine* **2011**, *22*, 507–14.

[96] YALOW, R. S.; BERSON, S. A. *Nature* **1959**, *184*, 1648–1649.

[97] Lequin, R. M. *Clinical chemistry* **2005**, *51*, 2415–8.

[98] Noble, R.; Weisberg, R. *J Water Health* **2005**, 381–392.

[99] Liu, G.; Liu, J.; Davis, T. P.; Gooding, J. J. *Biosensors & bioelectronics* **2011**, *26*, 3660–5.

[100] Homola, J. *Analytical and bioanalytical chemistry* **2003**, *377*, 528–39.

[101] Yonzon, C. R.; Jeoung, E.; Zou, S.; Schatz, G. C.; Mrksich, M.; Van Duyne, R. P. *Journal of the American Chemical Society* **2004**, *126*, 12669–76.

[102] Cao, C.; Sim, S. J. *Biosensors & bioelectronics* **2007**, *22*, 1874–80.

[103] Brookst, I. *Analytical biochemistry* **1993**, *212*, 457–468.

[104] Smith, E.; Corn, R. *Applied Spectroscopy* **2003**, *57*, 320A–340A.

[105] Lee, H.; Nedelkov, D. *Analytical chemistry* **2006**, *78*, 6504–6510.

[106] Lijfas, S. *Pure & Appl. Chem* **1995**, *67*, 829–834.

[107] Lfk, S.; Johnsson, B.; Rijnnberg, I. *Colloids and Surfaces B Biointerfuces, 1* **1993**, *1*, 83–89.

2 Electrografting of Diazonium Derived Thick Films on Gold Using High Reduction Potentials

2.1 Introduction

The applications of organic films on metal surfaces are extensive. From paints and varnishes in the auto industry to microelectronic chip packaging and biocompatible coatings. The ability to construct robust organic films with the desired chemical and physical properties is highly valuable. With this varying degree of applications for organic films it's no wonder that there are so many methods used for their construction on metal surfaces. Plasma deposition[1], spin coating[2], vapor deposition[3], electrochemical deposition[4], self-assembly[5], and electrografting[6, 7] are all commonly used methods. Electrografting, which is often confused with electrodeposition, is particularly useful as it allows the deposition of thin organic films bonded to a surface. An electro-initiation step is required only for the grafting step. The adsorbed radical then initiates polymerization and results in a propagation of the film.

Diazonated compounds were first described in the mid-19th century and are commonly used in organic chemistry for the synthesis of many compounds, such as azo dyes.[8] It wasn't until more recently that the use of diazonium compounds to modify surfaces has been utilized. First published by Pinson in 1992,[9] aryl diazonium salts can be used to modify a variety of conductive surfaces, including: gold, carbon, copper, platinum, and silicon.[10][11][12] Additionally, diazonium derived layers have been shown to out-perform SAM's in thermal stability,[13] potential cycling,[14] ultrasonication,[15] and storage in ambient conditions.[9] The versatility of diazonium surface modification has led to its employment in a number areas. Molecular electronics, biomedical applications, sensors, and energy conversion have all seen growing use of diazonium modified surfaces.[16][17][13][10]

Diazonium Salt	Reduction Potential, V vs. SCE
4-Nitrobenzenediazonium	+0.20
4-Bromobenzenediazonium	+0.02
Benzenediazonium	-0.06
4-t-Butylbenzendiazonium	-0.10
4-Methylbenzenediazonium	-0.16
4-Diethylaminobenzendiazonium	-0.56

Table 2.1: Literature reduction potentials of various diazonium salts on glassy carbon.

Diazonium cations have been shown to graft to surfaces through a variety of meth-

ods, including the use of reducing agents[18], ultrasonication[19], heating[20], mechanical grafting[21], photochemistry[22], or electrochemistry[6, 23, 24, 11]. The latter being the most prevalent method; it has been used to deposit a number a diazonium salts. Table 2.1 shows a number of diazonium cations reduced using electrochemistry; the relatively low reduction potentials exemplify the ease of reduction of these molecules.

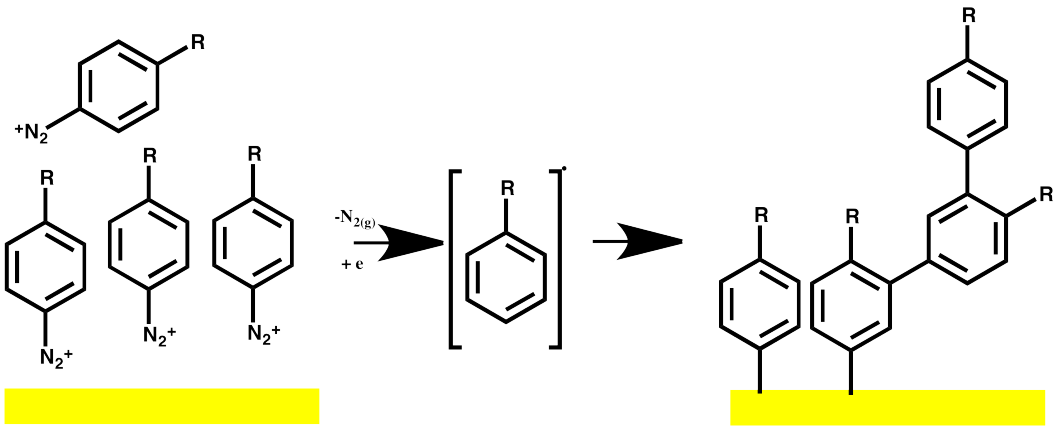

Figure 2.1: Proposed mechanism of diazonium derived layer deposition. Diazonium salts are reduced to form radical intermediates, which bond to the electrode surface capable of multilayer formation.

Diazonium cations can be either spontaneously[25] or electrochemically reduced at the surface of a conductor. In both cases it is believed that the aryl layer forms through a radical intermediate. Free electrons from an electrode induce radical formation of a diazonium cation. The radicals then bind to the substrate due to the proximity at which reduction occurs, forming a covalent bond on the surface.[26, 7, 27] Figure 2.1 shows the mechanism in which diazonium surface modification occurs. This mechanism results in a kind of radical polymerization in which newly formed aryl radicals bind to the aryl rings of molecules that previously bound to the surface. This results in multilayers that tend to be relatively disordered. While diazonium salts are not in the strictest sense electrografted, as there is no propagation of film growth without an applied potential, this attatchment mechanism allows for a high degree of control over film thickness. The general structure of diazonium derived layers is that of polyphenylene layers bonded together through either the 3, 4, or 5 position of the aryl ring in relation to the diazonium group.[28] These films are easily characterized through spectroscopic techniques as the aromatic ring or the substituent groups result in distinct bands pertaining to their signature. IR spectroscopy, Raman spectroscopy, ToF-SIMS and XPS are all commonly used in the structural determination of diazonium derived

layers. An interesting feature of this process is the formation of a bond between a number of different surfaces and the organic layer. This surface-layer bonding provides tremendous stability as diazonium derived layers have shown high stability at ambient condition, thermal stability, and electrochemical stability.

Previously it has been shown that diazonium derived layers can be constructed with thicknesses ranging anywhere from sub-monolayer to hundreds of nanometers depending on the deposition conditions, solvents, or substrates.[29, 30] It has been demonstrated that the thickness of diazonium derived films can be controlled with a number of different electrochemical techniques. Cyclic voltammetry, potential steps, and pulsed wave voltammetry have all been used to prepare a variety of different diazonium derived layers of various thickness on a variety of substrates.[29, 23, 31]

The work presented in this chapter looks at the grafting of a number of different diazonium derived films on gold and controlling film thickness of these layers using the applied reduction potential. Thick diazonium derived layers will be facbricated using extremely negative reduction potentials. Also the information on the structure and stability of diazonium derived films of various thicknesses will be presented. Molecular layers derived from phenylacetic acid diazonium (dPAA) and nitroazobenzene diazonium (dNAB) were formed via cyclic voltammetry and chronoamperometry using various reduction potentials. Successful deposition of dPAA and dNAB was determined spectroscopically with infrared reflection absorption spectroscopy (IRRAS) and X-ray photoelectron spectroscopy (XPS). Film thickness measurements, extent of multilayer formation, and topographic information were determined with atomic force microscopy (AFM).

2.2 Experimental

2.2.1 Diazonium Salt Synthesis

Diazonium salts were prepared according to a modified procedure from Starkey *et al.*[32] One mole of appropriate aniline derivative was dissolved in a molar excess of fluoroboric acid (Fischer Chemical) with a minimal amount of deionized (18MΩ) water at 0°C with constant stirring. A chilled solution with 1.2 mole sodium nitrite (Sigma-Aldrich) in a minimal amount of water was added drop-wise until the reaction was complete, the presence of excess sodium nitrite was tested for with potassium iodine starch paper. The product was then filtered with a glass frit and washed successively with 5 mL portions of cold ether

(Fischer Chemicals) and cold deionized (18MΩcm) water. The product was then recrystallized using acetonitrile (Fischer Chemicals) and ether (Fischer Chemicals) and filtered, the recrystallization procedure was repeated two more times. The product was dried under vacuum and stored at -20°C over desiccant until needed.

2.2.2 Substrate Preparation

Glass microscope slides (Fischer Scientific) were cleaned in piranha solution, 3:1 H_2SO_4 and H_2O_2, for 10 min. After cleaning in piranha solution slides were rinsed with deionized (18MΩ) water, blown dry with $Ar_{(g)}$, and placed in the thermal evaporator (Torr International). Metal films of 10 nm chromium and 300 nm gold were deposited at a pressure of 4 $\times 10^{-6}$ mbar. Following deposition slides were store under house vacuum until needed. [Warning: Piranha solution should be handled with extreme care; it is a strong oxidant and reacts violently with many organic materials. It also presents an explosion danger. All work should be performed in a fume hood.]

2.2.3 Surface Modification

Prior to surface modification substrates were cleaned with either a 3:1 H_2SO_4 and H_2O_2hot piranha solution for 10 min or with a UV ozone cleaner for 10 min. Following cleaning in piranha slides were rinsed with deionized (18MΩ) water, blown dry with $Ar_{(g)}$, and placed in a three-electrode cell. Substrates cleaned with ozone were placed directly in the three-electrode cell. Various 1 mM diazonium salt solutions containing 0.1 M NBu_4BF_4supporting electrolyte were electrochemically grafted by either cyclic voltammetry or chromoamperometry. The cycling potentials and the potential steps depended on the particular diazonium salt used. A Pine Bipotentiostat model AFCPI controlled by Aftermath software (version 1.2.4532) along with a $Ag/AgNO_3$ reference electrode and platinum mesh counter electrode were used. Note that for high potential experiments no supporting electrolyte was used.

2.2.4 Infrared Reflection Absorption Spectroscopy

Infrared reflection absorption spectroscopy (IRRAS) measurements were made with a Matson Infinity FT-IR spectrometer set to a glancing angle of 80° equipped with a mercury-cadmium-tellurium detector cooled to 77 K with liquid N_2. Background spectra were collected from deuterated octadecanethiol monolayers on gold. Samples were purged with

$N_{2(g)}$for 10 min and spectra were collected over 1000 scan with a resolution of 2 cm^{-1}. Spectra were analyzed with Essential FT-IR software.

2.2.5 X-ray Photoelectron Spectroscopy

Samples were analyzed using X-ray photoelectron spectroscopy (XPS) using a AXIS Ultra spectrometer (Kratos Analytical) at the Alberta Centre for Surface Engineering and Sciences (ACSES). Samples were measured at a base pressure below 10^{-7}Pa using a monochromatic Al Kα source (hν = 1486.7 eV). Survey spectra were taken from 1000 eV to 0 eV binding energy using a analyzer pass energy of 160 eV at a resolution of 0.3 eV.

2.2.6 Atomic Force Microscopy and Film Thickness Measurements

Atomic force microscopy (AFM) imaging and film thickness measurements were performed under ambient conditions using using a Nanoscope IIIa Multimode^{TM} (Digital Instruments). Rectangular Si cantilevers with reflective Al coatings (Olympus) were used with a force constant and oscillating frequency of 20 N/m and 300 ± 10 kHz, respectively. Film thickness measurements were performed by "scratching" a 1 μm^2area with high force in contact mode. A 5 μm^2area was then re-imaged in tapping mode, a cross-sectional profile was then taken. Control "scratches" were preformed on bare substrates to ensure forces were not sufficient to damage the substrate.

2.3 Results and Discussion

2.3.1 Deposition and Spectroscopic Characterization of Diazonium Derived Films Using Cyclic Voltammetry

Voltammetry is an electrochemical technique in which the potential of a working electrode is scanned linearly over a set range versus a reference electrode and the resulting current is measured. This current can be either reductive or oxidative in nature and is typically proportional to the concentration of the analyte. Cyclic voltammetry is commonly used to graft diazonium derived films to conductive surfaces. Gold substrates were modified with 1 mM phenylacetic acid diazonium salt (dPAA) and nitroazobenzene diazonium salt (dNAB) solutions using a three electrode cell. The potential was cycled from 500 mV to -800 mV for solutions containing dPAA and from 400 mV to -800 mV for solutions containing dNAB against a Ag/Ag^{+}reference electrode at 10 mV/s. The successful attachment of these

diazonium salts was qualitatively confirmed with infrared reflection absorption spectroscopy (IRRAS) and X-ray photoelectron spectroscopy (XPS). Figure 2.2 (Top) shows a typical cyclic voltammogram (CV) for dPAA electrografted on gold. A large cathodic peak is present at E_p= -325 mV, indicating the reduction of dPAA. As the potential is swept back the absence of an oxidative peak indicates the irreversibility of the reaction.[33] The typical CV for dNAB (Figure 2.2, bottom) has a reduction peak at E_p= -274 mV, also lacking an oxidation peak on the return sweep.

The magnitude of the reduction peak current can be described by a diffusion controlled system. For diffusion controlled systems, assuming the reduction follows Nernstian conditions and is a one electron reduction, the peak current, i_p, is given by: [33]

$$i_p = 0.4463 \left(\frac{F^3}{RT}\right)^{1/2} A C_o^* D_o^* \nu^{1/2} \tag{2.1}$$

Where, F is the Faraday constant, A is the electrode area, C_o^* is the bulk concentration, D_o^* is the diffusion coefficient, ν is the sweep rate, R is the ideal gas constant, and T is the absolute temperature, From equation 2.1 it can be seen that the peak current, i_p, is directly proportional to diffusion coefficient, all other variables between the two different diazonium species should be identical. The smaller dPAA should have a larger diffusion coefficient compared to that of dNAB, resulting in a higher peak current. This is observed in the CV's of the two species, as dPAA has a peak current approximately 3 times larger than that of dNAB. Additionally, uncertainties in the concentrations of the bulk diazonium salts could account for some of these differences. dPAA is prepared from a precursor with 97% purity where as dNAB's precursor purity is 90%. Furthermore, slight differences in electrode area could also effect the peak current. These differences in peak currents do not necessarily mean that more dPAA was grafted to the gold surface but only an indication of the efficiency of the reduction process in solution.

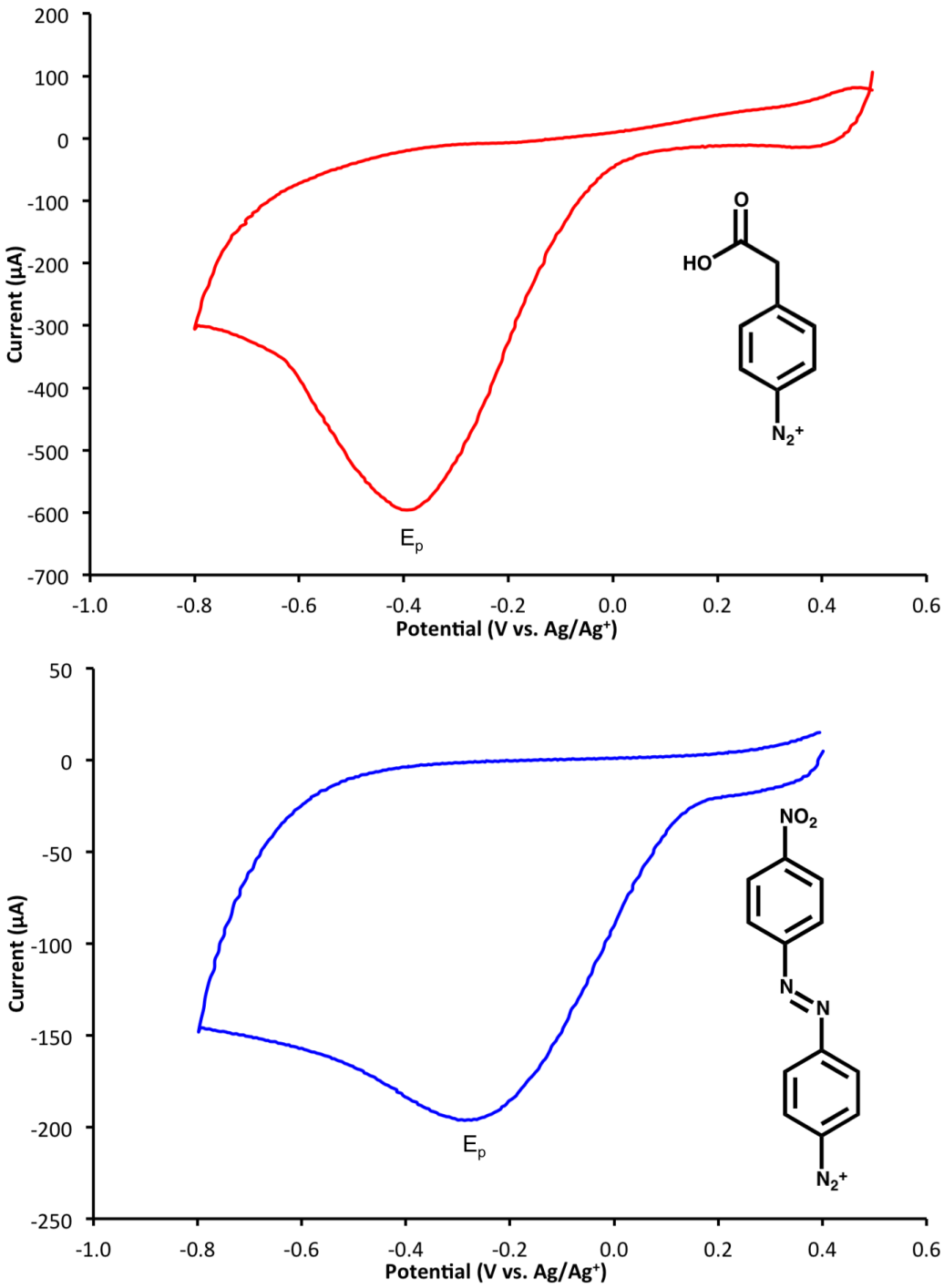

Figure 2.2: Cyclic volammogram of 1 mM dPAA (Top) and dNAB (Bottom) grafted from 500 mV to -800mV at 10 mV/s on gold containing 0.1 M NBu_4BF_4supporting electrolyte.

Figure 2.3 presents the IRRAS spectrum of dPAA grafted on gold using cyclic voltammetry. The potential was cycled from 500 mV to -800 mV for 1 cycle against a Ag/Ag^+reference electrode. The spectrum shows many bands characteristic of carboxylic acids and aryl rings,

strongly indicating the presence of dPAA on the surface. The strong peak at 1718 cm^{-1} has been assigned to the C=O stretch. The benzene ring stretching modes have been assigned to the peaks at 1603 cm^{-1} and 1509 cm^{-1}. Furthermore, the peaks at 1269 $cm^{-1}$and 821 cm^{-1} have been assigned to the C-O stretch and CH out of plane bending, respectively. No significant peak is observed at the 2200-2300 cm^{-1} region (not shown in the spectrum), which would correspond to the $N{\equiv}N^{+}$ stretching mode of the diazonium salt, confirming the loss of dinitrogen during the electrografting reaction.

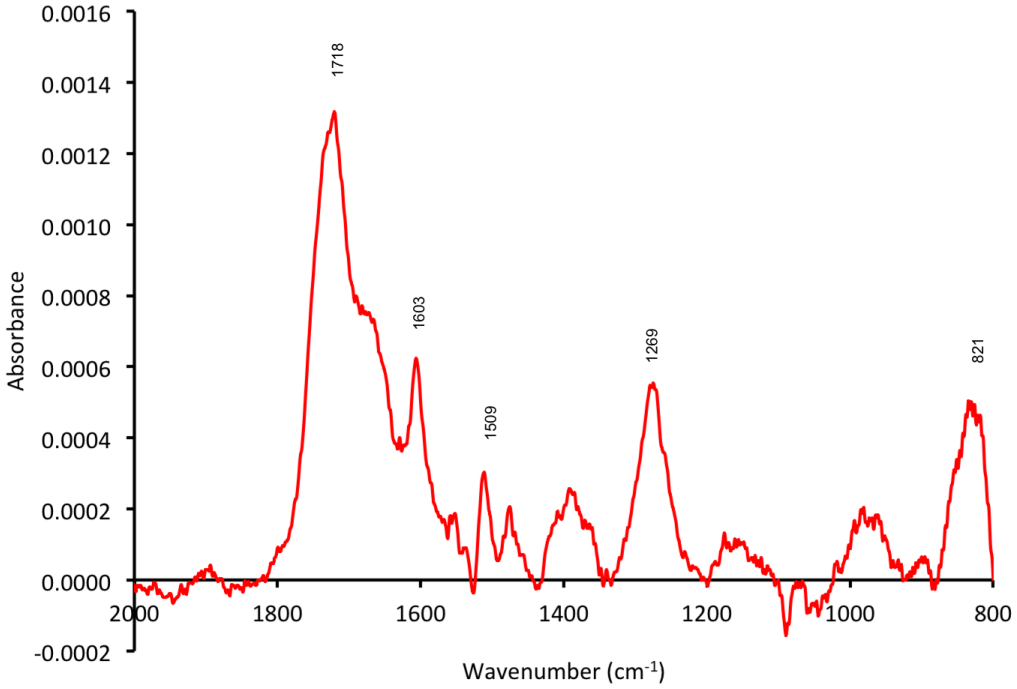

Figure 2.3: Infrared reflection absorption spectrum of 1 mM dPAA deposited with cyclic voltammetry from 500 mV to -800mV at 10 mV/s on gold

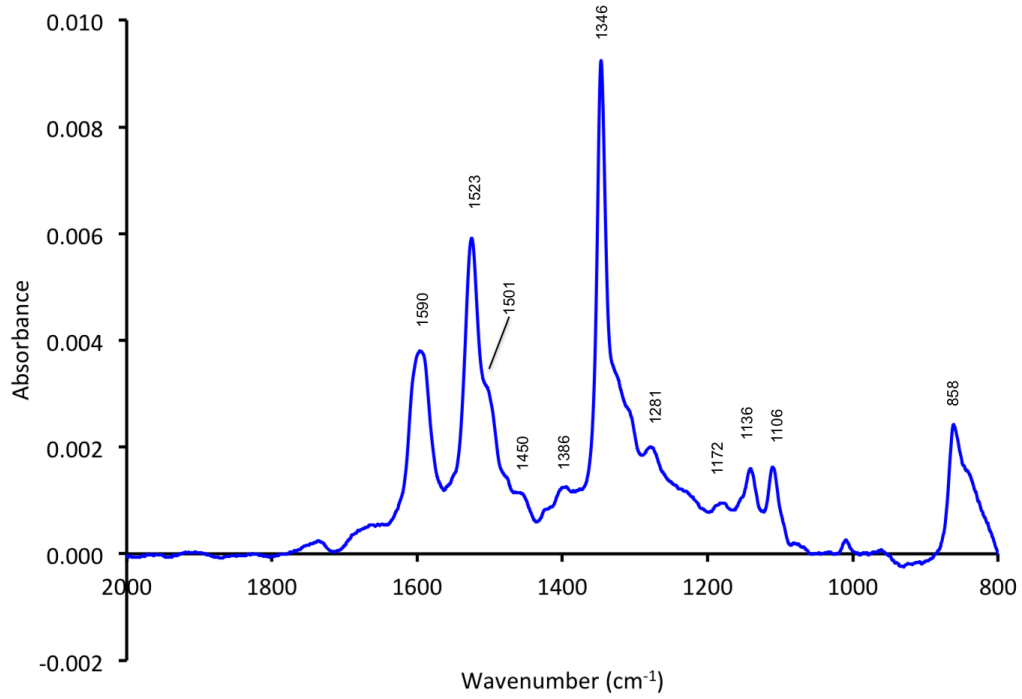

Figure 2.4: Infrared reflection absorption spectrum of 1 mM dNAB deposited with cyclic voltammetry from 400 mV to -800mV at 10 mV/s on gold

Figure 2.4 presents the IRRAS spectrum of dNAB deposited on gold. Similarly to that of dPAA, this spectrum has many characteristic of dNAB. Strong peaks at 1523 cm^{-1} and 1346 cm^{-1} have been assigned to the asymmetric and symmetric NO_2 stretches, respectively. Peaks at 1590 $cm^{-1}$and the shoulder at 1501 cm^{-1}represent the benzene ring stretching modes and the peak at 858 cm^{-1} has been assigned to the CH out of plane bending mode. Additionally, phenyl-N and phenyl-NO_2 stretches can be seen at 1136 $cm^{-1}$and 1106 cm^{-1}, respectively. Finally, N=N and N=N-ring stretching modes are present at 1450 $cm^{-1}$and 1386 cm^{-1}. Note the large negative peaks present at 2100 cm^{-1} and 2200 cm^{-1} which correspond to the deuterated thiol layer of the background slide. Examination of the peak intensities indicate that much more dNAB was deposited under these conditions compared to dPAA. Comparing the peak intensities of the benzene ring stretching modes of dPAA and dNAB at 1603 cm^{-1} and 1590 cm^{-1}, respectively. dNAB has greater peak intensities, by nearly a factor of 10, indicating a much thicker layer was grafted.

Additionally, the diazonium derived films were characterized with XPS. Figures 2.5 and 2.6 show high-resolution XPS spectra for the C1s, O1s, and N1s regions characteristic of

dPAA and dNAB grafted on gold using cyclic voltammetry. Peaks were fit with CasaXPS software. The C1s region of dPAA exhibits three distinct peaks. The strongest peak at 284.4 eV corresponds to the C=C/CH carbons of the aromatic ring. Two smaller peaks at 285.3 eV and 288.9 eV correspond to the C-O carbon and the C=O carbon, respectively. Furthermore, the ratios between the large peak and the two smaller peaks is approximately 6:1, which is what would be expected from a layer of dPAA molecules. The O1s region of dPAA shows two relatively strong peaks. The first for the C-O oxygen at 532.0 eV and the second at 533.4 eV for the C=O oxygen. The N1s region of dPAA shows a small peak representative of a -N=N- nitrogen at 399.9 eV. Indicating that the reduction dPAA results in azo linkages within the film.

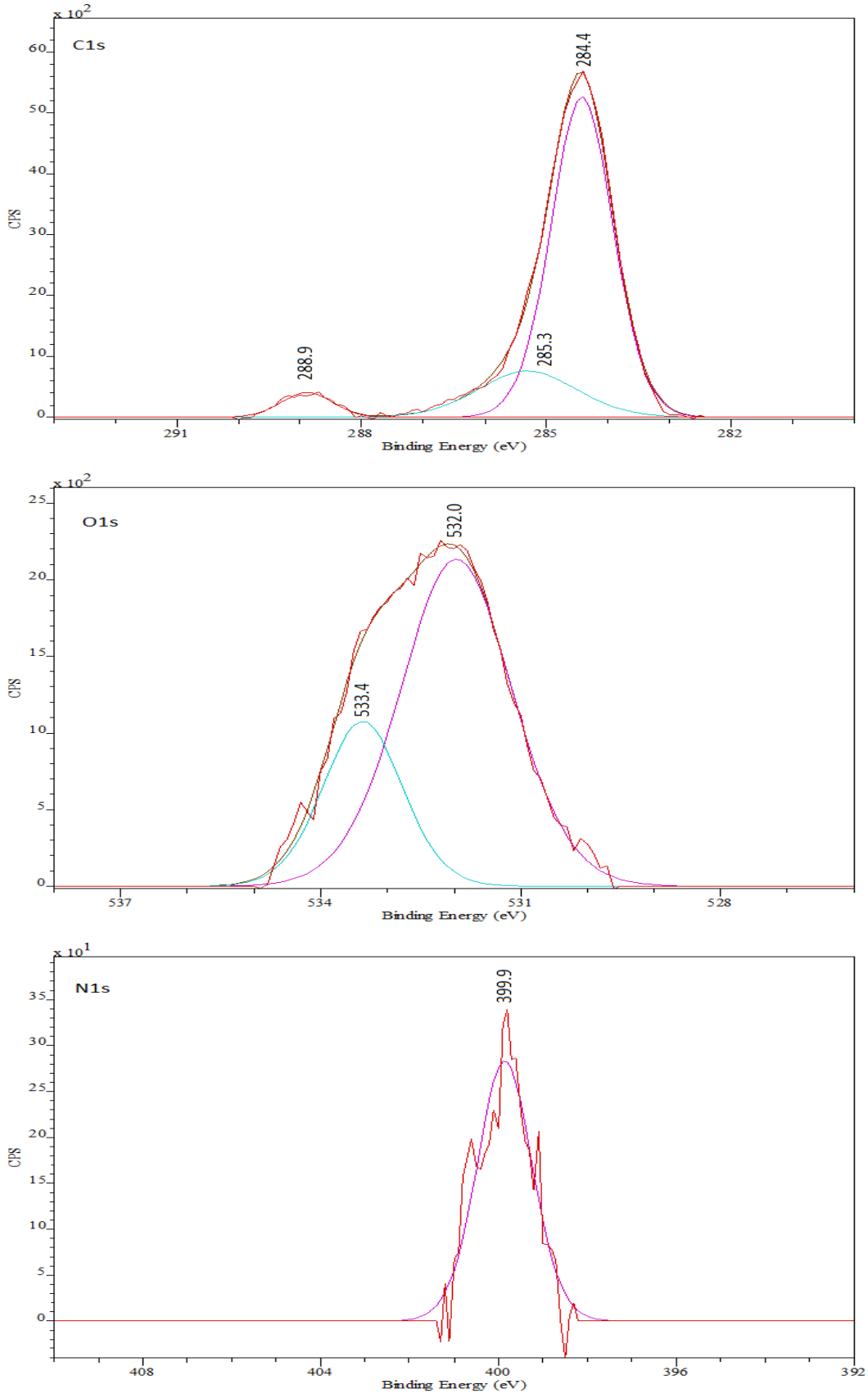

Figure 2.5: High-resolution x-ray photoelectron spectra of 1 mM dPAA deposited on gold

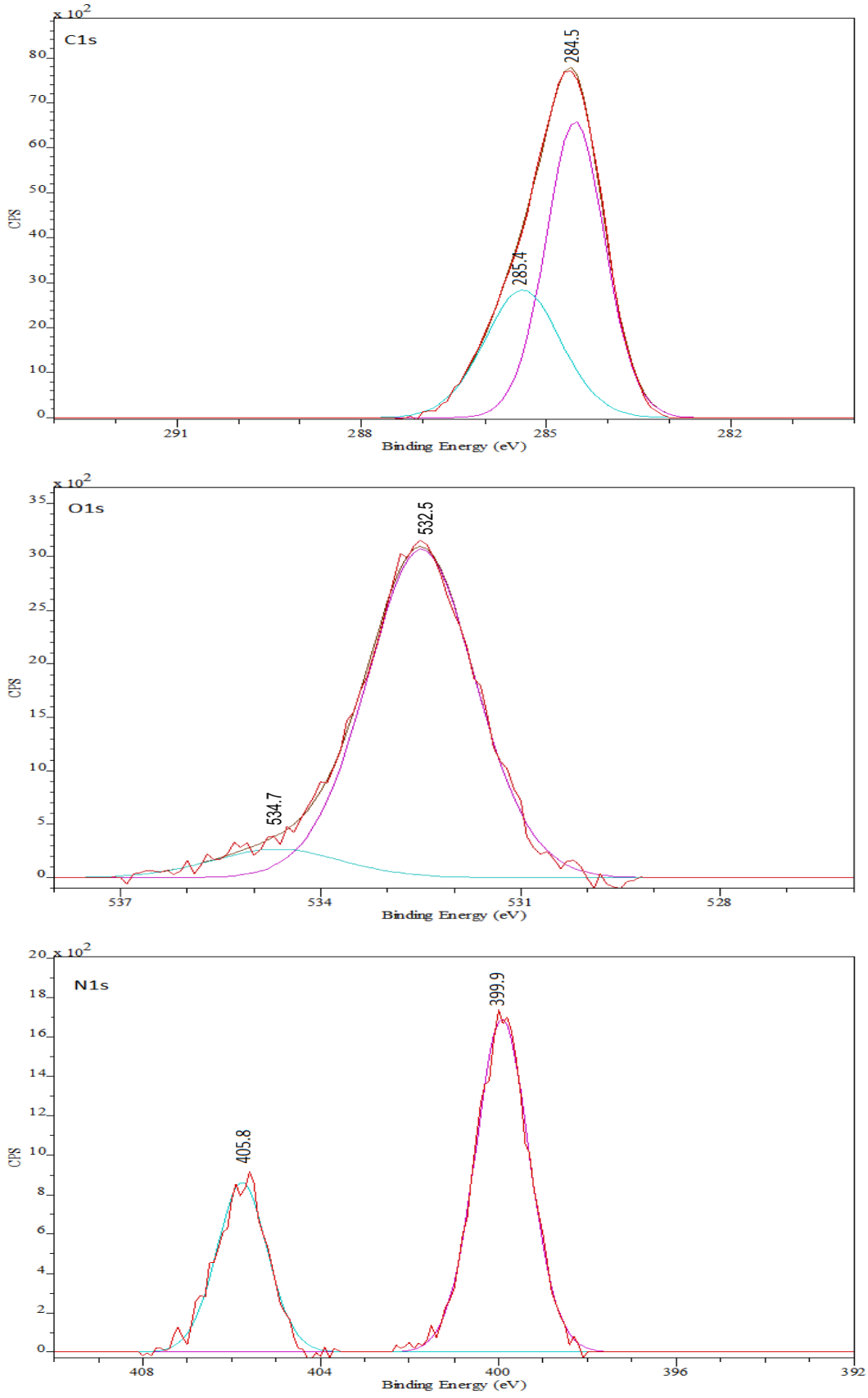

Figure 2.6: High-resolution x-ray photoelectron spectra of 1 mM dNAB deposited on gold

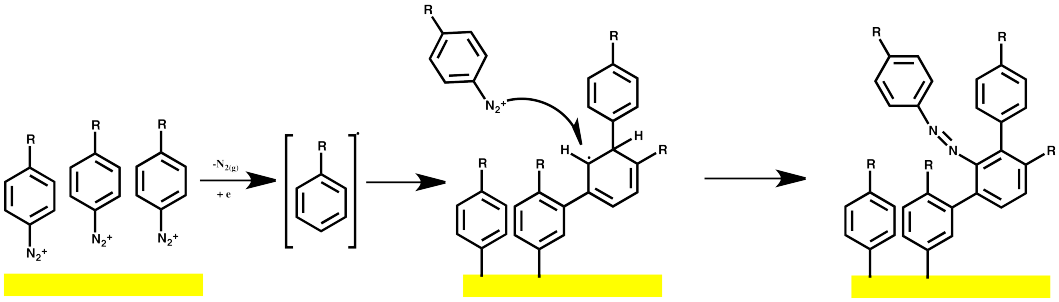

Figure 2.7: Mechanism of azo linkage formation within a diazonium derived layer. Adapted from reference [34].

The C1s region of dNAB has peaks at 284.5 eV and 285.4 eV representing the C=C/CH carbons and C-N carbons, respectively. The O1s region has a peak for the -NO_2 oxygens at 532.5 eV. Finally, the N1s region of dNAB shows two strong peaks corresponding to the -N=N- nitrogens at 399.9 eV and the -NO_2 nitrogens at 405.8 eV. Based on the characteristic peaks seen in the IRRAS and XPS spectra, as well at information attained from the CV's, it was determined that gold surfaces were successfully modified with dPAA and dNAB. The effect of reduction potentials on diazonium derived layer formation was subsequently studied.

2.3.2 Deposition and Spectroscopic Characterization of Diazonium Derived Films Using Highly Negative Reductive Potentials

The effect on film formation using a high reduction potential to graft diazonium salts was studied and compared to the grafting of diazonium salts using more traditional reduction potentials, from the previous section. Gold substrates were modified with 1 mM solutions of dPAA and dNAB using a three electrode cell. The potentials were initially cycled from positive to negative voltages with a switching potential of -5 V against a Ag/Ag^+reference electrode at 10 mV/s. The films were characterized with IRRAS, and XPS. Figure 2.8 presents the CV of dPAA with a switching potential of -5 V. Between 0 and -1 V this CV of dPAA looks very similar to that presented in figure 2.2, as there is a large cathodic peak present at E_{p1}= -325 mV with a similar peak current. As a more negative potential is applied a second cathodic peak is observed at E_{p2}= -1678 mV, indicating the reduction of some other species in solution. It's possible that this is the reduction of the diazonium radical to an anion,[34] although this would hinder film formation. The same situation is evident in the CV of dNAB. A cathodic peak present at E_{p1}= -274 mV, identical to that

of figure 2.2, and a second peak at E_{p2}= -1145 mV is present on the shoulder of the first reductive peak. For both diazonium species a large current is maintained throughout the reduction until the potential is swept back where no oxidative peaks are observed.

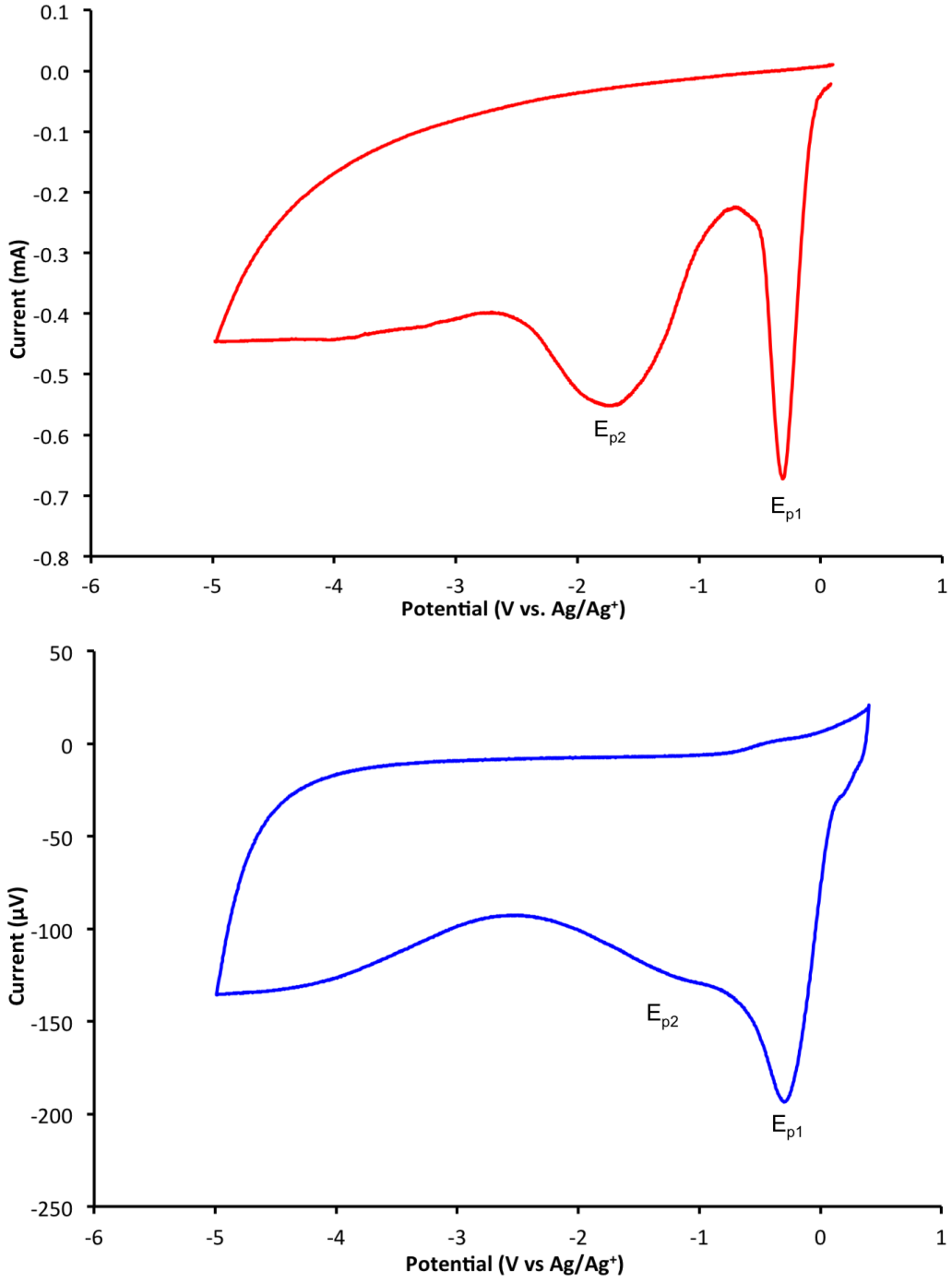

Figure 2.8: Cyclic volammogram of 1 mM dPAA (Top) and dNAB (Bottom) grafted from 100 mV to -5000mV at 10 mV/s on gold, no electrolyte was used.

Upon examination of the IRRAS spectra of diazonium derived films using these high reductive potentials many of the same peaks are observed as in their more traditional reduction potential counterparts. The intensities of certain peaks have changed. Giving some indications towards the structure of the films. Figure 2.9 shows the IRRAS spectrum of dPAA deposited using cyclic voltammerty with a switching potential of -5 V. The peak intensities have increased by around a factor of 10, indicating much more dPAA was grafted. The strong peak at 1703 cm^{-1} has been assigned to the C=O stretch. The benzene ring stretching modes have been assigned to the peaks at 1604 $cm^{-1}$and 1510 cm^{-1}. The peak at 1259 cm^{-1} has been assigned to the C-O stretch. Furthermore, peaks at 1153 $cm^{-1}$and 831 cm^{-1} have been assigned to the CH in-plane bending and CH out of plane bending, respectively. The peak at 1452 cm^{-1} has been assigned to a N=N stretch mode, indicating the presence of some azo linkages within the film. Furthermore, notice the difference in absorbance intensities of the C=O stretch and the ring stretching modes between the spectra of dPAA deposited with normal and high reduction potentials, seen in table 2.2. The films deposited with high reduction potentials appear to have a much higher ratio of aryl rings to carboxyl groups. Possibly indicating the reduction of the carboxyl group at these high potentials or a change in surface orientation.

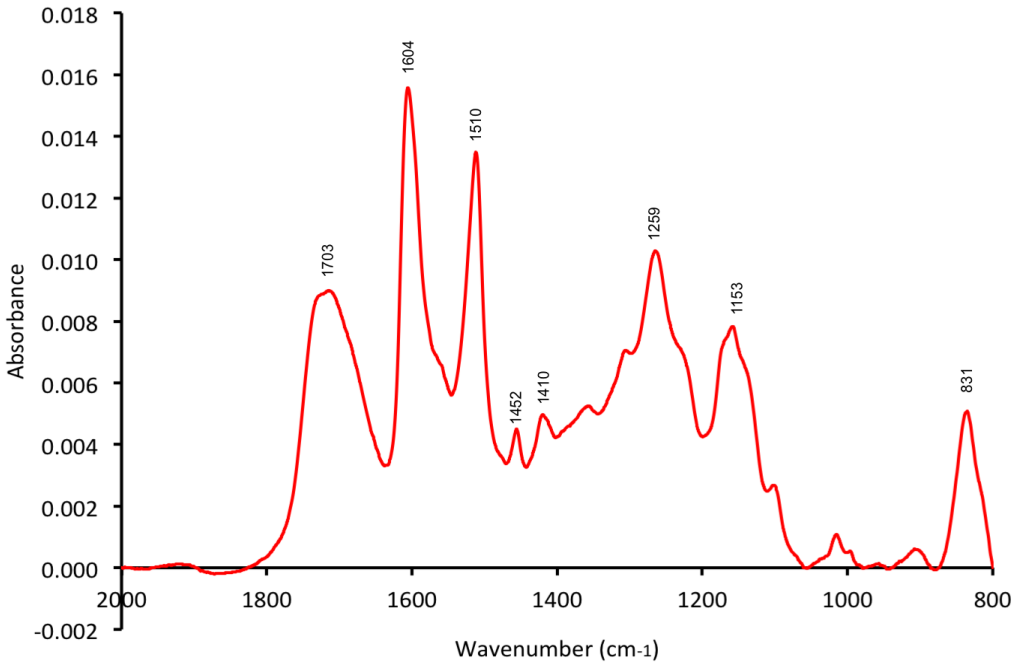

Figure 2.9: Infrared reflection absorption spectrum of 1 mM dPAA grafted with cyclic voltammetry from 0 mV to -5000mV at 10 mV/s on gold

dPAA -0.8 V Switching Potential

Bands (cm^{-1})	Intensity (peak height $\times 10^{-3}$)	Assignment
1718	1.34	C=O stretch
1603, 1509	0.652, 0.324	aromatic C=C stretch
1269	0.578	C-O stretch
821	0.552	C-H out-of-plane bend

dPAA -5 V Switching Potential

Bands (cm^{-1})	Intensity (peak height $\times 10^{-3}$)	Assignment
1703	9.28	C=O stretch
1604, 1510	15.2, 13.8	aromatic C=C stretch
1452	5.53	N=N stretch
1259	10.7	C-O stretch
1153	8.58	C-H in-plane bend
831	5.47	C-H out-of-plane bend

Table 2.2: Summery of IRRAS peak assignments and height for dPAA films using traditional and high reductive potentials.

The IRRAS spectrum of dNAB deposited using cyclic voltammetry with a switching potential of -5 V, shown in figure 2.10, also shows much larger peak intensities. Again, indicating the deposition of much more aryl groups on the surface. Strong peaks at 1523 cm^{-1} and 1346 cm^{-1} have been assigned to the asymmetric and symmetric NO_2 stretches, respectively. Peaks at 1590 $cm^{-1}$and the shoulder at 1499 cm^{-1}represent the benzene ring stretching modes and the peak at 858 cm^{-1} has been assigned to the CH out of plane bending mode. Additionally, phenyl-NN and phenyl-NO_2 stretches can be seen at 1137 $cm^{-1}$and 1106 cm^{-1}, respectively. Finally, N=N and N=N-ring stretching modes are present at 1450 $cm^{-1}$and 1386 cm^{-1}.

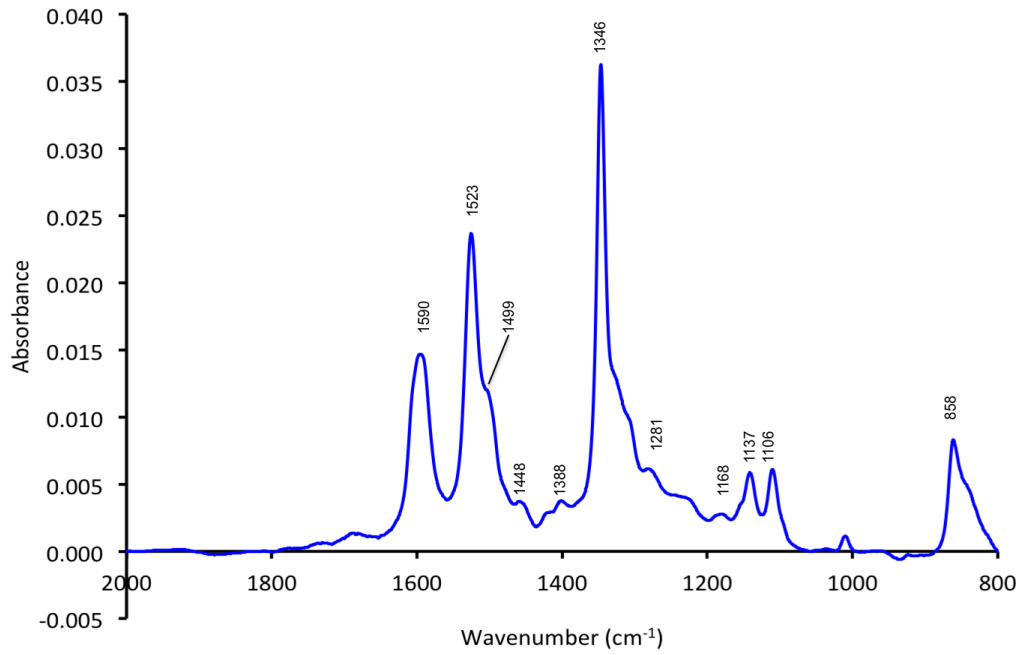

Figure 2.10: Infrared reflection absorption spectrum of 1 mM dNAB grafted with cyclic voltammetry from 400 mV to -5000mV at 10 mV/s on gold

dNAB -0.8 V Switching Potential

Bands (cm^{-1})	Intensity (peak height $\times$ 10^{-3})	Assignment
1590, 1501	3.96, 3.04	aromatic C=C stretch
1523, 1346	6.02, 9.21	asymmetric, symmetric NO_2 stretch
1450, 1386	1.18, 1.23	N=N, N=N-ring
1136	1.86	phenyl-N
1106	1.88	phenyl-NO_2
858	2.54	C-H out-of-plane bend

dNAB -5 V Switching Potential

Bands (cm^{-1})	Intensity (peak height $\times$ 10^{-3})	Assignment
1590, 1499	14.9, 12.3	aromatic C=C stretch
1523, 1346	24.6, 36.2	asymmetric, symmetric NO_2 stretch
1450, 1386	4.32, 4.43	N=N, N=N-ring
1137	5.89	phenyl-N
1106	6.04	phenyl-NO_2
858	7.87	C-H out-of-plane bend

Table 2.3: Summery of IRRAS peak assignments for dNAB using traditional and high reductive potentials.

The XPS spectra of high reduction potential diazonium derived layers were also used to characterize these film. The results are summarized in table 2.4 comparing the films grafted using high reduction potentials to those grafted using traditional reduction poten-

tials, presented in the previous section. Many of the peaks are nearly identical to that of the diazonium derived films grafted using normal reduction potentials. However, there are a few key differences that provide information about the structure of the films. The Au 4f regions of the diazonium derived layers grafted at normal reduction potentials show two strong peaks at 83 eV and 87 eV. In the Au 4f regions of the high reduction samples no peaks are evidence, indicating an increased shielding from the thicker grafted layers. Additionally, the N1s region of the dPAA film grafted with high potentials has a much stronger peak at 400 eV compared to its traditional potential counterpart, which is evident of significant azo linkages within the film. Based on the peak areas of the N1s region it was determined that in dPAA films deposited with low reduction potentials the elemental composition of azo groups within the film was 2.84 %; whereas, for dPAA grafted with high potentials the composition was 14.14 %. The structure of dNAB films appears to be nearly identical based on the elemental compositions.

Peak	Assignment	Binding Energy (eV), Elemental Composition (%)			
		dPAA -0.8 V	**dPAA -5 V**	**dNAB -0.8 V**	**dNAB -5 V**
C1s	C=C/CH	284.4, 46.67	284.7, 36.37	284.5, 33.70	284.5, 31.22
	C-O or C-N	285.3, 10.74	285.3, 23.98	285.4, 18.89	285.4, 23.21
	C=O	288.9, 3.01	289.2, 0.86		
O1s	C-O or NO_2	532.0, 27.00	532.1, 16.46	532.5, 24.39	532.8, 23.51
	C=O	533.4, 9.72	533.6, 8.16	534.7, 2.49	534.9, 2.33
N1s	N=N	399.9, 2.84	400.3, 14.14	399.9, 13.55	400.2, 12.44
	NO_2			405.8, 6.98	405.9, 7.28
Au4f		83.6	no peak	83.8	no peak
		87.5		87.5	

Table 2.4: XPS spectral analysis of dPAA and dNAB grafted using normal and high reduction potentials. Note that for the elemental composition the gold peaks were excluded to allow for direct comparison of diazonium derived film structure.

The effect of highly negative reduction potentials on diazonium derived layers was spectroscopically studied using IRRAS and XPS. Based on this data it appears that using higher reduction potentials results in much thicker films. The mechanism by which this occurs will be discussed in a subsequent section, as well as a characterization of the multilayer formation of diazonium derived layers using high reduction potentials.

2.3.3 Effect of Reduction Potentials on Multilayer Formation of Diazonium Derived Films

The effect of high reduction potentials on the multilayer formation of diazonium derived films was studied using chronoamperometry. Amperometry is an electrochemical technique in which changes in current generated by oxidation or reduction are monitored directly with time while the potential is held constant at the working electrode with respect to the reference. The current monitored is directly proportional to the concentration of electroactive species in the sample. The lack of a scanning potential is what marks the key difference between amperometry and voltammetry. For this work gold substrates were modified with 1 mM dPAA and dNAB solutions using a three electrode cell. The potential was stepped to a specific potential against a Ag/Ag^{+}reference electrode and held at that potential for a desired amount of time. The amount of electroactive species reduced was monitored electrochemically and the extent of multilayer formation was examined with atomic force microscopy (AFM). Note that for these electrochemical experiments using high reduction potentials no supporting electrolyte was used. The reasons for this will be discussed in this section. Figures 2.11 and 2.12 show the current response of dNAB grafted with potential steps of -1 V to -8 V and of dPAA grafted from -1 V to -5 V, respectively. In both samples there is a large initial spike of current corresponding to reduction of all the electroactive species near the electrode surface. After this the concentration of electroactive species near the electrode is nearly zero and the current is totally controlled by mass transfer. The magnitude of the current is proportional to the concentration of electroactive species. As the reductive potential is made more negative the current increases, reducing more diazonium in solution.

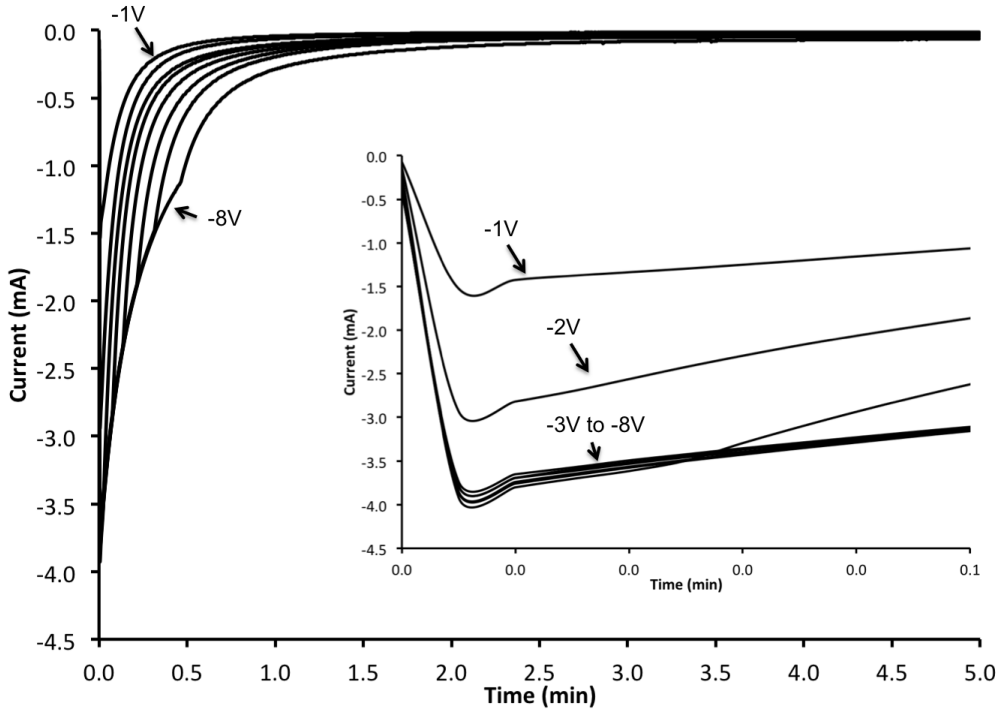

Figure 2.11: Chronoamperometric responce for a 1 mM dNAB solution grafted at -1V to -8V, with 1V intervals.

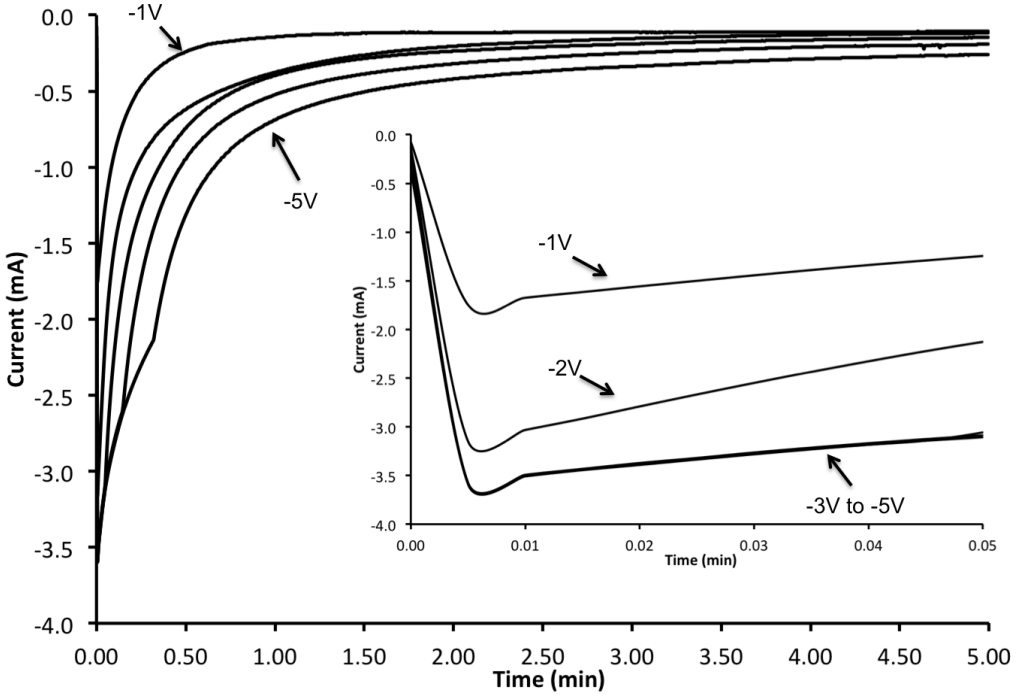

Figure 2.12: Chronoamperometric responce for a 1 mM dPAA solution grafted at -1V to -5V, with 1V intervals.

In most electrochemical systems an excess amount of nonelectroactive (in the electrochemical window) supporting electrolyte is added to eliminate the contribution of migration in mass transfer of the electroactive species. However, when high reduction potentials are applied this is not the case. Let us look at a situation using a solution containing 0.1 M NBu_4BF_4 to electrochemically reduce 1 mM dPAA at high potentials. Figure 2.13 shows the current response for dPAA containing electrolyte reduced with potential steps of -1 V to -4 V. The curve exhibits a much greater magnitude of current compared to solutions with no electrolyte. For example in the current responce curve of an applied potential of -4 V without electrolyte an initial current spike of -3.5 mA is observed. The current quikly levels off to around -0.5 mA. Whereas, in the current responce curve of an applied potential of -4 V with electrolyte an initial current spike of -100 mA is observed. This current is maintained throughout the entire experiment. As mentioned above the electrolyte should be nonelectroactive. At these high applied potentials it's likely that the electrolyte is being reduced. Since the current is proportional to the amount of electroactive species this results in the large currents observed. However, the large observed currents does not necessarily mean that diazonium ions were grafted to the gold surface, which was investigated with IRRAS.

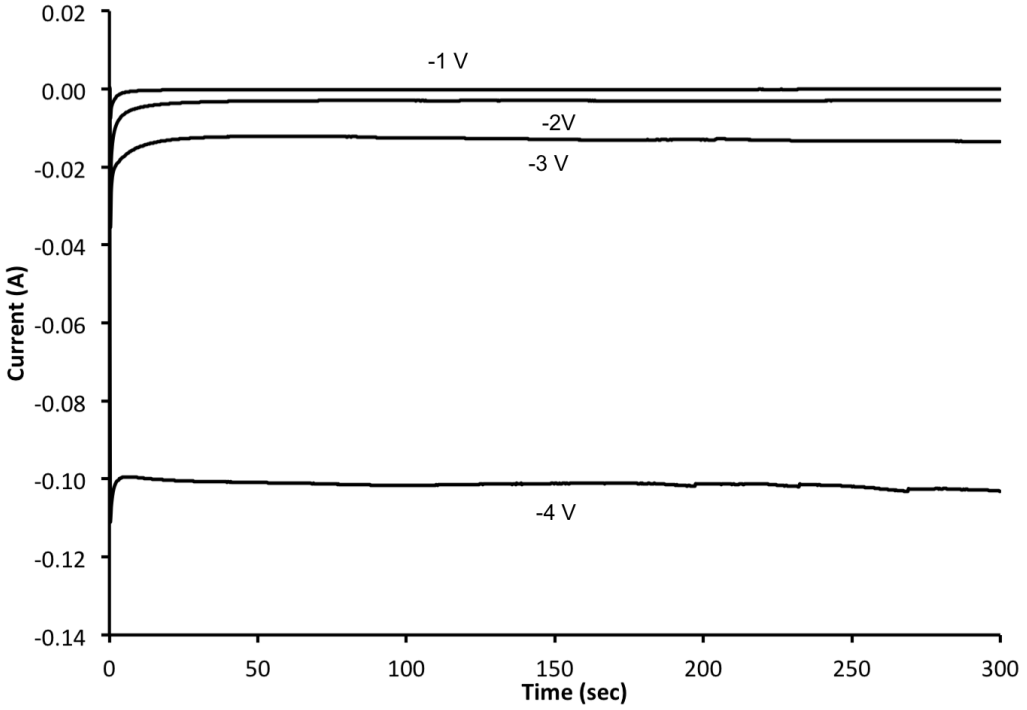

Figure 2.13: Chronoamperometric responce for a 1 mM dPAA solution containing 0.1 M NBu_4BF_4 deposited at -1V to -4V, with 1V intervals.

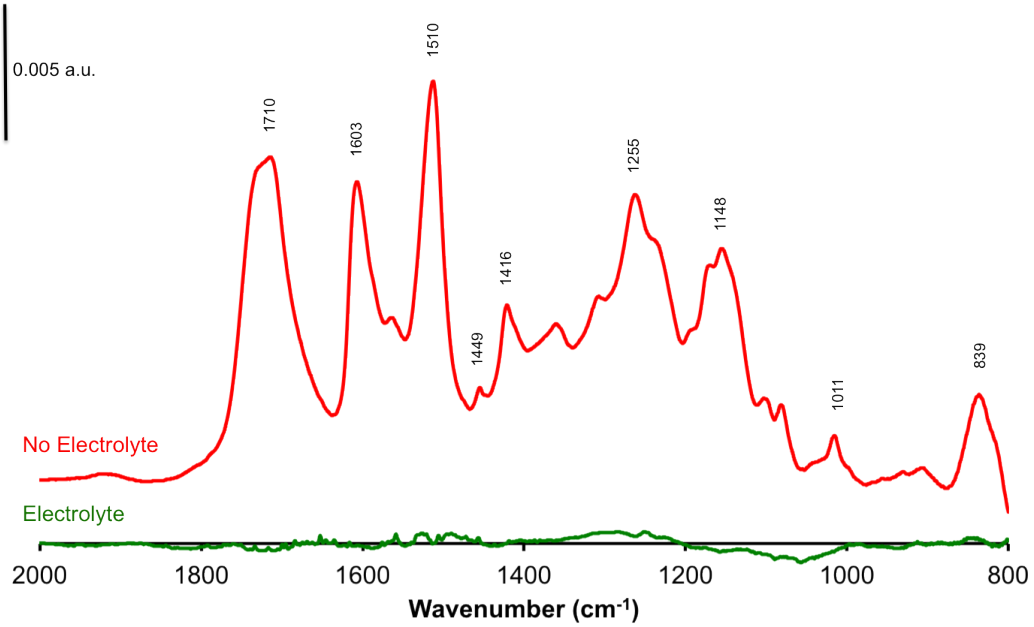

Figure 2.14: IRRAS spectra of 1 mM dPAA reduced with a -4 V potential step in solutions containing no electrolyte and 0.1 M NBu_4BF_4 electrolyte.

Figure 2.14 shows the IRRAS spectra of 1 mM dPAA electrochemically reduced using a potential step of -4 V in solutions containing no electrolyte and 0.1 M electrolyte. The reduction of dPAA in the solution without electrolyte resulted in intense peaks in the IRRAS spectrum, indicating a thick layer of dPAA grafted to the gold surface. The strong peak at 1710 cm^{-1} has been assigned to the C=O stretch. The benzene ring stretching modes have been assigned to the peaks at 1603 $cm^{-1}$and 1510 cm^{-1}. The peak at 1255 cm^{-1} has been assigned to the C-O stretch. Furthermore, peaks at 1148 $cm^{-1}$and 839 cm^{-1} have been assigned to the CH in-plane bending and CH out of plane bending, respectively. Whereas, the electrolyte containing solution resulted in no grafting. In fact only the -1 V potential step experiment resulted in any grafting for solutions containing supporting electrolyte. Although, during the experiment a dark red precipitate was observed in the electrochemical cell. To identify the precipitate some of the solution containing the precipitate was deposited on a gold coated slide and allowed to dry, once dry an IRRAS spectrum was obtained. Figure 2.15 shows the IRRAS spectrum of this precipitate which displays many of the characteristic peaks of a dPAA derived layer. However, there is a marked difference, a greatly reduced peak is present for the C=O stretch. There are two possible causes of this. Such high applied

potentials could result in the reduction of the carboxylic acid functional group, although this is unlikely since this hasn't been observed in any of the IRRAS spectra of grafted films. More likely is the orientation of the molecule on the surface. If this precipitate is just a cluster of PAA spotted on the surface then many of the molecules will be parallel with the surface. Due to the surface selection rules of IRRAS this will greatly reduce the peak intensity from the C=O stretch. During the electrochemical reduction of diazonium cations the radicals bind to the electrode surface due to their proximity to the electrode surface. With the electrolyte reducing in solution there will be many more reactive molecules in solution. The reduced diazoniums and electrolyte can then react with each other, polymerize and precipitating out of solution.

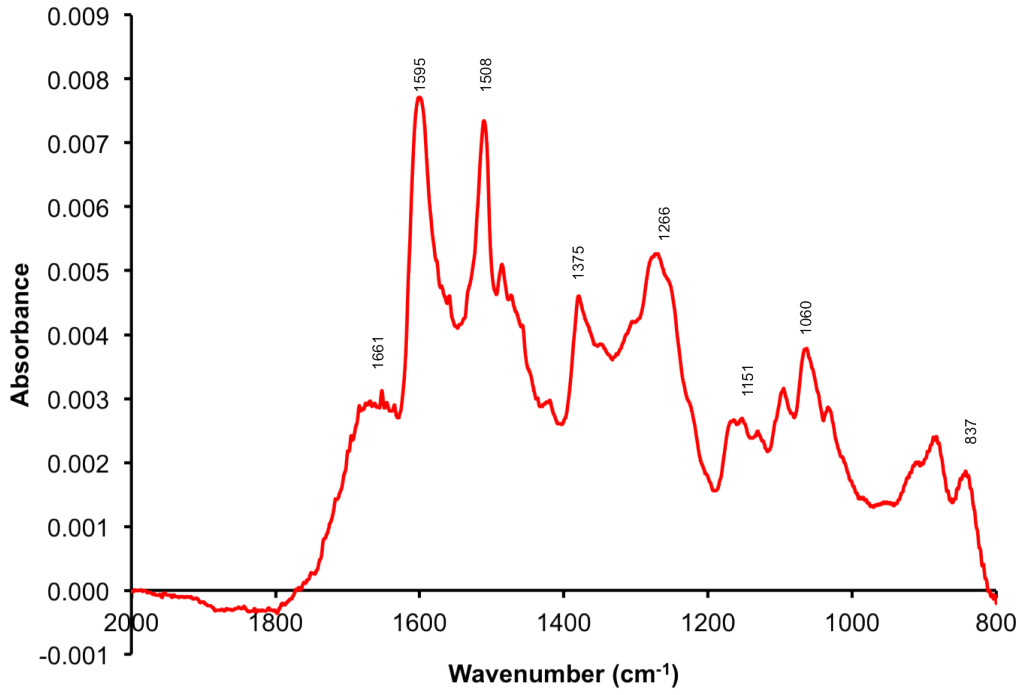

Figure 2.15: IRRAS spectrum of polymerized dPAA deposited on gold surface.

The addition of a supporting electrolyte is to eliminate the contribution of migration in mass transfer of the electroactive species. Most electrochemical theory assumes the addition of a supporting electrolyte. At any point in solution during electrolysis, the current, i, is made up of combinations of diffusion and migration of all species, j, given by:[33]

$$i = \left(\frac{AF}{RT}\right)\left(\frac{\partial \phi}{\partial x}\right)\sum_j z_j^2 D_j C_j + FA\sum_j z_j D_j \frac{\partial C_j}{\partial x} \tag{2.2}$$

where A is the area of a planar electrode, F is the Faraday constant, R is the resistance, T is the absolute temperature, ϕ is the potential gradient, z is the number of moles of electrons transferred, D is the diffusion coefficient, and C is the bulk concentration. The migrational component is the first term and the diffusion component is the second term. Near an electrode the electroactive species are transported by both diffusion and migration. The flux of an elctroactive species at the surface controls the rate of reaction and the current recorded. For our purposes the expression for i can be reduced to:

$$i = i_m + i_d$$

where i_m is the current due to migration and i_d is the current due to diffusion that contribute to the total flux of the elctroactive species. The direction of the two components depends on the direction of the electric field and the charge of the electroactive species. In the case of diazonium cations being reduced at a gold cathode i_m and i_d are in the same direction, resulting in a increase in the total flux of the reaction. With no electrolyte the conductivity of the solution is less, but the mass transfer of electroactive species will be higher. Increased mass transfer of electroactive species, largely driven by migration, results in more diazonium cations moving towards the electrode where they are reduced and bind to the electrodes surface forming thick films.

The topography and thickness of diazonium derived aryl films grafted at different reduction potentials were obtained by atomic force microscopy (AFM). To determine the thickness of deposited films, AFM "scratching" measurements were performed on modified gold electrodes. This method involves repeatedly rastering the AFM tip over the surface with enough force to remove the deposited aryl layer but not enough force to damage the substrate below. The affected area (1 μm^2) is re-imaged over a larger area (5 μm^2) with tapping mode AFM. From the images a cross sectional profile across the bare substrate and the intact film provides information on layer thickness. To ensure that forces used were not enough to damage the gold substrate, bare gold substrates were scratch with high forces and re-imaged.

Figure 2.16 shows the image of an unmodified thermally evaporated gold substrate and a substrate modified with dPAA. The unmodified surface is relatively rough (rms $\sim$ 2 nm) composed of many small gold crystallites. The re-image after scratching, figure 2.16b, shows no modification to the surface from the forces applied. Figures 2.16c and d show the AFM

images of a dPAA modified gold surface before and after scratching. A cross-sectional profile is then taken, the data points averaged, and the height measured, figure 2.17.

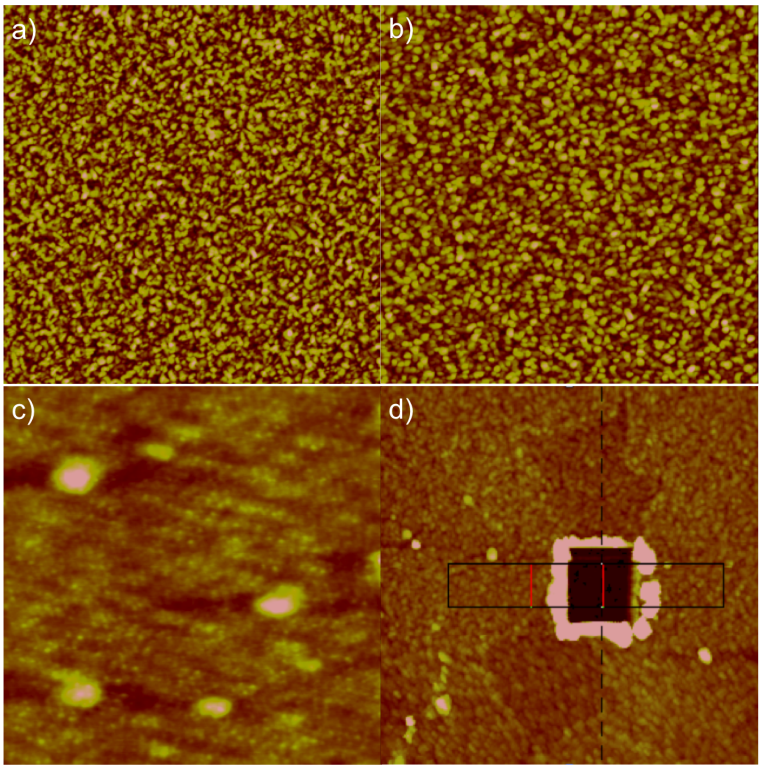

Figure 2.16: AFM height images of a) bare gold substrate b) bare gold substrate after scratching c) dPAA modified gold substrate d) dPAA modified gold substrate after scratching. Images are 5 μm^2.

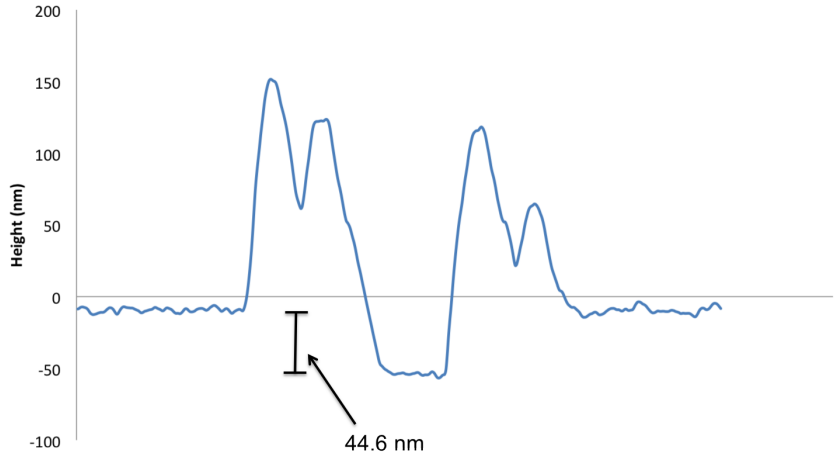

Figure 2.17: AFM cross-sectional profile of dPAA film.

The grafted layer thickness of dNAB and dPAA was monitored as a functional of electrochemical reduction potential. From figure 2.18 the effect of reduction potential on film

thickness is evident. Higher potentials result in thicker films and *vice versa*. The growth of the layers as reduction potential is increased is linear, with dNAB and dPAA resulting in layers of a similar maximum thickness. One noticeable difference between the plots is the y-intercept. dNAB has a positive intercept, while dPAA's intercept is negative. This is expected as dNAB readily spontaneously grafts to gold surfaces, resulting in layer $\sim$8 nm thick. On the other hand dPAA does not reduce spontaneously on gold surfaces.

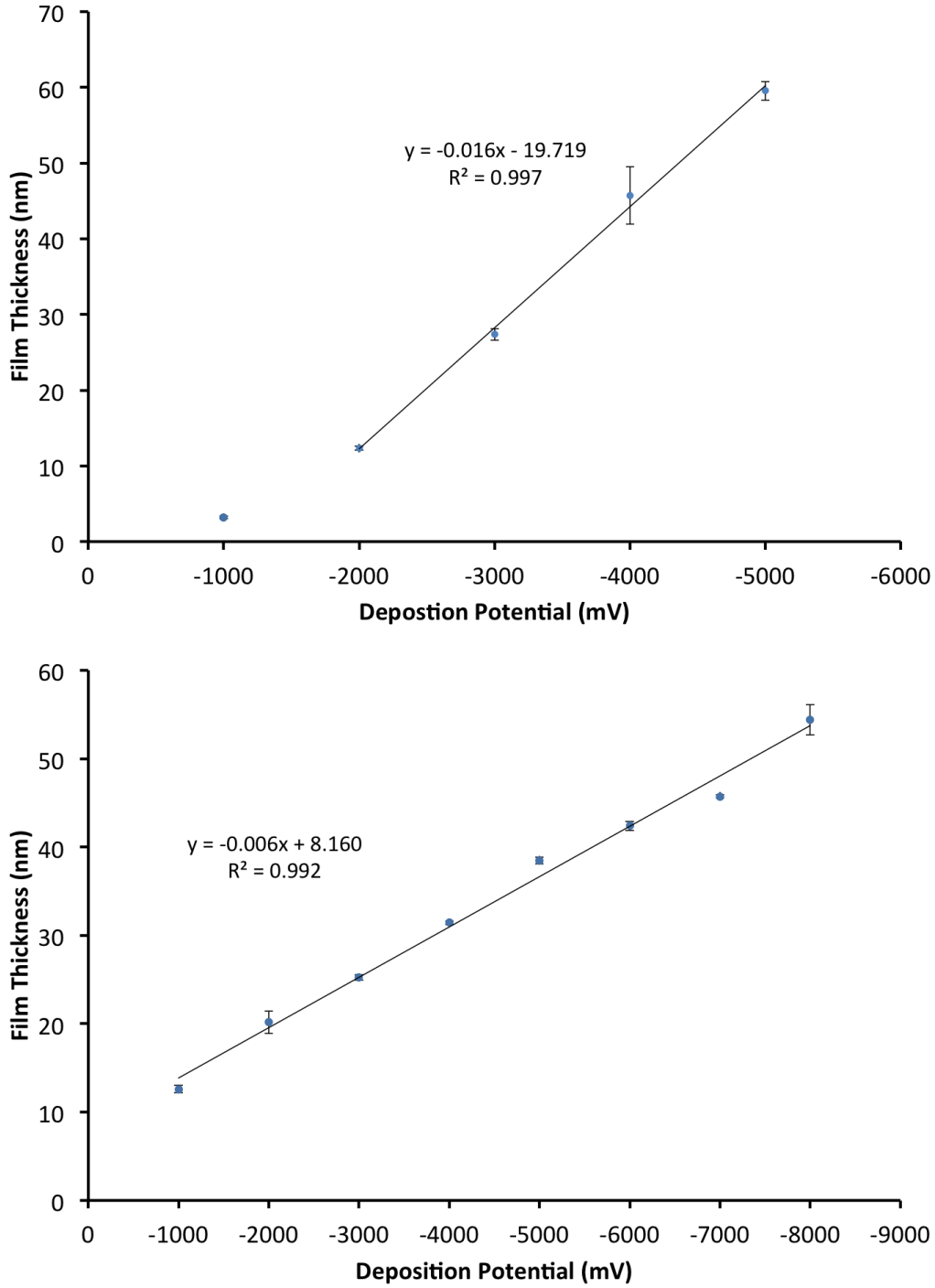

Figure 2.18: AFM Film thickness measurements of 1 mM dPAA and dNAB grafted at various reduction potentials using chronoamperometry.

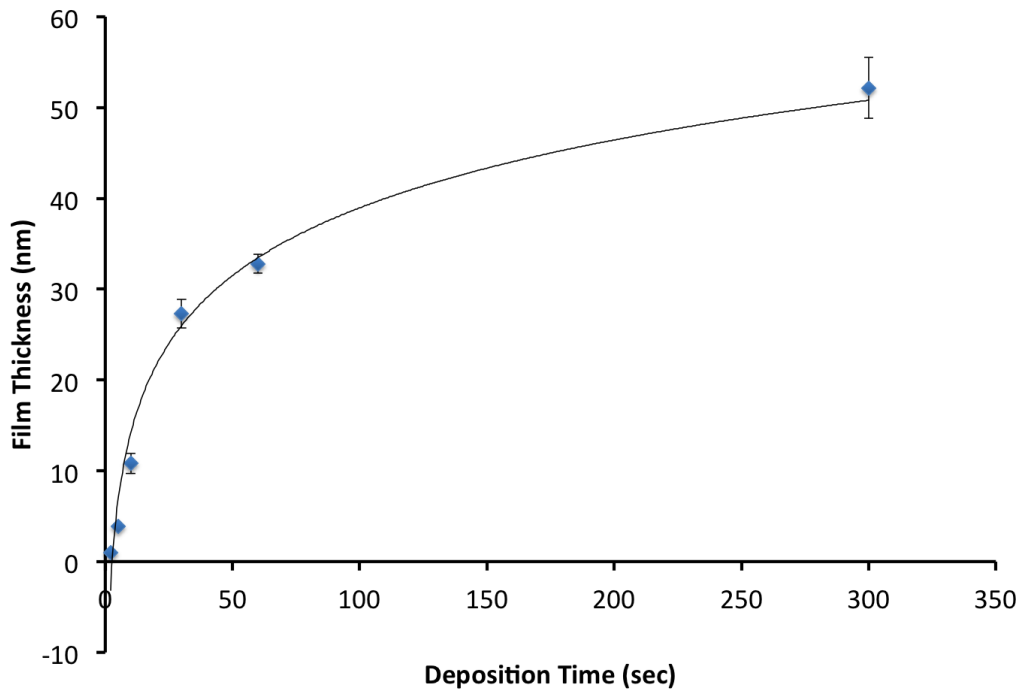

Figure 2.19: AFM Film thickness measurements of 1 mM dPAA deposited at -4V using chronoamperometry for various times.

The magnitude of film growth with respect to time was also studied. A 1mM dPAA solution was electrochemically grafted to gold using chronoamperometry with the potential stepped to -4 V *versus* the reference electrode for different amounts of time. The thickness of the grafted layers were determined with AFM. Evident from Figure 2.19 film growth is initially quite quick and then begins to plateau. As the film grows thicker the barrier to charge transfer increases. However, since at -4 V driving force remains constsant, film growth is slowed at longer times. Applying a larger driving force by increasing the reduction potential the barrier to charge transfer is overcome resulting in a thicker film. Theoretically if the potential is continually increased the film should continue to grow thicker and thicker, as long as the solvent is not reduced. However, this is also limited by the capabilities of the potentiostat.

The effect of increasing reduction potentials on multilayer formation of electrochemically grafted diazonium derived films on gold was studied with AFM and IRRAS. Increasing reduction potentials seems to form thicker diazonium derived films. Additionally, migration appears to play a key role in the creation of such films. Solutions that contained supporting electrolyte, negating the effect of migration, resulted in no grafted organic layer.

2.3.4 Mechanism Governing the Growth of Diazonium Derived Films Using Highly Negative Reduction Potentials

Previous work in the literature has demonstrated the formation of diazonium derived thick films through successive voltammetric cycles.[35, 6, 30] However, no work has demonstrated the formation of thick diazonium films as a function of reduction potentials. For the preparation of electrochemically grafted thick films the transfer of electrons from the electrode to the outer surface must take place. Several examples in the literature have achieved this by inclusion of a redox system in the layer that permits electron transfer through the layer. Work presented by Daasbjerg *et al.* showed the preparation of thick nitrobenzene diazonium derived films using cyclic voltammetry by successive increasing of the potential window. If the reductive potential window only allowed for the reduction of the diazonium group the film thickness was limited to ∼10 nm. If the potential range was increased to include the reduction of the nitro group, the film thickness increased to a maximum of 86 nm. These experiments were also performed on methylbenzene diazonium salt, which contains no redox active species other than the diazonium group. In this case film thickness was limited to ∼10 nm.[30] In previous sections of this chapter the preparation of thick diazonium derived films has been presented using diazonium salts that contain electroactive R-groups, such as nitro groups.

In an effort to determine if a highly negative reduction potential results in the formation of thick diazonium derived films without the presence of a redox active species within the film to mediate electron transfer, the successive electrochemical cycling of dNAB and benzene diazonium (dB) were performed. In figure 2.20 the CV of dNAB grafted to a gold surface using a switching potential of -3 V vs. the reference electrode is presented. A large reductive peak (E_{p1}) corresponds to the reduction of the diazonium group to the radical, the smaller peak (E_{p2}) corresponds to the reduction of the radical to the anion. The formation of the anion should hinder film formation, although it is possible when such high potentials are applied that any effect the anion would have is simply negated by large driving force of the reaction. On the successive voltammetric scan the peak (E_{p3}) is believed to correspond to the reduction of the nitro group of the grafter aryl molecules, with each scan the peak increases in intensity as more molecules are bound to the surface.

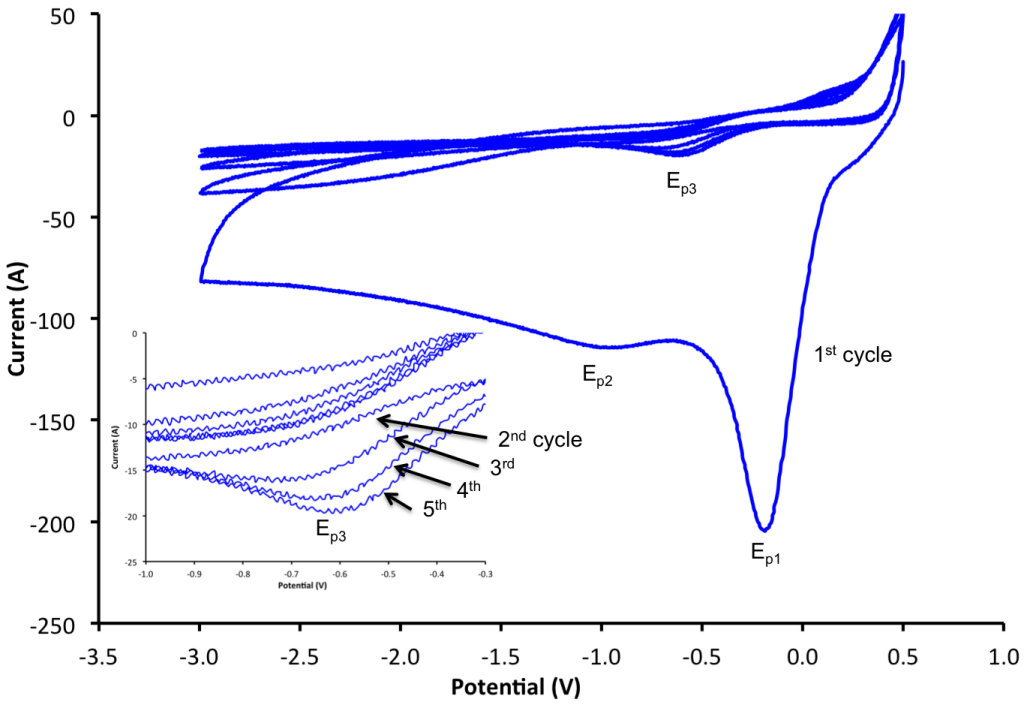

Figure 2.20: Cyclic voltammagram of 1mM dNAB in ACN deposited with a switching potential of -3V for 5 cycles.

Figure 2.21 presents the CV of dB grafted to a gold surface using a switching potential of -3 V vs. the reference electrode. Similar to that of dNAB a large reductive peak E_{p1} corresponds to the reduction of the diazonium to the radical and the smaller peak E_{p2} corresponds to the reduction of the radical to the anion. On the successive voltammetric scans a third peak E_{p3} is observed, although in this case the peak cannot be due to the reduction of redox active functional groups. It is unclear what this peak is due to although the same results are observed for methylbenzene diazonium, which also lacks a redox active functional group. Regardless of the identity of this third reduction peak applying a high reduction potential to these diazonium salts results in thick films. The maximum thickness of a number of different diazonium derived aryl films were obtained by AFM. Some contained redox active species and some did not. Films with thicknesses of ten's of nanometers can be obtained with a variety of substituents para to the diazonium functional group.

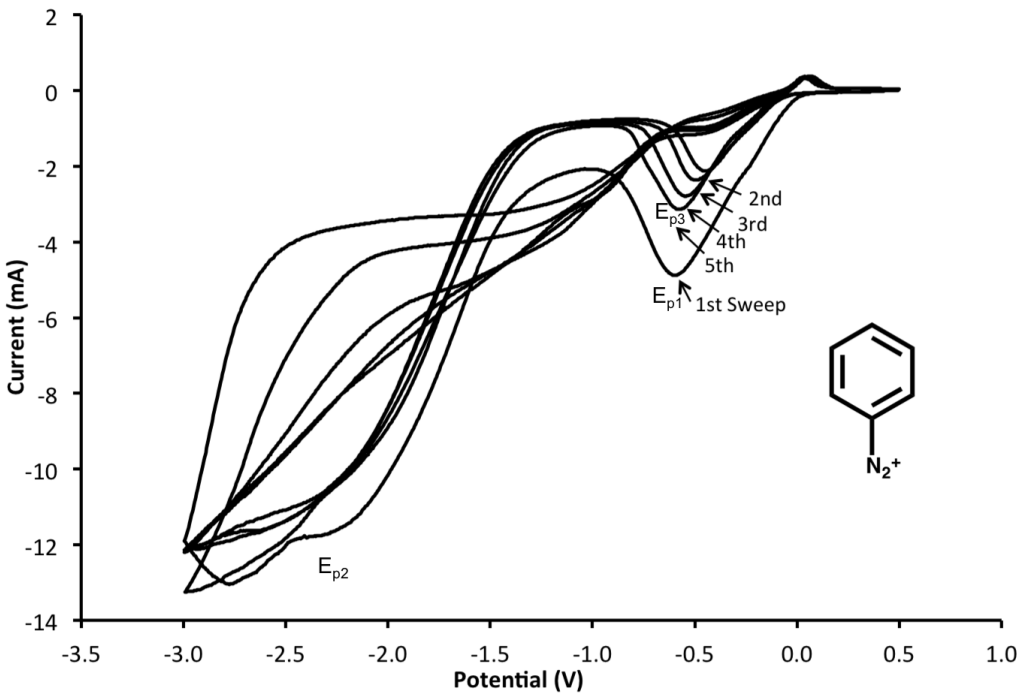

Figure 2.21: Cyclic voltammagram of 1mM dB in ACN deposited with a switching potential of -3V for 5 cycles.

Name	Structure	Method	Thickness
phenylacetic acid	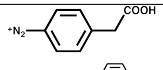	CA -5 V, 5 min	61 nm
nitroazobenzene	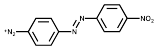	CA -8 V, 5 min	56 nm
benzene	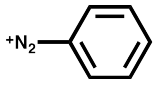	CV 0.5 to -3 V, 5 cycles, 10 mV/s	42 nm
methylbenzene	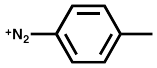	CA -3 V, 5 min	118 nm
bromobenzene	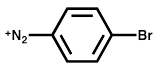	CA -4 V, 5 min	87 nm

Table 2.5: Diazonium salts that have been deposited on gold using high negative reduction potentials.

Table 2.5 presents the maximum thickness of a variety of different diazonium derived layers. When high reduction potentials are used it appears that the presence of a redox active probe within the film is not necessary for thick film growth. The use of these high potentials is applying such a large driving force for the reaction. Electron tunneling can take place over much larger distances then would be possible using lower reduction potential.

The effect of high reduction potentials on multilayer formation of electrochemically

grafted diazonium derived films with and without redox active probes on gold was studied with electrochemistry and AFM. The presence of redox probes within the aryl film is not necessary when high reduction potentials are used.

2.3.5 Stability of Thick Diazonium Derived Films

A key feature of diazonium derived films is the formation of a bond between the aryl layer and the surface (carbon, Si, or metal). [26, 7] This bond results in results in high stability of the organic layers in a number of adverse environments. Diazonium derived layers have been shown to be stable under ambient conditions for up to six months.[9] They also show high stability against ultrasonication, thermal treatments, potential cycling, and mechanical forces. They have also been shown to outperform many other surface modification techniques (SAM's) under certain conditions.[13] [14] [15] Stability of diazonium derived layers has previously been well studied. The goal of this work was simply to confirm that the thick aryl films formed using high reduction potentials are indeed grafted to the surface and are not merely physisorbed to the surface or are large polymerized units trapped in the film by other aryl molecules.

Sonicate	dPAA thin	dPAA thick	dNAB thin	dNAB thick
before treatment	$1.35 \pm 0.12 \times 10^{-3}$	$1.13 \pm 0.45 \times 10^{-2}$	$9.06 \pm 0.98 \times 10^{-3}$	$3.71 \pm 0.20 \times 10^{-2}$
after treatment	$8.69 \pm 0.19 \times 10^{-4}$	$1.07 \pm 056 \times 10^{-2}$	$7.46 \pm 1.12 \times 10^{-3}$	$3.23 \pm 0.46 \times 10^{-2}$
% of Original	**64.3**	**95.1**	**82.3**	**87.3**
Reflux				
before treatment	$1.33 \pm 0.15 \times 10^{-3}$	$1.37 \pm 0.37 \times 10^{-2}$	$9.73 \pm 0.59 \times 10^{-3}$	$3.65 \pm 0.56 \times 10^{-2}$
after treatment	$6.68 \pm 0.30 \times 10^{-4}$	$1.04 \pm 0.87 \times 10^{-2}$	$6.48 \pm 0.98 \times 10^{-3}$	$2.95 \pm 0.67 \times 10^{-2}$
% of Original	**50.3**	**76.0**	**66.6**	**80.7**

Table 2.6: IRRAS peak height measurements of C=O stretch band at 1703 $cm^{-1}$for dPAA and symmetric NO_2stretch at 1346 $cm^{-1}$for dNAB before and after sonication in acetonirile for 1 hour or refluxing in acetonitrile for 1 hour. Films were prepared by chromoamperometry using 1 mM precursor solutions. For thin film the potential was stepped to -1 V for 5 min, and for thick films was stepped to -5 V for 5 min.

dPAA and dNAB films on gold were prepared by stepping the potential to either -1 V for thin films or -5 V for thick films against a Ag/Ag^{+}reference electrode and held for 5 minutes. IRRAS was used to monitor the stability of the films by collecting spectra before and after exposing the film to either sonication or refluxing in acetonitrile.. The difference in peak height was monitored and used as a qualitative measure of film stability. From table 2.6 it would seem that the films grafted using high reduction potentials are just as if not

more stable than their lower potential counterparts. All the films appear to be more stable under unltrasonication compared to refluxation. Between thin and thick films derived from dPAA there is a significant difference in the stability. For dNAB the difference between thin and thick films is not as great, but the thick films still show more resilience.

2.4 Conclusion

This work has shown the successful modification of gold electrodes using electrochemical grafting of diazonium salts. dPAA and dNAB were used to modify gold surfaces using a variety of electrochemical techniques. The effect of reduction potential on film formation was studied. It was determined that using higher reduction potentials results in thicker films and that this increase in thickness is linear with respect to the applied reduction potential. The formation of thick films is largely driven by migration. To form diazonium derived films using high reduction potentials the omittance of supporting electrolyte is preferred as electrolyte leads to polymerization of the aryl radicals in solution preventing film formation. Additionally, the presence of a redox active functional group does not appear to be necessary to mediate thick film growth, as has been stated previously in the literature. When such high potentials are applied the driving force of the reaction is large enough to overcome the charge transfer barrier from the film deposited on the electrode surface allowing films thickness to increase with potential. Finally, the stability of films deposited using high reduction potentials was compared to films prepared with lower more traditional potentials. Under the conditions used it appears that films grafted with high reduction potentials are more stable than their low potential counterparts. Highly controllable stable organic films, like the ones presented here, have potential applications in electronic, portective coatings, energy conversion, and sensors.

References

[1] Anders, A. *Surface and Coatings Technology* **1997**, *93*, 158–167.

[2] Natsume, Y.; Sakata, H. *Thin solid films* **2000**, 30–36.

[3] Mahan, J. E. *Physical Vapor Deposition of Thin Films*; Wiley: New York, 2000.

[4] Brewer, G. **1973**.

[5] Porter, M. D.; Lipert, R. J.; Siperko, L. M.; Wang, G.; Narayanan, R. *Chemical Society reviews* **2008**, *37*, 1001–11.

[6] Haccoun, J.; Vautrin-Ul, C.; Chaussé, A.; Adenier, A. *Progress in Organic Coatings* **2008**, *63*, 18–24.

[7] Bélanger, D.; Pinson, J. *Chemical Society reviews* **2011**, *40*, 3995–4048.

[8] Konstantinou, I. K.; Albanis, T. a. *Applied Catalysis B: Environmental* **2004**, *49*, 1–14.

[9] Delamar, M.; Hitmi, R.; Pinson, J.; Saveant, J. M. *Journal of the American Chemical Society* **1992**, *114*, 5883–5884.

[10] Mahouche-Chergui, S.; Gam-Derouich, S.; Mangeney, C.; Chehimi, M. M. *Chemical Society reviews* **2011**, *40*, 4143–66.

[11] Downard, A. *International Journal of Nanotechnology* **2009**, *6*, 233–244.

[12] Anariba, F.; DuVall, S. H.; McCreery, R. L. *Analytical chemistry* **2003**, *75*, 3837–44.

[13] Mahmoud, A. M.; Bergren, A. J.; Pekas, N.; McCreery, R. L. *Advanced Functional Materials* **2011**, *21*, 2273–2281.

[14] Paulik, M.; Brooksby, P.; a.D. Abell; a.J. Downard *Journal of Physical Chemistry C* **2007**, *111*, 7808–7815.

[15] Shewchuk, D. M.; McDermott, M. T. *Langmuir : the ACS journal of surfaces and colloids* **2009**, *25*, 4556–63.

[16] Corgier, B. P.; Marquette, C. a.; Blum, L. J. *Journal of the American Chemical Society* **2005**, *127*, 18328–32.

[17] Polsky, R.; Harper, J. C.; Dirk, S. M.; Arango, D. C.; Wheeler, D. R.; Brozik, S. M. *Langmuir : the ACS journal of surfaces and colloids* **2007**, *23*, 364–6.

[18] Wildgoose, G. G.; Leventis, H. C.; Davies, I. J.; Crossley, A.; Lawrence, N. S.; Jiang, L.; Jones, T. G. J.; Compton, R. G. *Journal of Materials Chemistry* **2005**, *15*, 2375.

[19] Bureau, C.; Pinson, J.; *No Title*; 2008.

[20] Evans, J.; Bénard, S.; Yu, P.; Clément, R. *Chemistry of materials* **2001**, 3813–3816.

[21] Pandurangappa, M.; Ramakrishnappa, T.; Compton, R. G. *Carbon* **2009**, *47*, 2186–2193.

[22] Zhao, W.; Tong, B.; Zhi, J.; Pan, Y.; Shen, J.; Shi, J.; Dong, Y. *Acta Physico-Chimica Sinica* **2010**, *26*, 822.

[23] Downard, A. *Electroanalysis* **2000**, *12*, 1085–1096.

[24] Downard, A. J.; Prince, M. J. *Langmuir* **2001**, *17*, 5581–5586.

[25] Jayasundara, D. R.; Cullen, R. J.; Soldi, L.; Colavita, P. E. *Langmuir : the ACS journal of surfaces and colloids* **2011**, *27*, 13029–36.

[26] Laurentius, L.; Stoyanov, S. R.; Gusarov, S.; Kovalenko, A.; Du, R.; Lopinski, G. P.; McDermott, M. T. *ACS nano* **2011**, *5*, 4219–27.

[27] Hurley, B. L.; McCreery, R. L. *Journal of The Electrochemical Society* **2004**, *151*, B252.

[28] Adenier, A.; Combellas, C.; Kanoufi, F.; Pinson, J.; Podvorica, F. I. *Chemistry of Materials* **2006**, *18*, 2021–2029.

[29] Kariuki, J. K.; McDermott, M. T. *Langmuir* **2001**, *17*, 5947–5951.

[30] Ceccato, M.; Bousquet, A.; Hinge, M.; Pedersen, S. U.; Daasbjerg, K. *Chemistry of Materials* **2011**, *23*, 1551–1557.

[31] Menegazzo, N.; Zou, Q.; Booksh, K. S. *New Journal of Chemistry* **2012**, *36*, 963.

[32] Strakey, E. *Organic Syntheses, Coll.* **1943**, *2*, 225.

[33] Bard, A. J.; Faulkner, L. R. *Electrochemical Methods: Fundamentals and Applications*, 2nd ed.; Wiely & Sons: New York, 2000.

[34] Chehimi, M. M. *Aryl Diazonium Salts. New Coupling Agents in Polymer and Surface Science*; Wiley-VCH Verlag: Weinheim, 2012.

[35] Adenier, a.; Barre, N.; Cabetdeliry, E.; Chausse, a.; Griveau, S.; Mercier, F.; Pinson, J.; Vautrinul, C. *Surface Science* **2006**, *600*, 4801–4812.

3 Controlling the Thickness of Diazonium Derived Films for Surface Plasmon Resonance (SPR) Immunoassays

3.1 Introduction

Diagnostic testing is largely concerned with the recognition and confirmation of the presence of disease, the control of that disease, and gauging the prognosis. This can be very difficult as it involves accurately detecting and quantifying a wide range of analytes. Simple species such as ions, to more complex molecules; drugs, metabolites, hormones, or proteins to whole cells such as viruses or bacterium have diagnostic interests.

Another important factor in the development of diagnostic testing for biological samples is the fact that these analytes are present in a complex biological matrix: blood, plasma, sweat, urine, or tissue biopsies. Therefore interferences from similar molecules and nonspecific interactions are a prevalent concern in bioassay development.

A critical step in bioassay development is the construction of a stable film to which biomolecules can be immobilized; furthermore, the ability to control structure and functionality of such films is extremely advantageous. Using a variety of microscopic and spectroscopic techniques the properties of such surfaces have been accurately obtained for a number of film derivation methods and employed in many different immunoassays.[1][2]

Since their discovery in the early 1980's by Nuzzo and Allara,[3] thiol and dithiol self assembled monolayers (SAM's) have been the preeminent method for modifying metal surfaces. Due to the relatively strong thiol-gold interaction as well as the ease of preparation and controllability of surface functionality SAM's have been used extensively in molecular electronics, biocompatible surfaces, chemical wettability, system fabrication, and biorecognition sensors.[4, 5, 6] However, the nature of the bonding is also the root of many of the problems associated with SAM's. The lability of the Au-S bond results in low thermal stability,[7] a narrow electrochemical window,[8] and is susceptible to oxidation.[9] Furthermore, a tightly packed monolayer is not ideal for all surface based applications.

Unlike SAM's, diazonium derived aryl layers form a covalent bond with the surface.[10, 11] This results in diazonium derived layers out-performing SAM's in thermal stability,[12] potential cycling,[13] ultrasonication,[14] and storage in ambient conditions.[15] Furthermore, their propensity for multilayer formation makes them ideal substrates for biorecognition based immunosensors as multilayers will result in surfaces with more sites available for

biomolecule immobilization, potentially resulting in higher sensitivity.

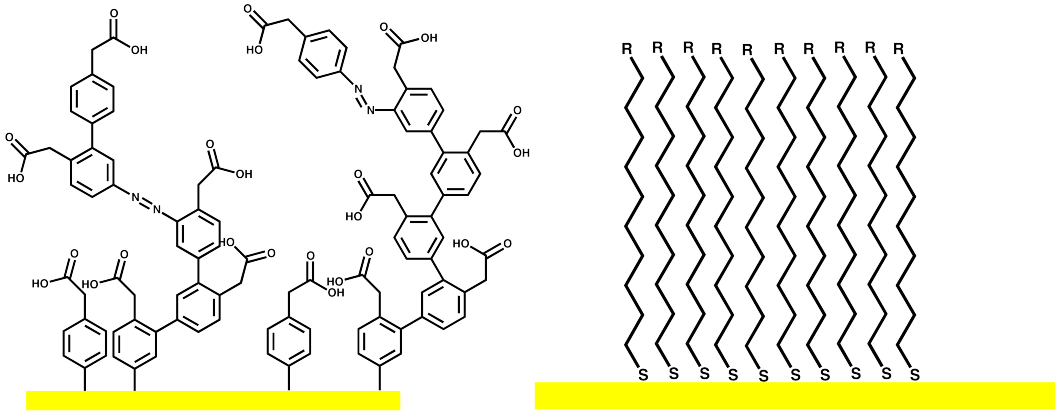

Figure 3.1: Potential immobilization sites of diazonium derived layer compared to SAM.

The wide range of para-substituted diazonium salts provided a pathway to tailor interfacial surface chemistry. The covalent attachment of glucose oxidase to a carbodiimide activated phenylacetic acid layer was one of the first reported biosensor applications using diazonium derived layers.[15] Since then other common methods of biomolecule immobilization have been demonstrated on diazonium derived surfaces; such as the generation of amine, maleimide, and nitriliotriacetic.[16] These surfaces have been used to facilitate the attachment of DNA, peptides, and proteins.[17][18][19]

Many analytical techniques have been used for the detection of binding events between biological entities. Probably the most common methods involve electrochemical detection, as it provides a highly sensitive robust platform for sensing.[19, 20, 16] However, there are also many other commonly used techniques, including fluorescence or chemiluminescence.[21][22] One drawback to these techniques is that they require modification of the analyte molecule prior to the assay, as the addition of either an electroactive, fluorescent, or luminescent probe is required to detect any binding events. Since labeling molecules involves chemical modification there is a risk the function may be impacted by the label.[23] Therefore, label-free techniques offer a particular advantage when it comes to the functional analysis of biological molecules. Surface plasmon resonance (SPR) allows for the simply label-free detection of analyte molecules and easy analysis of binding affinities.

Another important factor in the development of diagnostic testing for biological samples is that the analytes are present in a complex biological matrix such as blood, plasma, sweat, urine, or tissue biopsies. Therefore interferences from similar molecules and nonspecific

interactions are a prevalent concern in bioassay development. To this end, two main classes of low-fouling materials exist: polyhydrophilic and polyzwitterionic.[24, 25] Both have been prepared using a number of different film derivation methods including: spin-coating, self-assembly, atom transfer radical polymerization, plasma treatments.[9] One universal aspect of low-fouling materials is that they require a high degree of control over functionality and structure during preparation.

The work presented in this chapter looks at using functionalized diazonium derived films on gold for surface plasmon resonance immunoassays. In this work phenylacetic acid diazonium salt (dPAA) was used to electrochemically modify a gold electrode using various electrochemical techniques. The ability to control surface converge was evaluated using infrared reflection absorption spectroscopy (IRRAS) and atomic force microscopy (AFM). The application of these surfaces as substrates for immunoassays was achieved through covalent attachment of antibodies to the activated surface. The attachment of protein to the surface was evaluated with IRRAS and SPR. Antibody-antigen binding was monitored using SPR and the impact of multilayer formation and surface roughness on immunoassay performance was studied. Diazonium salts were also used to electrochemically modify gold with potential low-fouling films. These films were characterized with IRRAS and the low-fouling abilities of these films were compared to poly-ethyleneglycol containing SAM's, a common film used to reduce non-specific adsorption, with surface based bioassays.

3.2 Experimental

3.2.1 Diazonium Synthesis

Diazonium salts were prepared according to a modified procedure from Starkey *et al.*[26] One mole of appropriate aniline derivative was dissolved in a molar excess of fluoroboric acid (Fischer Chemical) with a minimal amount of deionized (18MΩ) water at 0°C with constant stirring. A chilled solution with 1.2 mole sodium nitrite (Sigma-Aldrich) in a minimal amount of water was added drop-wise until the reaction was complete, the presence of excess sodium nitrite was tested for with potassium iodine starch paper. The product was then filtered with a glass frit and washed successively with 5 mL portions of cold ether (Fischer Chemicals) and cold deionized (18MΩ) water. The product was then recrystallized using acetonitrile (Fischer Chemicals) and ether (Fischer Chemicals) and filtered, the recrystallization procedure was repeated two more times. The product was dried under vacuum

and stored at -20°C over desiccant until needed.

3.2.2 IRRAS Substrate Preparation

Glass microscope slides (Fischer Scientific) were cleaned in piranha solution, 3:1 H_2SO_4 and H_2O_2, for 10 min. After cleaning in piranha solution slides were rinsed with deionized (18MΩ) water, blown dry with $Ar_{(g)}$, and placed in the thermal evaporator (Torr International). Metal films of 10 nm chromium and 300 nm gold were deposited at a pressure of 4 $\times 10^{-6}$mbar. Following deposition slides were stored under house vacuum until needed. [Warning: Piranha solution should be handled with extreme care; it is a strong oxidant and reacts violently with many organic materials. It also presents an explosion danger. All work should be performed under a fume hood.]

3.2.3 Electrochemical Surface Modification

Prior to surface modification substrates were cleaned with either a 3:1 H_2SO_4 and H_2O_2 hot piranha solution for 10 min or with a UV ozone cleaner for 10 min. Following cleaning in piranha slides were rinsed with deionized (18MΩ) water, blown dry with $Ar_{(g)}$, and placed in a three-electrode cell. Substrates cleaned with ozone were placed directly in the three-electrode cell. 1 mM phenylacetic acid diazonium salt solutions were electrochemically grafted by either cyclic voltammetry or chromoamperometry. The cycling potentials and the potential steps depended on the particular diazonium used. A Pine Bipotentiostat model AFCPI controlled by Aftermath software (version 1.2.4532) along with a $Ag/AgNO_3$ reference electrode and platinum mesh counter electrode were used.

3.2.4 Surface Activation and Protein Immobilization

After electrochemical surface modification, substrates were activated with a solution of 0.4 M N-(3-dimethylaminopropyl)-N'-ethylcarbodmiimide hydrochloride (EDC) (Sigma) and 0.1 M N-hydroxysuccinimide (NHS) (Sigma). The activated surfaces were then modified with polyclonal rabbit immunoglobulinG antibody goat host (a-rIgG) (MP Biomedicals), any unreacted NHS groups were reacted with 1 M ethanolamine (Sigma). The substrates were backfilled with a 0.01 % solution of bovine serum albumen (BSA) (Sigma) for 30 minutes.

3.2.5 Infrared Reflection Absorption Spectroscopy

Infrared reflection absorption spectroscopy (IRRAS) measurements were made with a Matson Infinity FT-IR spectrometer set to a glancing angle of 80° equipped with a mercury-cadmium-tellurium detector cooled to 77K with liquid N_2. Background spectra were collected from deuterated octadecanethiol monolayers on gold. Samples were purged with $N_{2(g)}$for 10 min and spectra were collected over 1000 scan with a resolution of 2 cm^{-1}. Spectra were analyzed with Essential Ft-IR software.

3.2.6 Atomic Force Microscopy and Film Thickness Measurements

Atomic force microscopy (AFM) imaging and film thickness measurements were performed under ambient conditions using a Nanoscope IIIa Multimode^{TM} (Digital Instruments). Rectangular Si cantilevers with reflective Al coatings (Olympus) were used with a force constant and oscillating frequency of 20 N/m and 300 ± 10 kHz, respectively. Film thickness measurements were performed by "scratching" a 1 μm^2area with high force in contact mode. A 5 μm^2area was then re-imaged in tapping mode, a cross-sectional profile was then taken. Control "scratches" were preformed on bare substrates to ensure forces were not sufficient to damage the substrate.

3.2.7 Surface Plasmon Resonance Measurements

Substrates were 1.8 cm × 1.8 cm squares of SF-10 glass (Schott) modified with 1 nm chromium and 45 nm gold films. Following surface modification surface plasmon resonance (SPR) measurements were made with a SPR Imager II (GWC Technologies). The substrates were place in the iflow cell and rinsed with 10 mM PBS buffer. Polyclonal rabbit IgG (goat host) solutions were prepared by dilution of the stock solution and were introduced continuously to the surface for 5 minutes at 0.1 mL/min followed by rinsing with buffer.

3.3 Results and Discussion

3.3.1 Preparation of Electrografted Diazonium Derived films for Immunoassays

Gold substrates were modified with 1 mM phenylacetic acid diazonium salt (dPAA) solutions using either cyclic voltammerty or chronoamperometry in a three electrode cell. For cyclic voltammetry the potential was cycled from 500 mV to -800 mV against a Ag/Ag^+reference electrode at 10 mV/s for one to five cycles of the potential window. For chronoamperometry

the potential was stepped from 0 V to the desired voltage and maintained for five minutes. The successful deposition of the organic layer was qualitatively confirmed with infrared reflection absorption spectroscopy (IRRAS). The thickness of the grafted films was measured with atomic force microscopy (AFM). Note that for this work no supporting electrolyte was used in any of the electrochemical grafting, even at low reduction potentials. It was determined that the electrolyte made no difference in the formation of the grafted layer at low potentials and hindered it at higher potential. Since for this work the monitoring of current was of no concern the electrolyte was left out of the experiments.

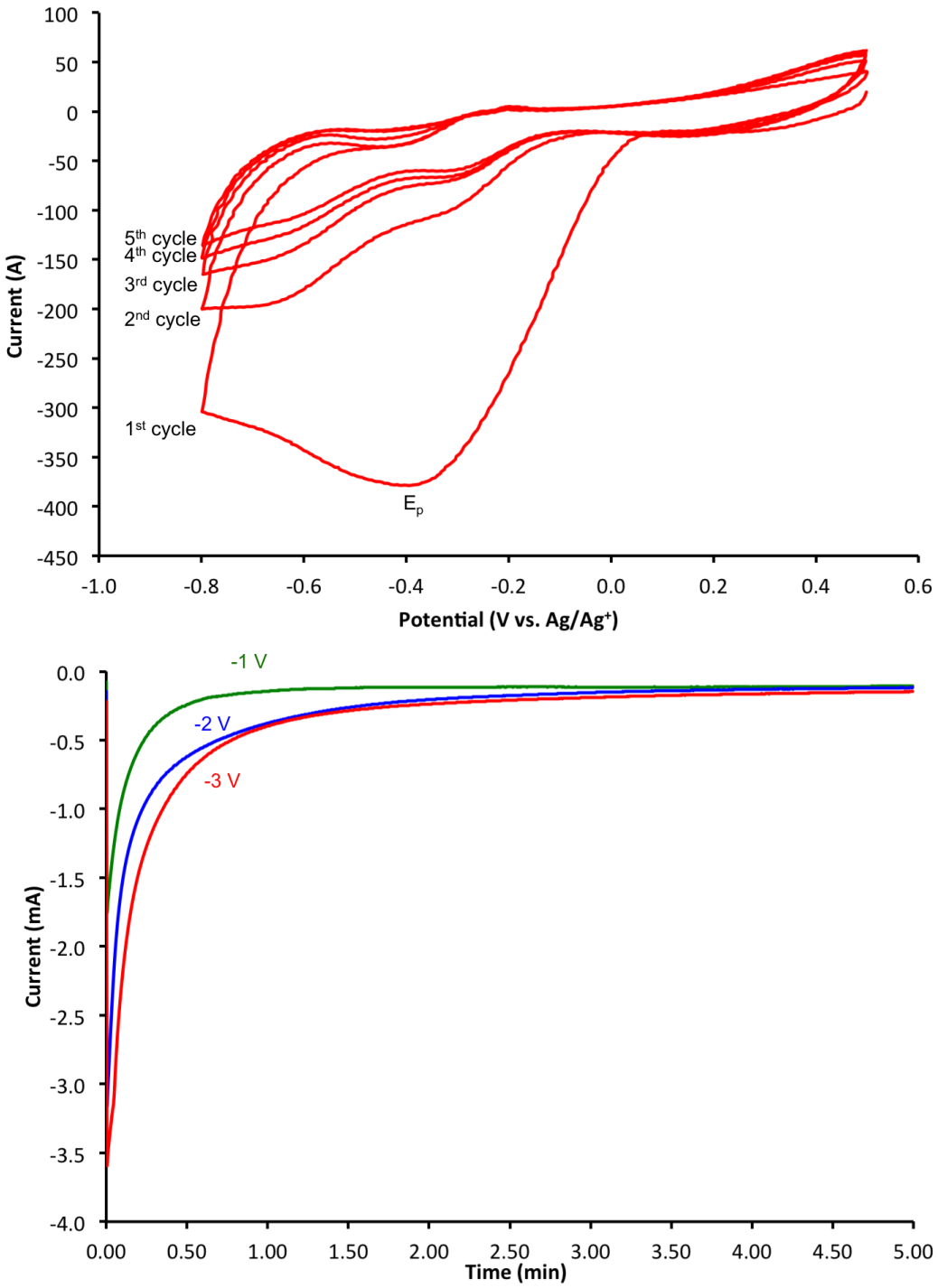

Figure 3.2: Cyclic voltammogram (Top) and current response curve (Bottom) of 1 mM dPAA grafted to gold under various conditions.

Figure 3.2 presents the cyclic voltammogram and current response curves of dPAA electrografted on gold. On the first potential cycle a large cathodic peak is present at E_p= -400

mV, indicating the reduction of dPAA at the electrode surface. As the potential is swept back the absence of an oxidative peak indicates the irreversibility of the reaction.[27] Additional potential cycles show a significant reduction in current, indicating the passivation of the electrode surface by grafting of aryl molecules. However, the reduction in overall current due to surface passivation does not indicate inhibition of further layer growth. In the current response curves there is a large initial spike of current corresponding to reduction of all the electroactive species near the electrode surface. Again the decrease in current corresponds to the passivation of the electrode surface.

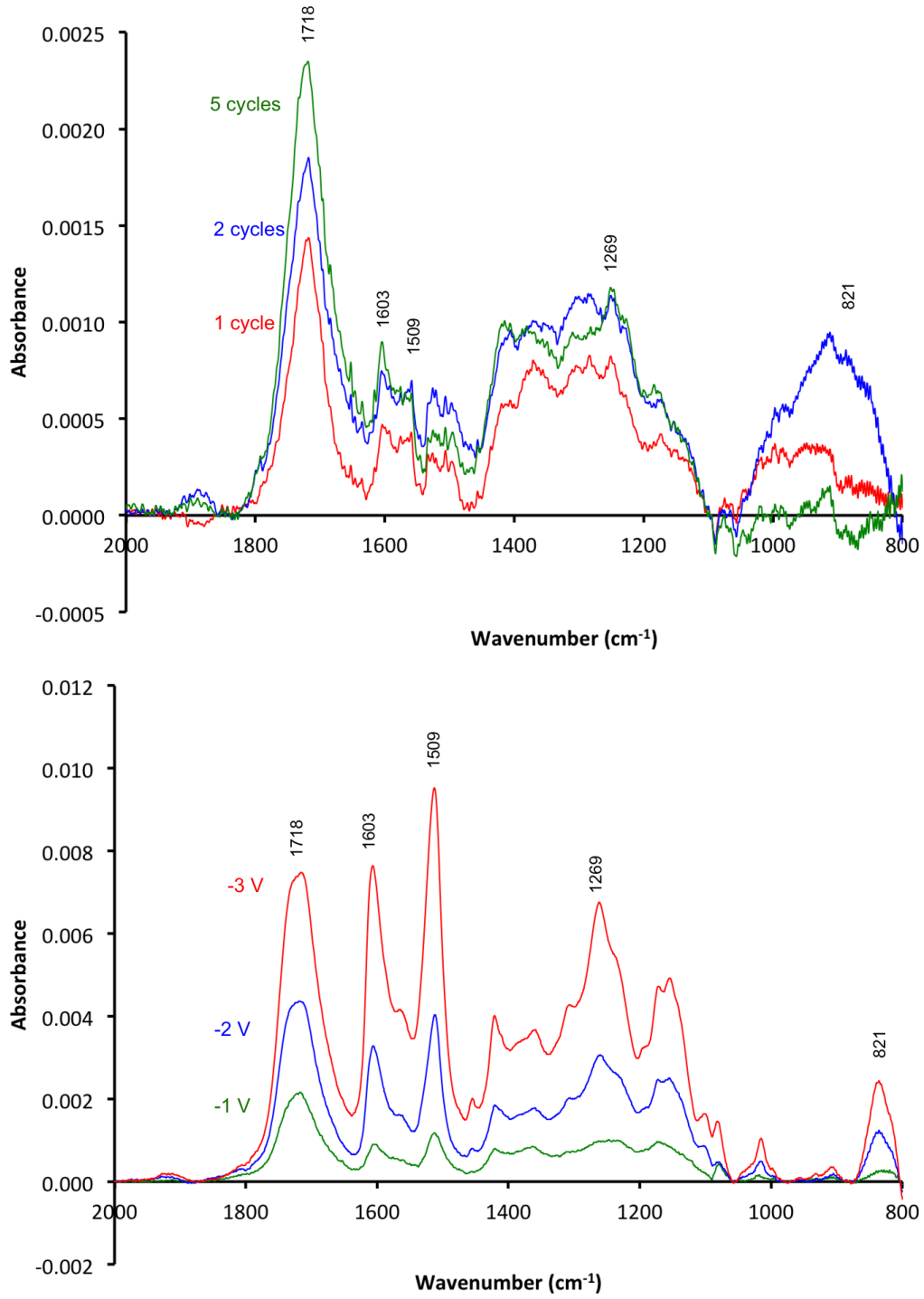

Figure 3.3: IRRAS spectra of dPAA derived films grafted with cyclic voltammetry (Top) and chronoamperometry (Bottom).

IRRAS was used to confirm surface attachment of dPAA to the gold surface and to help probe the growth of the grafted layers. Figure 3.3 contains IRRAS spectra for dPAA derived

films grafted with CV (Top) and chronoamperometry (Bottom). The spectra shows many peaks characteristic of carboxylic acids and aryl rings, strongly indicating the presence of dPAA on the surface. The strong peak at 1718 cm^{-1} has been assigned to the C=O stretch. The benzene ring stretching modes have been assigned to the peaks at 1603 $cm^{-1}$and 1509 cm^{-1}. Furthermore, the peaks at 1269 $cm^{-1}$and 821 cm^{-1} have been assigned to the C-O stretch and CH out-of-plane bending, respectively. Additionally, the IRRAS spectra give an indication to the thickness of the grafted layers as the absorbance is proportional to the amount of material present. With each successive voltammic cycle or as the reduction potentials are increased the intensities of the IRRAS peaks increases, indicating the presence of a thicker film.

Grafting Method	Thickness (nm)	# of Molecular Layers
1 cycle	2.4 ± 0.2	5.4
2 cycles	4.6 ± 0.3	10.2
5 cycles	6.6 ± 0.1	14.6
-1 V	4.4 ± 0.2	9.6
-2 V	14.4 ± 0.3	31.7
-3 V	27.8 ± 0.8	61.5

Table 3.1: Film thickness measurements determined by AFM scratching. The uncertainty of the thickness is the standard deviation of the mean of 3 measurements. The # of molecular layers are estimated assuming a PAA molecule is 0.459 nm in length.

To determine the thickness of deposited films, AFM "scratching" measurements were performed on modified gold electrodes. The height of the aryl film was used to estimate the number of aryl layers grafted to the surface. The height of a phenylacetic acid molecule orientated perpendicular to the surface was estimated to be 0.459 nm, using PyMOL software. Table 3.1 shows that aryl film thickness increases with electrochemical cycles and reduction potential (from chapter 2). These thicker layers potentially have more sites available for surface activation and biomolecule immobilization. Which should result in a larger response in an immunoassay. The effect of layer thickness on surface activation and protein immobilization will be examined in the next section.

3.3.2 Modification of Electrografted dPAA Derived Films for Immunoassays

A critical step in construction of any surface based immunoassay is the immobilization of a receptor molecules on the surface. Maximizing the number of receptor molecules should result in a larger response when detecting the analyte of interest, as more target molecules can be captured per unit area, increasing sensitivity. After electrochemical surface modifi-

cation, dPAA derived films were activated with a solution of 0.4 M EDC and 0.1 M NHS for 30 minutes. The activated surfaces were then modified with polyclonal anti-rabbit IgG (goat host), any unreacted NHS groups were deactivated with 1 M ethanolamine. The presence of characteristic functional groups was monitored with IRRAS throughout the surface modification process.

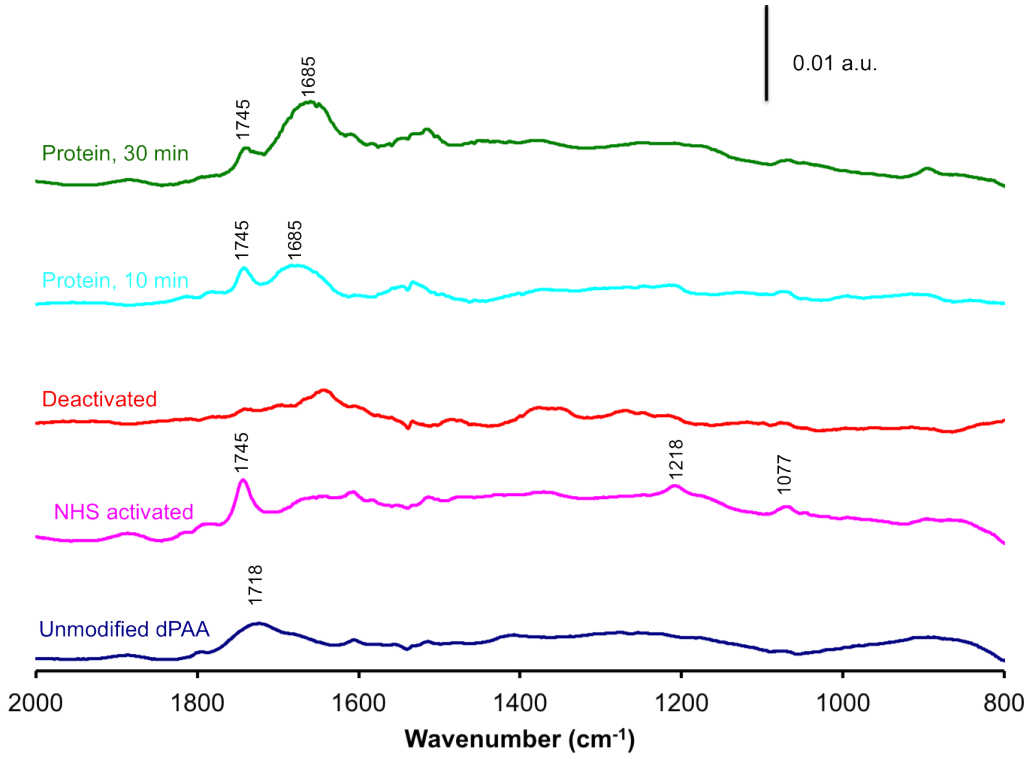

Figure 3.4: IRRAS spectra of dPAA derived layer during NHS activation and protein immobilization.

Figure 3.4 presents the IRRAS spectra of dPAA derived films at various stages of the surface modification process. The dPAA derived films have a strong peak at 1718 cm^{-1} characteristic of the C=O stretch of phenylacetic acid. Upon activation with EDC/NHS for 30 minutes the peak shifts to 1745 cm^{-1} arising form the C=O stretch of the succinimidyl ester. Also the strong bands at 1218 cm^{-1} (C-N-C stretch) and 1077 cm^{-1}(N-C-O stretch) confirm the activation with the succinimidyl group. After surface activation, substrates were immersed in a 667 nM solution of rabbit IgG to monitor the covalent attachment of protein to the surface. The spectra of samples immersed in protein solution for 10 and 30 minutes are shown. The growth of the amide I band at 1685 cm^{-1} can be used to monitor protein binding. After 30 minutes immersed in protein solution the IRRAS spectra showed

no significant change in the amide band indicating that 30 minutes is enough time to reach saruration. Not all the succinimidyl ester groups react with protein evident by the band at 1745 cm^{-1} remaining after protein immobilization. Therefore, after immersion in protein slides were reacted with 1 M ethanolamine to deactivate any unreacted NHS groups and prevent non-specific binding.

The differences in surface activation and protein binding of the dPAA derived films prepared using different electrochemical methods was also evaluated with IRRAS. Table 3.2 displays the peak intensities of the characteristic bands after surface activation and protein binding of dPAA derived films grafted with cyclic voltammetry and chronoamperpmetry. For both grafting methods it is clear that that as thicker films are grafted to the surface that more acid groups are being activated with NHS and more protein is binding to the activated surfaces. Using cyclic voltammetry to graft films the intensity of the protein amide band increased 1.44× from 1 cycle to 5 cycles. Using chronoamperometry the band intensity increased 3.85× from -1 V to -3 V, indicating much more protein was bound to the thicker films. Plotting these peak intensities as a function of thickness, Figure 3.5, shows that the increase in amide band intensities is not particularily linear with respect to film thickness. Indicating that as layer thickness increases not all of the activatible (-COOH) groups within the film are having protein immobilized. This is not unexpected as a normal IgG molecule has a diameter of approximately 15 nm in solution and 20-40 nm on a surface.[28] With this large size it is unlikely that proteins will penetrate very far into the surface of the dPAA derived layers. Therefore, the increased protein binding capacity of thicker films likely comes from the surface morphology of the films.

Grafting Method	**1715 cm^{-1}**	**1745 cm^{-1}**	**1685 cm^{-1}**
1 cycle	1.696	3.964	2.319
2 cycles	1.971	4.135	2.719
5 cycles	2.964	4.962	3.332
-1 V	2.058	4.224	2.154
-2 V	5.261	6.567	4.012
-3 V	10.49	11.23	8.921

Table 3.2: IRRAS peak intensities ($\times 10^{-3}$) of dPAA carboxyl group (1715 cm^{-1}) NHS ester (1745 cm^{-1}) and protein amide (1685 cm^{-1}) of dPAA derived films.

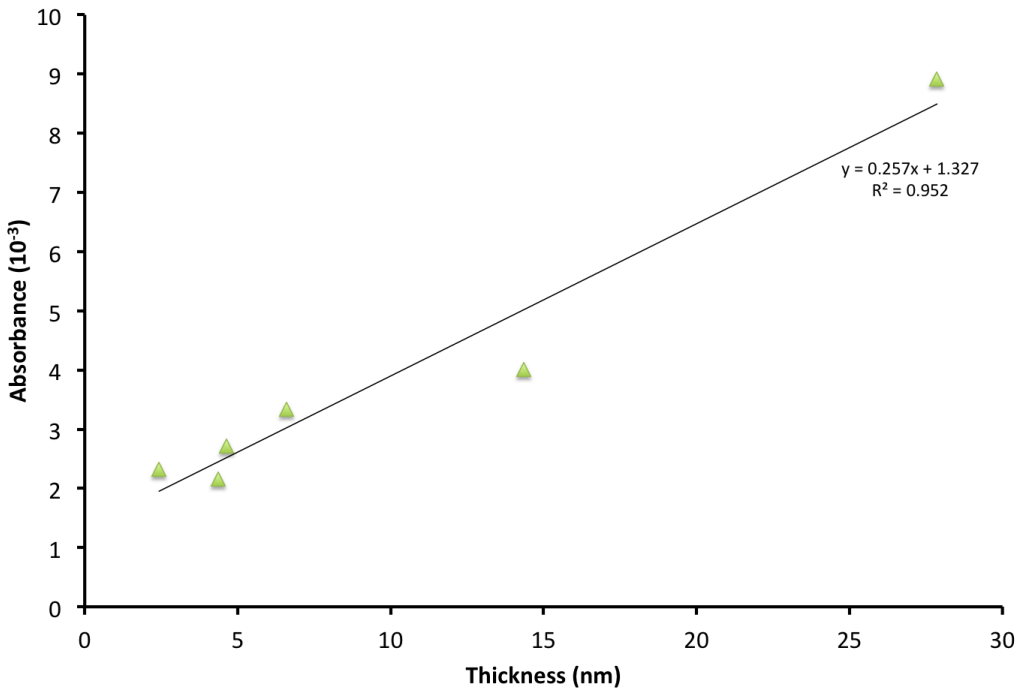

Figure 3.5: IRRAS peak intensities ($\times$ 10^{-3}) of protein amide (1685 cm^{-1}) bands plotted against film thickness.

The overall film morphology is likely to play a role in the number of antibodies immobilized. AFM was used to probe film morphology as measured by surface roughness. The effect of surface roughness on protein binding capacity of dPAA derived films grafted using various electrochemical methods was then examined. Figure 3.6 shows the AFM images of dPAA derived films grafted with cyclic voltammetry (1 and 5 cycles) and chronoamperometry (-3 V for 5 minutes). The 1 cycle image appears to be quite uniform with many small clusters of dPAA covering the surface. The film grafted with 5 cycles appears to be much less uniform (i.e. rougher) with large peaks and valleys. This is also observed for films deposited at -3 V for 5 minutes, but to an even greater degree. The rms roughness values of films grafted with cyclic voltammetry and chronoamperometry can be seen in Table 3.3. The roughness of dPAA derived films increases with successive voltammetric cycling or increased reduction potential (i.e. thicker films).

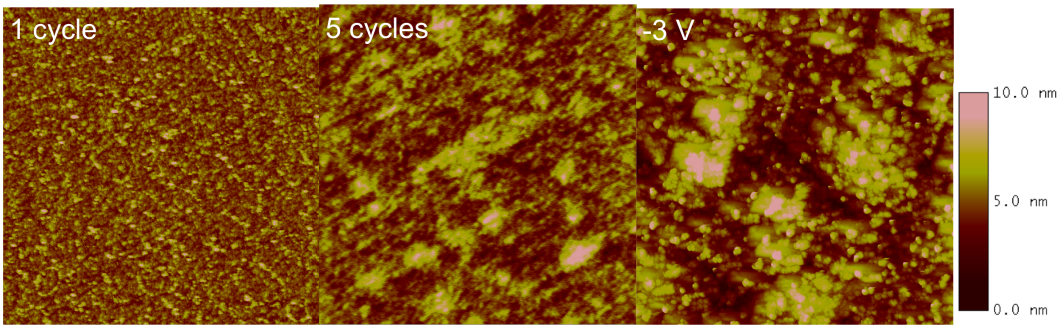

Figure 3.6: AFM height images of dPAA derived films grafted with 1 cycle, 5 cycles, and -3 V on thermally evaporated gold. Images are 5 μm^2.

Grafting Method	RMS Roughness (nm)
1 cycle	2.0 ± 0.1
2 cycle	2.5 ± 0.1
5 cycle	3.2 ± 0.2
-1 V	2.5 ± 0.3
-2 V	3.0 ± 0.3
-3 V	3.7 ± 0.4

Table 3.3: AFM rms roughness measurements of dPAA derived films grafted on gold with cyclic voltammetry and chronoamperometry. The uncertainty in the roughness is the standard deviation of the mean of 3 measurements.

To further characterize and control protein immobilization, the binding of rabbit a-IgG on dPAA derived surfaces was measured at various concentrations of protein solutions using SPR. Prior to immobilization of the antibodies, the dPAA derived surface was activated with 0.4 M EDC and 0.1 M NHS for 30 minutes. The SPR chip was allowed to equilibrate in PBS buffer for 10 minutes then was exposed to a series of a-rIgG solutions from low to high concentrations. The surface was then rinsed with PBS buffer for 10 minutes to remove any unbound protein. Figure 3.7 plots the fractional coverage (θ) versus the concentration of the antibody. The values for θ were determined from $\%\triangle R$ values and normalized to θ_{max} by fitting to a langmuir model. It is evident from Figure 3.7 that the amount of adsorbed protein increases sharply at low concentrations and reaches a plateau at higher concentrations, were the dPAA derived surface may be completely saturated with antibody. The immobilization of antibodies to the surface of dPAA derived films grafted with different electrochemical parameters was also examined with SPR.

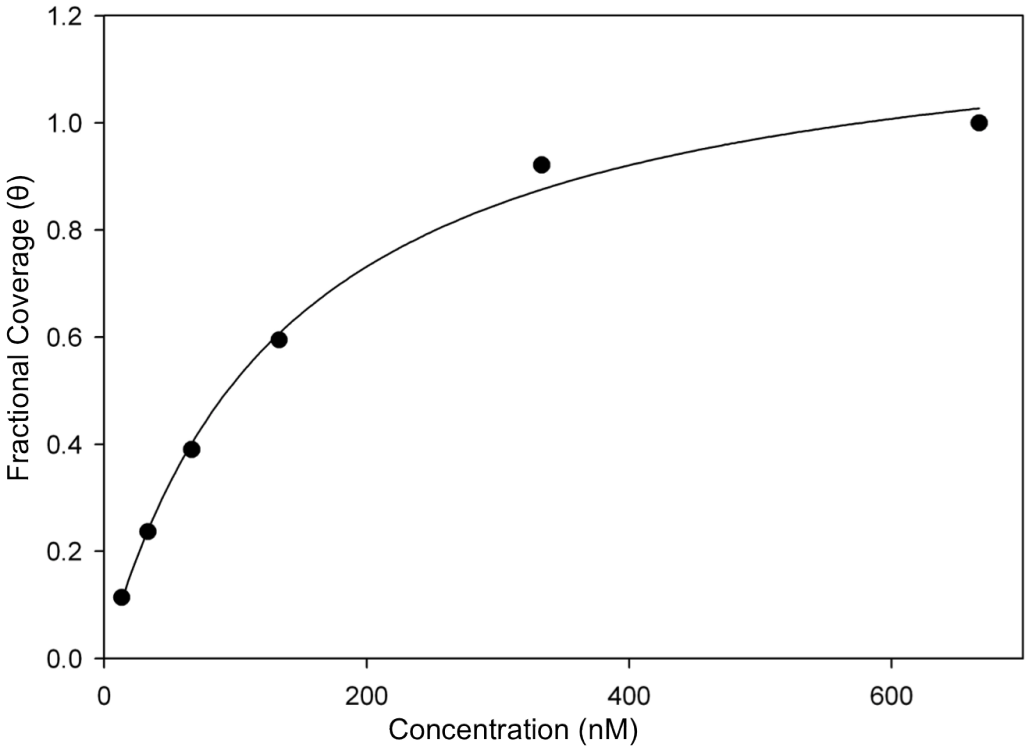

Figure 3.7: Isotherm describing the immobilization of a-rIgG to a NHS-activated dPAA layer. dPAA was deposited using chronoamperometry with a potential step of -1 V for 5 minutes.

Figure 3.8 presents the maximum response of the antibody immobilization to surfaces grafted with different electrochemical methods. Comparing these values to Table 3.3 it is clear that the amount of immobilized antibody increases with surface roughness and thickness. Since the %△R values are high (over 20%) the values are not linear with the number of proteins immobilized on the surface. It has been shown for constant angle SPRimaging theat the %△R is linear with surface coverage up to 10-15 %.[29] However, these %△R values can still be used to compare the coverage of protein on the different surfaces. An increase in antibody immobilization should lead to a larger response in the antibody-antigen immunoassays.

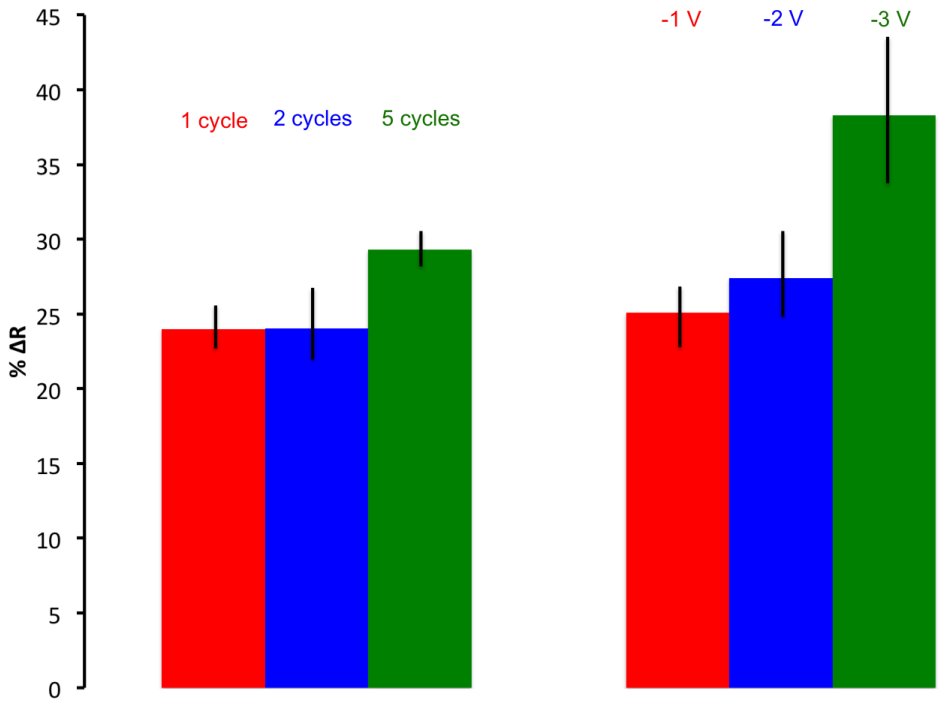

Figure 3.8: SPR %△R values of 667 nM rabbit a-IgG binding to NHS activated dPAA derived surfaces.

3.3.3 Surface Plasmon Resonance Immunoassays Using dPAA Derived Films

The goal of this project was to develop and evaluate the usefulness of a surface formed by the electrochemical reduction of dPAA as a support for SPR immunoassays. Gold surfaces were electrografted with dPAA derived layers of varying thicknesses and surface roughness using cyclic voltammetry and chronoamperometry and used for further functionalization. The surface functionalization is shown in Figure 3.9 and involved the activation of the carboxylic acid groups with EDC/NHS chemistry. The NHS-activated surfaces were then used to covalently immobilize antibodies to the surface. Any unreacted NHS groups were deactivated with 1 M ethanolamine and the surface was backfilled with a 0.1 % solution of BSA, to help prevent nonspecific adsorption.

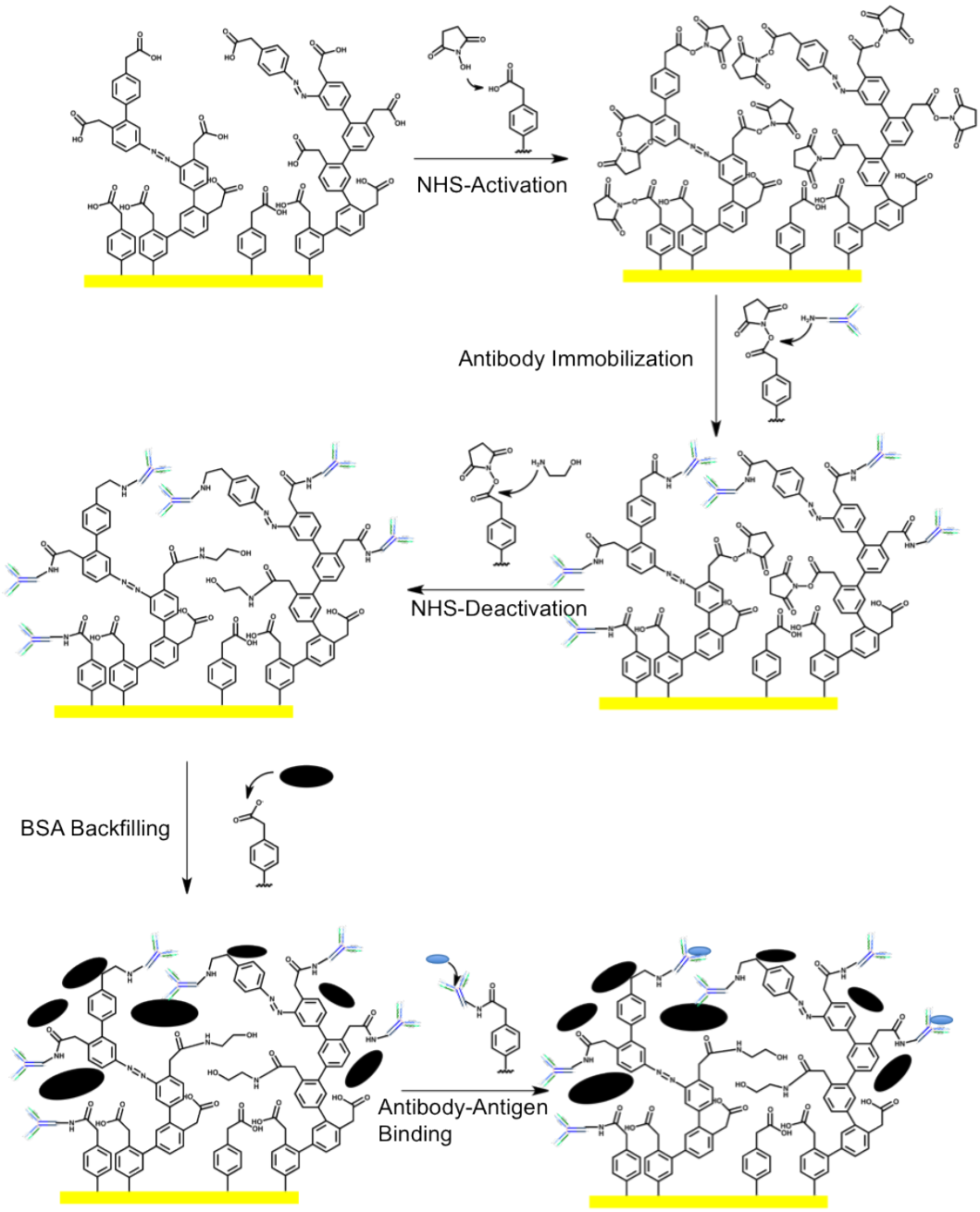

Figure 3.9: Surface preparation of dPAA derived layers for SPR immunoassays.

The performance of the antibody chips were evaluated by incubating them with solutions of increasing concentration of antigen (rabbit IgG) and monitoring the response with SPR. Binding curves were constructed to investigate the impact of electrochemical grafting conditions employed to pre-functionalize the chip surface. The curves were fit with a one-site

saturation ligand binding model:

$$\%\triangle R = \frac{\%\triangle R_{max}[C]}{K_d + [C]} \tag{3.1}$$

where $\%\triangle R_{max}$ is an asymptotic value obtained from the regression analysis, $[C]$ is the concentration of antigen in solution, and K_d is the dissociation constant. In this study the reciprocal of the K_d value obtained from the regression analysis will be reported as K_{ADS} (where $K_{ADS} = 1/K_d$). Antigen binding curves, and the accompanying fitting parameters, for the biochips derived from dPAA layers grafted using cyclic voltammetry are shown in Figure 3.10 and Table 3.4. Comparison of the K_{ADS} values, a measure of the antibody-antigen interaction strength, show no significant differences with values all in the low 10^7 M^{-1}range. These values are comparable to those previously reported in the literature.[30] Examination of the $\%\triangle R_{max}$ values, a measure of the amount of antigen bound, does show a dependence on the underlying dPAA derived layer. The films grafted using 1 or 2 voltammetric cycles showed nearly identical results, with both surfaces resulting in a $\%\triangle R_{max}$ value of 9.2. Whereas the films deposited with 5 voltammetric cycles resulted in a $\%\triangle R_{max}$ value nearly 21 % higher at 11.1, indicating more antigen was bound. Also shown in Figure 3.10 is the non-specific binding due to goat IgG. It is not surprising that there is some cross reactivity between the IgG molecules from different species. They are polyclonal antibodies and have identical fragment crystallizable regions. The point of this was to show that any signal due to non-specific adsorption will be low at these concentrations and not have much effect on the assay.

The antigen binding results are closely related to the amount of antibody immobilized on the surface. Figure 3.8 in the previous section shows the amount of immobilized antibody for various dPAA derived films. Films grafted with 1 and 2 voltammetric cycles were nearly identical while the 5 cycles immobilized $\sim$ 20 % more antibody. A high antibody surface density leads to a larger observed signal as more antigens are captured from solution.

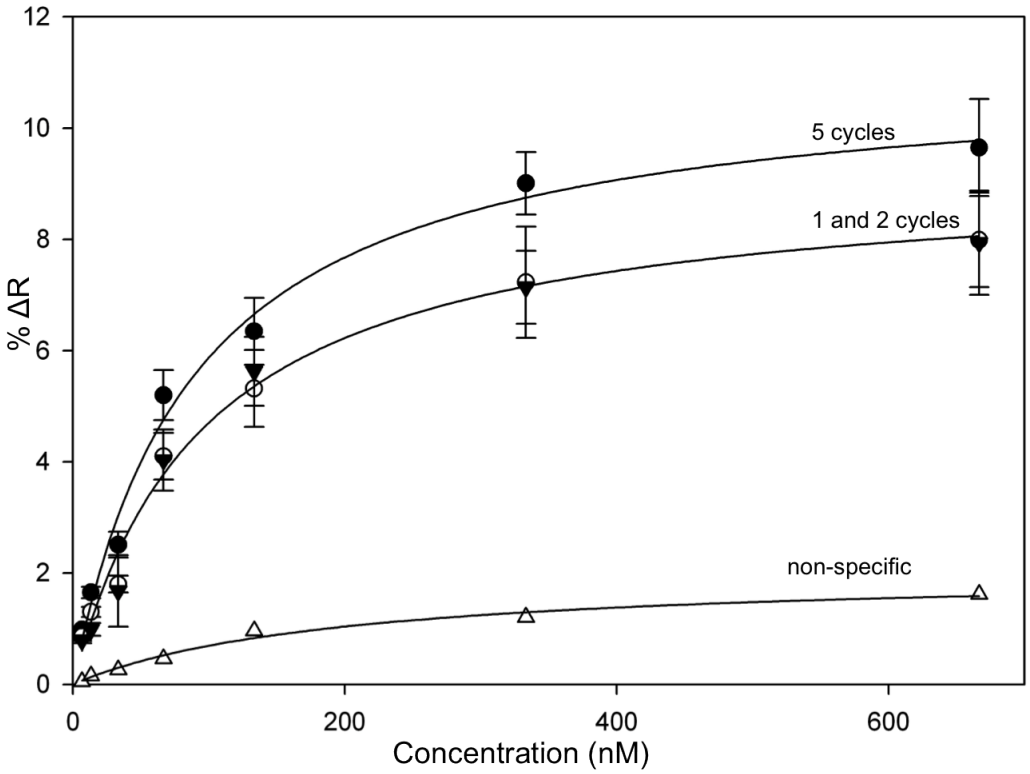

Figure 3.10: SPR antibody-antigen binding response curve for dPAA derived films grafted using cyclic voltammetry.

Grafting Method	$\mathbf{R^2}$	$\mathbf{K_{ADS}}$ $\mathbf{(M^{-1})}$	$\mathbf{\%\triangle R_{max}}$
1 cycle	0.9869	$1.0 \pm 0.2 \times 10^7$	9.2 ± 0.4
2 cycles	0.9842	$1.2 \pm 0.3 \times 10^7$	9.2 ± 0.4
5 cycles	0.9881	$3.1 \pm 0.9 \times 10^7$	11.1 ± 1.1

Table 3.4: Curve fitting parameters using a one site saturation ligand binding model for antigen binding curves obtained on modified dPAA derived surfaces grafted with cyclic voltammetry.

Studies were also performed on electrografted dPAA derived layers using chromoamperometry. The antigen binding curves and fitting parameter are shown in Figure 3.11 and Table 3.5. As in the previous example, comparisons of the K_{ADS} values suggest that the strength of the antibody-antigen interactions are similar on all surfaces. The amount of bound antigen ($\%\triangle R_{max}$) again showed a dependence on the grafting conditions of the dPAA derived layers. The films grafted using a potential step of -1 V had a $\%\triangle R_{max}$ value of 8.5. Whereas films grafted at -2 V or -3 V had $\%\triangle R_{max}$ values of 10.4 or 13.2, respectively. This corresponds to an increase of 22 % for the films grafted at -2 V and 55 % for films grafted at -3 V. Again these values are closely related to the amount of immobilized

antibody on the surface.

Comparing the $\%\triangle R_{max}$ values for dPAA films grafted with cyclic voltammetry and chronoamperomtry suggests that the roughness of the films, not the thickness, plays a large role in the antigen binding response as the films deposited using CV and CA had very similar $\%\triangle R_{max}$ values and very similar roughness measurements, whereas their thicknesses were quite different. If we examine the two films which had the highest antigen binding, either 5 cycle CV or -3 V CA. We can see that films deposited with 5 cycles had a roughness of 3.2 nm and a thickness of 6.6 nm which resulted in a $\%\triangle R_{max}$ value of 11.1; whereas, films deposited using -3 V had a roughness of 3.7 nm and a thickness of 27.8 nm with a $\%\triangle R_{max}$ value of 13.2. Clearly surface morphology is playing a major role in antigen binding capacity.

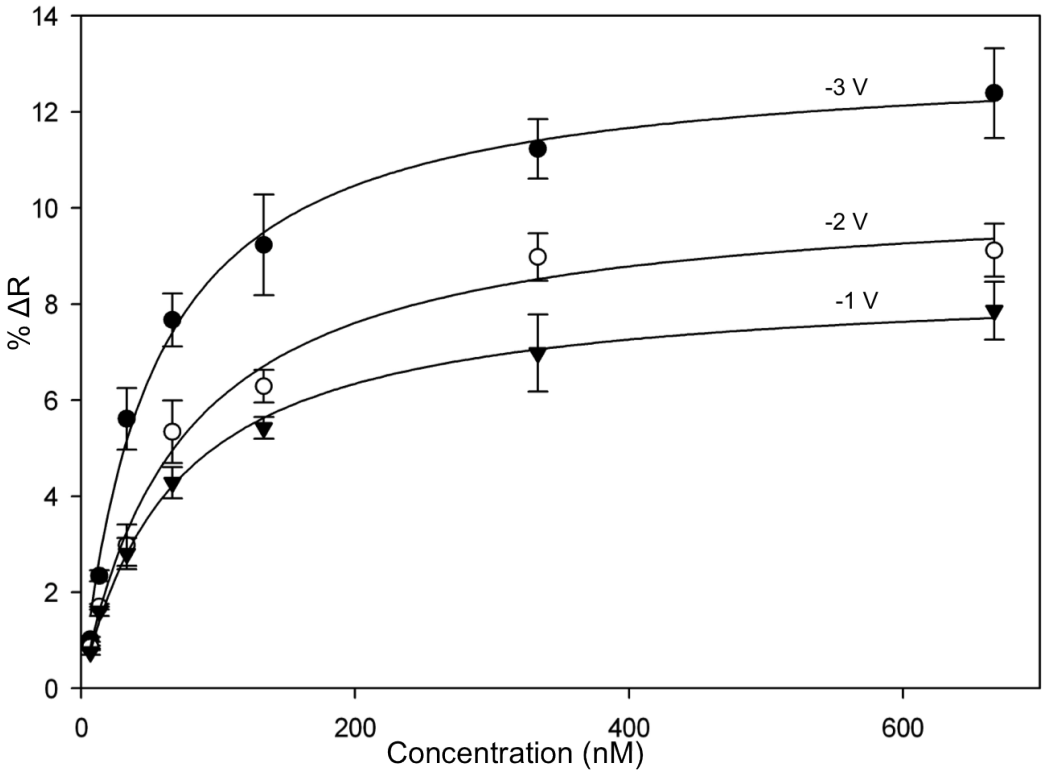

Figure 3.11: SPR antibody-antigen binding response curve for dPAA derived films grafted using chronoamperometry.

Grafting Method	$\mathbf{R^2}$	$\mathbf{K_{ADS}\ (M^{-1})}$	$\mathbf{\%\triangle R_{max}}$
-1 V	0.9967	$1.7 \pm 0.1 \times 10^7$	8.5 ± 0.2
-2 V	0.9878	$1.3 \pm 0.3 \times 10^7$	10.4 ± 0.4
-3 V	0.9919	$2.0 \pm 0.2 \times 10^7$	13.2 ± 0.4

Table 3.5: Curve fitting parameters using a one site saturation ligand binding model for antigen binding curves obtained on modified dPAA derived surfaces grafted with chronoamperometry.

The %△R values obtained following incubation with the lowest concentration of antigen were used to determine the limit of detection (LOD) for the various surfaces used for the binding assays.

$$LOD = 3\sigma_{blank} + blank \tag{3.2}$$

The values obtained from equation 3.2 were converted to a concentration using the linear fit obtained from the least squares analysis shown in Figure 3.12.

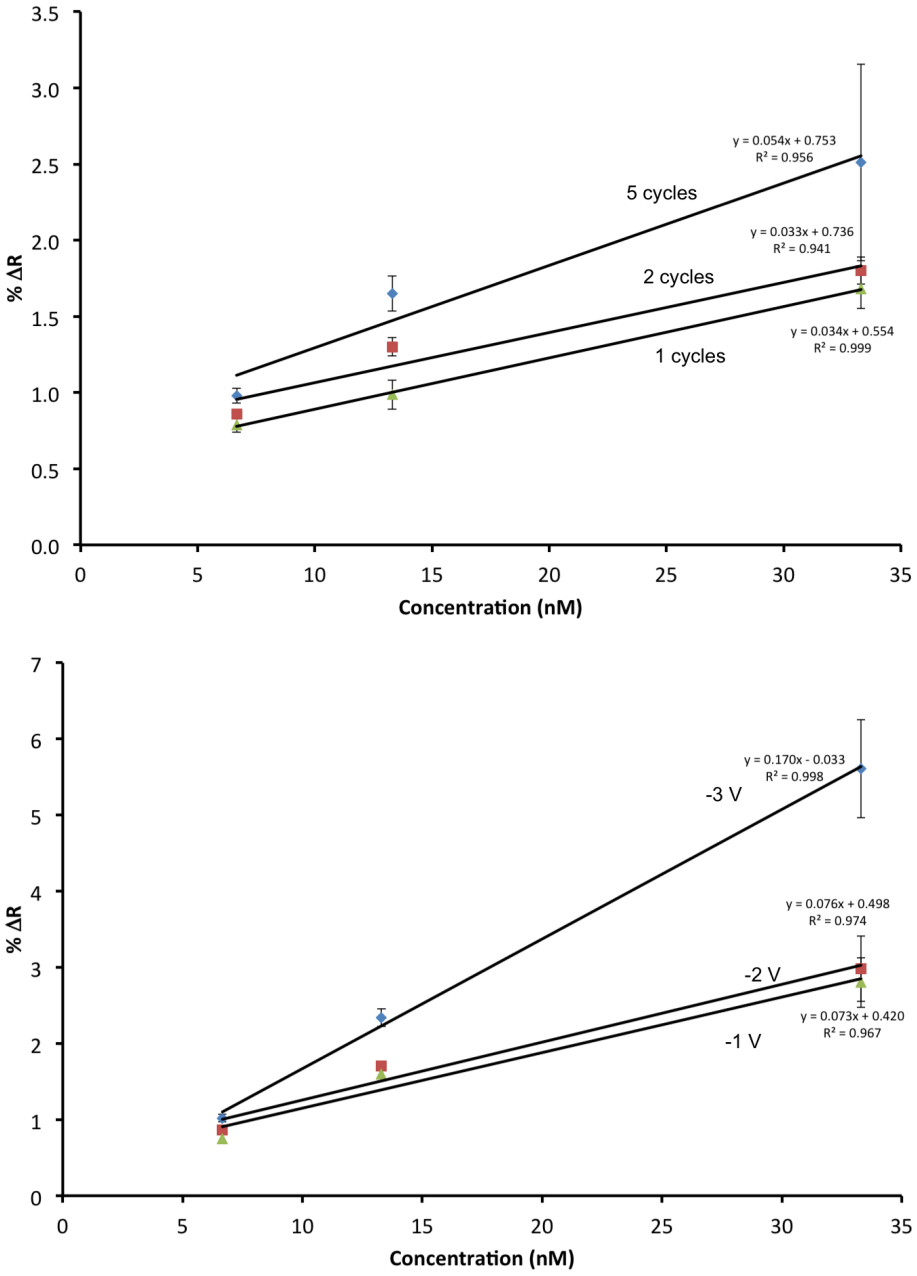

Figure 3.12: SPR response following incubation with low concentration of rIgG.

Grafting Method	LOD (nM)
1 cycle	44.6
2 cycle	40.4
5 cycle	24.4
-1 V	22.6
-2 V	21.1
-3 V	12.4

Table 3.6: LOD of dPAA derived films used for antibody-antigen immunoassay.

Table 3.6 presents the LOD's of dPAA derived films using cyclic voltammetry and chronoamperometry. The LOD's ranged from 44.6 nM for the thinnest film (grafted using cyclic voltammetry for 1 cycle) to 12.4 nM for the thickest film (grafted using chronoamperometry with a potential step of -3 V), an improvement of $\sim$3.6$\times$. While these may not be the lowest LOD's reported for surface based immunoassays (low nM) they are consistent with other substrates used for SPR based immunoassays monitoring the label-free binding of an anti-IgG IgG system.[31] By optimizing NHS activation and antibody immobilization the LOD's can be easily increased by an order of magnitude. Further evidence of the difference between the layers is witnessed when examining the slope of the linear fits in Figure 3.12. The slope of the fits for the dPAA derived layers increases form 0.034 to 0.170 for the different grafting conditions used. A higher slope reflects more sensitive antigen detection. This increase in sensitivity is probably due to a combination of increased antibody density and proper surface orientation of the immobilized antibodies.

3.3.4 Low-Fouling Diazonium Derived Films

Another critical aspect in bioassay development is the prevention of non-specific interactions. In the previous section the non-specific binding of a goat IgG to rabbit a-IgG was shown to be relatively low when compared to the binding of the analyte of interest. However, this was an idealized sample containing only one possible interference in a buffer solution. In diagnostic testing for biological samples analytes are usually present in complex biological matrixes such as blood, plasma, or urine, that contain thousands of different molecules that could interfere with the assay. In order to reduce the possibility of non-specific interactions occurring many immunoassays employ some type of low-fouling surface. In the immunoassay performed in the previous section this was done by backfilling the substrate with BSA. Backfilling with another protein is a common method for reducing non-specific adsorption, as it is relatively quick and simple. Although, the backfilling protein may also cover many

of the possible binding sites for the analyte of interest, reducing the response of the assay. Other common methods for reducing non-specific adsorption involve the incorporation of low-fouling materials into the substrate of the assay. A common material used to reduce non-specific adsorption are polyethylene glycol (PEG) SAM's; however, these materials are subject to oxidation in most biochemically relevant solutions.[9] Therefore the development of diazonium derived low-fouling films was investigated in order to utilize the covalent nature of diazonium derived films.

There are two main classes of low-fouling materials, polyzwitterionic and polyhydrophilic. For both materials it is believed that the low-fouling ability is tightly correlated to the formation of a hydration layer near the surface, which provides a physical and energetic barrier to resist non-specific adsorption.[32, 9] In this work we developed a zwitterionic diazonium derived layer and a hydrophilic diazonium derived layer for use as potential non-fouling substrates. Diagrams of these diazonium derived surfaces can be seen in Figures 3.13 and 3.14.

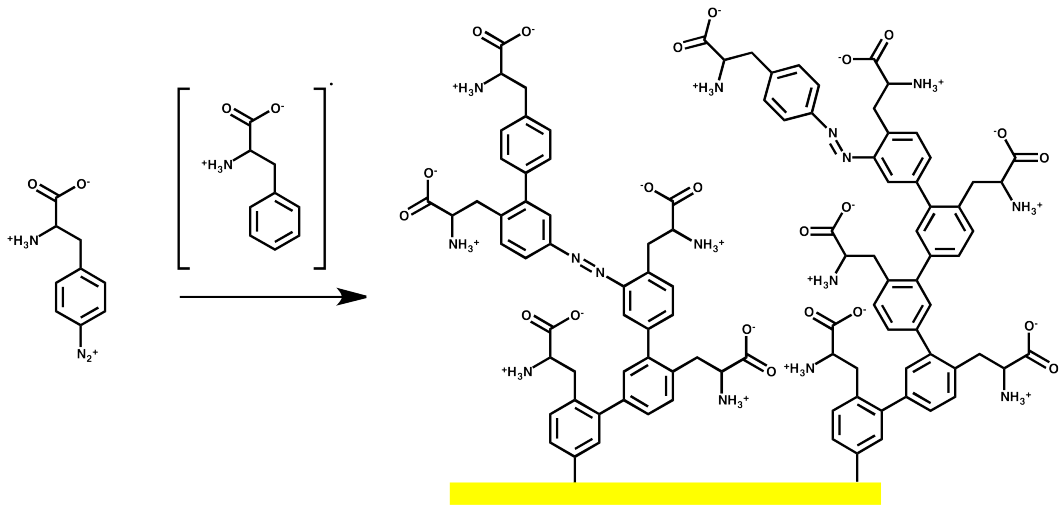

Figure 3.13: Preparation of zwitterionic diazonium derived films with potential low-fouling properties.

The polyzwitterionic films were prepared by synthesizing the phenylalanine diazonium (dPA) from the appropriate aniline precursor. The films were then grafted to gold using chronoamperometry and their low-fouling abilities tested.

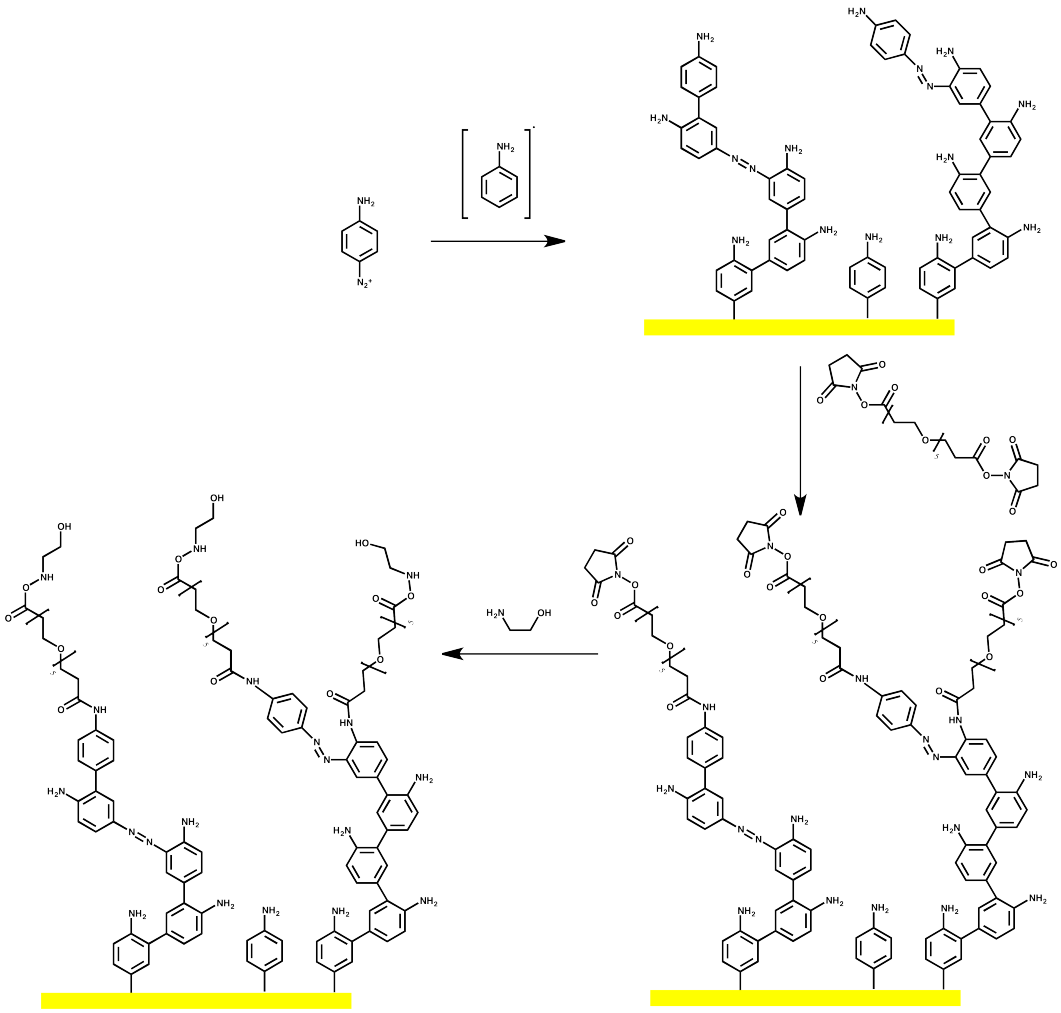

Figure 3.14: Preparation of hydrophilic diazonium derived films with potential low-fouling properties.

The polyhydrophillic films were prepared by synthesizing aminophenyl diazoniumsalt from its aniline precursor and grafting it to gold surface using chronoamperometry. The dAP derived surface was then modified with Bis(NHS)PEG_5. For the purposes of testing the low-fouling abilities of these films the unreacted NHS groups were deactivated with 1 M ethanolamine, although a receptor molecule could easily be attached for use in an immunoassay.

Gold substrates were modified with 1 mM phenylalanine diazonium salt (dPA) or 1 mM aminophenyl diazonium salt (dAP) solutions using chronoamperometry in a three electrode cell. The potential was stepped to -1 V against a Ag/Ag^+reference electrode. The successful deposition of this diazonium salts was qualitatively confirmed with infrared reflection absorption spectroscopy (IRRAS). Figure 3.15 (Top) presents the IRRAS spectrum of dPA,

with many bands characteristic to dPA. The peak at 1735 cm^{-1} has been assigned to the C=O stretch. The intense peak at 1629 cm^{-1}has been assigned to a combination of NH deformation and C=C stretching modes. The peak at 1510 cm^{-1} has also been assigned to a C=C stretching mode. Furthermore, the peaks at 1387 $cm^{-1}$and 826 cm^{-1} have been assigned to the COO^- symmetric stretch and CH out of plane bending, respectively. Figure 3.15 (Bottom) presents the IRRAS spectrum of dAP (before PEG-linker modification) also with many characteristic bands. The peak at 1674 cm^{-1} has been assigned to the NH deformation mode. The strong peaks at 1629 $cm^{-1}$and 1514 cm^{-1} have been assigned to the C=C aromatic stretching modes. The peak at 1282 cm^{-1} has been assigned to the NH stretch. The peak at 831 cm^{-1} has been assigned to the CH out of plane bending. The inset shows the dAP derived surface after PEG-linker modification, the band at 1742 cm^{-1} has been assigned to the C=O stretch of PEG.

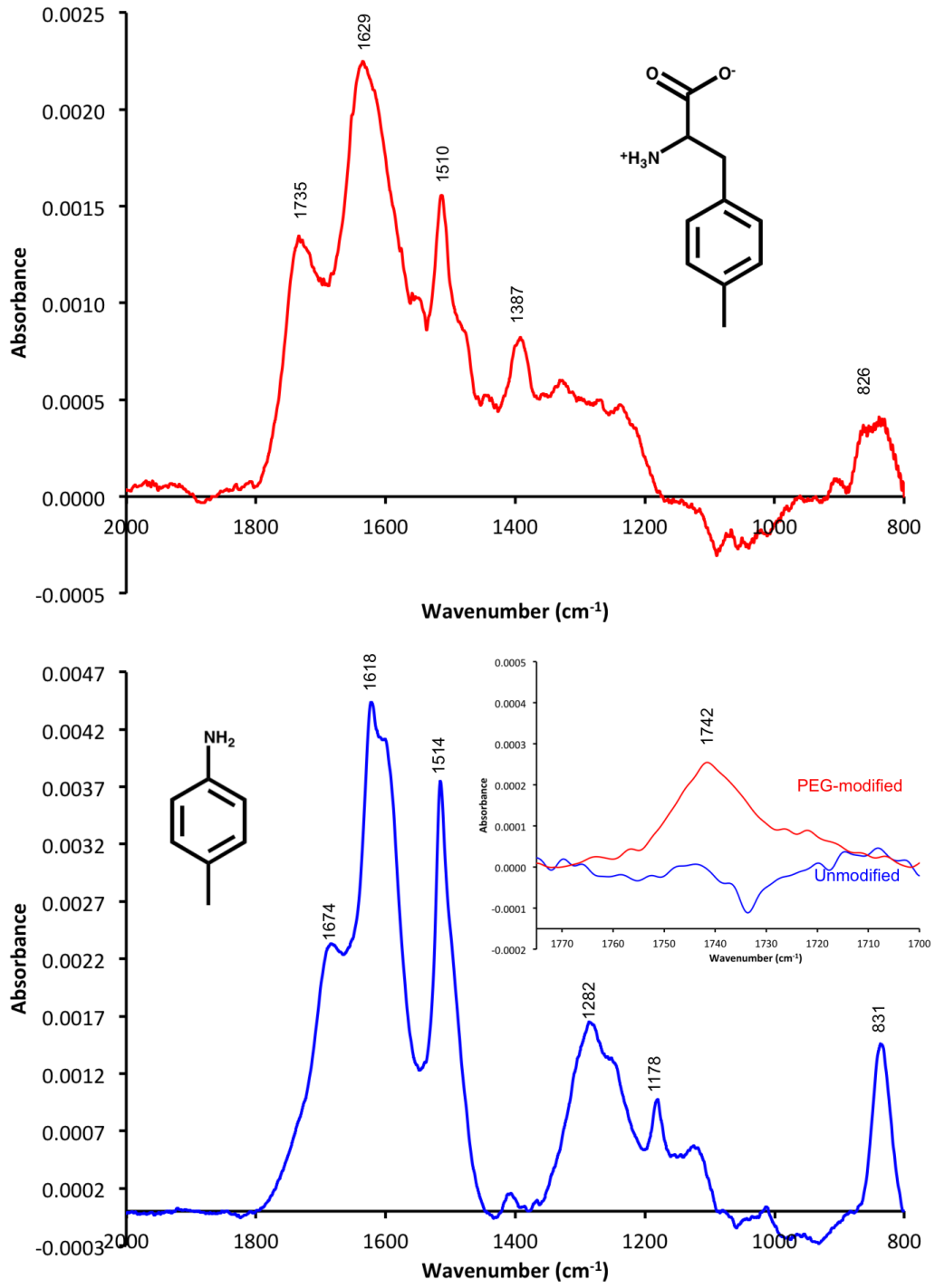

Figure 3.15: IRRAS spectra of dPA and dAP grafted to gold. Grafted with chronoamperometry with a potential step of -2 V for 5 minutes.

After modification of the gold surfaces the low-fouling abilities of these films were tested with SPR. Modified SPR chips were allowed to equilibrate in PBS buffer (pH 7.4) for 5 minutes. The chips were then exposed to 1 mg/mL solutions of bovine serum albumin

(BSA), lysozyme, or fibrinogen for 5 minutes. The chips were then rinsed with PBS buffer for 5 minutes. The %△R was measured and used to calculate the amount of irreversibly bound non-specifically adsorbed protein (Nonspecific protein adsorption (ng/cm^2) = 15.75×%△R + 0.05). An example SPR sensorgram can be seen in Figure 3.16.

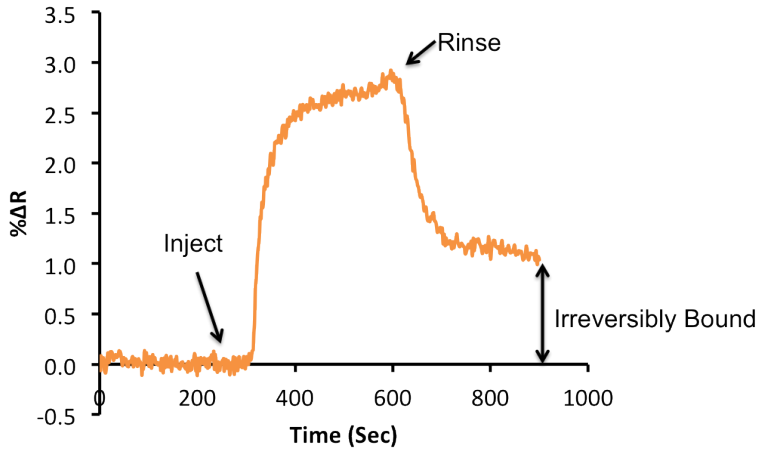

Figure 3.16: SPR sensorgram measuring non-specific adsorption.

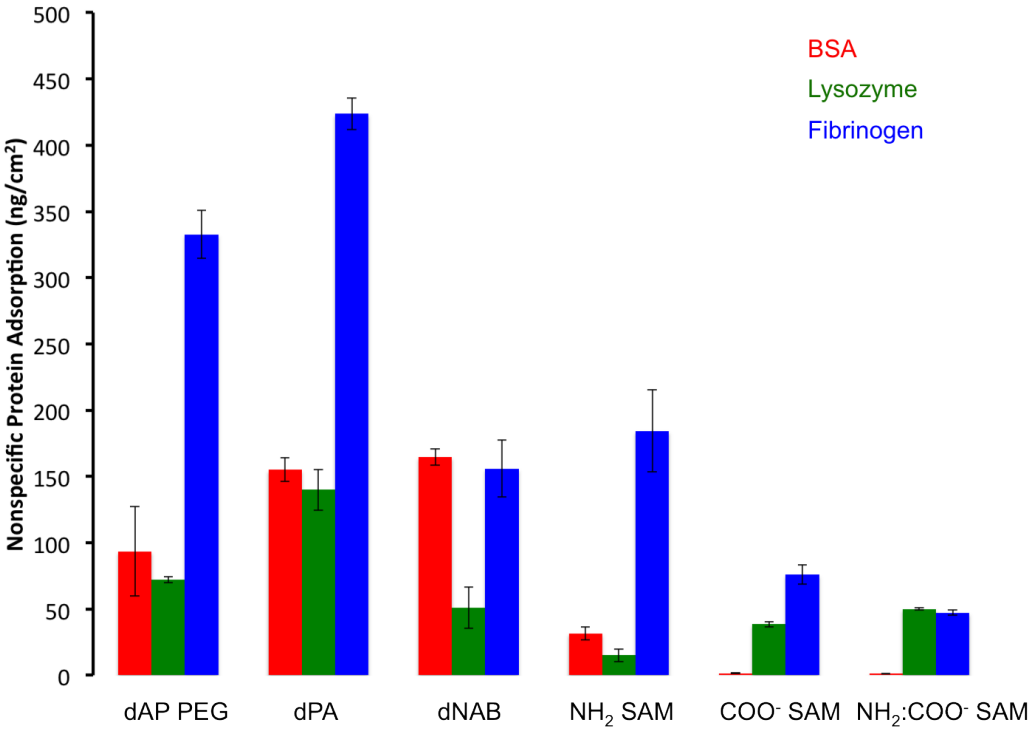

Figure 3.17: Irreversibly bound protein concentration determined by SPR of diazonium derived films and SAM's (HS-C_{11}-EG_6-R).

The low-fouling abilities of the diazonium derived films were tested and compared to that of various thiol-derived PEG-SAM films, a commonly used surface for reducing non-specific adsorption. Films of nitroazobenzene (dNAB) were also tested and used as a baseline for a standard diazonium derived film. Figure 3.17 shows the concentration of irreversibly bound protein on diazonium derived and PEG-SAM's surfaces exposed to 1 mg/mL solutions of BSA, lysozyme, or fibrinogen. These proteins were chosen because they are relatively common in biological samples and have varying physical properties. Additionally, fibrinogen is a key protein involve in the process of clotting, which makes it especially "sticky". From this data it appears that the diazonium derived films had significantly more non-specific protein adsorption then the PEG-SAM's. The diazonium films had an average protein adsorption of 137 ng/mm^2 for BSA, 88 ng/mm^2 for lysozyme, and 304 ng/mm^2 for fibrinogen. Whereas the PEG-SAM films had average adsorption values of 11 ng/mm^2, 34 ng/mm^2, and 102 ng/mm^2, respectively. Ironically it seems the dNAB derived layers had the best overall ability to resist non-specific adsorption out of the diazonium derived layers. The adsorption of the proteins appears to be highly dependent on the charge of the surface. Lysozyme has an isoelectric point of 11.4, at pH = 7.4, this will results in a net positive charge. Whereas, BSA and fibrinogen have net negative charges with isoelectric points of 4.7 and 5.5, respectively. Examination of the SAM layers shows that surfaces with the same charge as the protein had less nonspecific adsorption compared to surfaces where the charges were opposing. The reason the diazonium derived films were less successful in resisting nonspecific adsorption is likely due to the general structure of diazonium layers. Relatively disordered polyphenylene layers results in a random distribution of the functional groups throughout the layer. For a film to have good low-fouling abilities a polydispersity of functional groups is key as any defect within the layer can result in protein adhesion. The diazonium derived layers appear to be too highly disordered, resulting in many defects throughout the films to which proteins can adsorb. However, the high control and stability of diazonium derived films still makes them an attractive method for controlling non-specific adsorption. Although more work needs to be performed to optimize these surfaces. Using different deposition conditions or different precursor moleules could lead to better control of non-specific interactions. This will be a subject of the future work section.

3.4 Conclusion

This work has shown the successful modification of gold substrates using electrografting of diazonium salts for use as supports for antibody immobilization in immunoassays. dPAA was used to modify gold substrates using cyclic voltammmetry and chronoamperometry to prepare films of varying thickness and surface roughness. These films were used for antibody immobilization and to monitor antibody-antigen binding. The effect of film thickness and roughness on antibody immobilization and antigen binding was studied. The immobilization of capture agents (antibodies) and the subsequent analyte binders (antigens) binding were shown to be highly dependent on surface roughness. As the roughness of the layers increases the binding capacity of antigen showed a 55% increase. The LOD's of these immunoassays was calculated to be in the low nM range, which is comparable with other surface based bioassays. Additionally, the use of diazonium derived films as potential low-fouling materials was studied. The non-specific adsorption of diazonium derived films was shown to be $\sim 4\times$ that of PEG SAM's. However, backfilling with BSA was shown to be a suitable method for contolling non-specific adsorption in certain situations with dPAA derived films.

References

[1] Bolduc, O.; Correia-Ledo, D.; Masson, J. *Langmuir* **2011**, 24–28.

[2] Yang, R.; Xu, J.; Ozaydin-Ince, G. *Chemistry of ...* **2011**, 1263–1272.

[3] Nuzzo, R. G.; Allara, D. L. *Journal of the American Chemical Society* **1983**, *105*, 4481–4483.

[4] Holmlin, R.; Chen, X.; Chapman, R.; Takayama, S. *Langmuir* **2001**, 2841–2850.

[5] Akkerman, H. B.; Blom, P. W. M.; de Leeuw, D. M.; de Boer, B. *Nature* **2006**, *441*, 69–72.

[6] Vericat, C.; Vela, M. E.; Benitez, G.; Carro, P.; Salvarezza, R. C. *Chemical Society reviews* **2010**, *39*, 1805–34.

[7] Kawaguchi, T.; Yasuda, H.; Shimazu, K.; Porter, M. D. *Langmuir* **2000**, *19*, 9830–9840.

[8] Monolayers, S.-A.; Delamarche, B. E.; Michel, B.; Biebuyck, H. A.; Gerber, C. *Advanced Materials* **1996**, *8*, 719–729.

[9] Chen, S.; Li, L.; Zhao, C.; Zheng, J. *Polymer* **2010**, *51*, 5283–5293.

[10] Bélanger, D.; Pinson, J. *Chemical Society reviews* **2011**, *40*, 3995–4048.

[11] Laurentius, L.; Stoyanov, S. R.; Gusarov, S.; Kovalenko, A.; Du, R.; Lopinski, G. P.; McDermott, M. T. *ACS nano* **2011**, *5*, 4219–27.

[12] Mahmoud, A. M.; Bergren, A. J.; Pekas, N.; McCreery, R. L. *Advanced Functional Materials* **2011**, *21*, 2273–2281.

[13] Paulik, M.; Brooksby, P.; a.D. Abell; a.J. Downard *Journal of Physical Chemistry C* **2007**, *111*, 7808–7815.

[14] Shewchuk, D. M.; McDermott, M. T. *Langmuir : the ACS journal of surfaces and colloids* **2009**, *25*, 4556–63.

[15] Delamar, M.; Hitmi, R.; Pinson, J.; Saveant, J. M. *Journal of the American Chemical Society* **1992**, *114*, 5883–5884.

[16] Gooding, J. *Electroanalysis* **2008**, *20*, 573–582.

[17] Liu, G.; Böcking, T.; Gooding, J. J. *Journal of Electroanalytical Chemistry* **2007**, *600*, 335–344.

[18] Corgier, B. P.; Bellon, S.; Anger-Leroy, M.; Blum, L. J.; Marquette, C. a. *Langmuir : the ACS journal of surfaces and colloids* **2009**, *25*, 9619–23.

[19] Polsky, R.; Harper, J. C.; Wheeler, D. R.; Dirk, S. M.; Arango, D. C.; Brozik, S. M. *Biosensors & bioelectronics* **2008**, *23*, 757–64.

[20] Liu, G.; Liu, J.; Davis, T. P.; Gooding, J. J. *Biosensors & bioelectronics* **2011**, *26*, 3660–5.

[21] Velusamy, V.; Arshak, K.; Korostynska, O.; Oliwa, K.; Adley, C. *Biotechnology advances* **2010**, *28*, 232–54.

[22] Noble, R.; Weisberg, R. *J Water Health* **2005**, 381–392.

[23] Ronkainen, N. J.; Halsall, H. B.; Heineman, W. R. *Chemical Society reviews* **2010**, *39*, 1747–63.

[24] Yebra, D. *Progress in Organic Coatings* **2004**, *50*, 75–104.

[25] Xiu, K. M.; Cai, Q.; Li, J. S.; Yang, X. P.; Yang, W. T.; Xu, F. J. *Colloids and surfaces. B, Biointerfaces* **2011**, *90*, 177– 183.

[26] Strakey, E. *Organic Syntheses, Coll.* **1943**, *2*, 225.

[27] Bard, A. J.; Faulkner, L. R. *Electrochemical Methods: Fundamentals and Applications*, 2nd ed.; Wiely & Sons: New York, 2000.

[28] Ouerghi, O.; Touhami, a.; Othmane, a.; Ouada, H. B.; Martelet, C.; Fretigny, C.; Jaffrezic-Renault, N. *Biomolecular engineering* **2002**, *19*, 183–8.

[29] Buzzeo, M. C.; Evans, R. G.; Compton, R. G. *Chemphyschem : a European journal of chemical physics and physical chemistry* **2004**, *5*, 1106–20.

[30] Kanda, V.; Kariuki, J. K.; Harrison, D. J.; McDermott, M. T. *Analytical chemistry* **2004**, *76*, 7257–62.

[31] Cao, C.; Sim, S. J. *Biosensors & bioelectronics* **2007**, *22*, 1874–80.

[32] Chen, S.; Zheng, J.; Li, L.; Jiang, S. *Journal of the American Chemical Society* **2005**, *127*, 14473–8.

4 Conclusions and Future Work

4.1 Conclusions

Polymers have unique characteristics not met by traditional materials. With the ability to be deposited on a surface and impart these characteristics to the desired substrate the work on organic coatings over the last 20 years has been extensive. With this in mind it is important to control the formation of the coating on the substrate as best as possible and to understand the linkage between the organic film and the substrate as best as possible. The work presented has detailed the use of diazonium salts to prepare thick aryl films on gold surfaces by the application of high reduction potentials. The mechanism of formation and stability of these films was investigated. Additionally, diazonium derived films were studied as substrates for SPR immunoassays and potential low-fouling surfaces.

Chapter 2 presented the modification of gold electrodes using the electrochemical grafting of phenylacetic acid and nitroazobenzene diazonium salts. The effect of reduction potential on film formation was studied. It was determined that using higher reduction potentials results in thicker films and that this increase in thickness is linear with respect to the applied reduction potential. The formation of thick films appears to be largely driven by migration. To form diazonium derived films using high reduction potentials the omittance of supporting electrolyte is preferred as electrolyte leads to polymerization of the aryl radicals in solution preventing film formation. Additionally, the presence of a redox active functional group does not appear to be necessary to mediate thick film growth, as has been stated previously in the literature.[1] When such high potentials are applied the driving force of the reaction is large enough to overcome the resistance from the film deposited on the electrode surface allowing film thickness to increase with potential. Finally, the stability of films deposited using high reduction potentials was compared to films prepared with lower more traditional potentials. Under the conditions used it appears that films grafted with high reduction potentials are more stable than their low potential counterparts.

Chapter 3 examined the electrochemical reduction of phenylacetic acid diazonium salt as surface chemistry for antibody immobilization and subsequent antigen detection. It was shown that the surface chemistry provided a suitable platform for antibody attachment. The effect of film thickness and roughness on antibody immobilization and antigen binding was studied. The immobilization of capture agents (antibodies) and the subsequent analyte binders (antigens) binding were shown to be highly dependent on surface roughness. As the

roughness of the layers increases the binding capacity of antigen showed a 55% increase. The LOD's of these immunoassays were calculated to be in the low nM range, which is comparable with other surface based bioassays.[2] Finally, diazonium salts were used to prepare potential low-fouling substrates. The non-specific adsorption of diazonium derived films was shown to be $\sim$4$\times$ that of PEG SAM's. Although, more work needs to be performed to optimize these surfaces. Using different deposition conditions or different precursor molecules could lead to better control of non-specific interactions.

4.2 Future Work

The electrochemical grafting of diazonium salts within this work has provided insight into the effect of reduction potential on film formation. The mechanism of formation and stability of these films was investigated. However, using the electrochemical, IRRAS, XPS, and AFM measurements to hypothesize about mechanism of film formation is difficult as no information is obtained that can be directly correlated to the observed peaks in the cyclic voltammograms. Belanger and coworkers have investigated the deposition of diazonium molecules on a electrode by monitoring the deposited mass during the electroreduction reaction with a quartz crystal microbalance (QCM) and correlating this with the charge transferred.[3] Using QCM to monitor the formation of diazonium derived layer grafted using high reduction potentials would potentially provide information on film formation during different stages of the electroreductive reaction.

In addition to diazonium salts the electrografting of organic molecules has been demonstrated using many precursors such as amines,[4] alcohols,[5] carboxylates,[6, 7] alkyl halides,[8] ammoniums,[9] sulfoniums,[10] iodoniums,[11] and vinylics.[12] The mechanisms for the electrografting from various precursors have been elucidated. While there are a few cases where the nature of the species that binds to the surface is unclear, it appears that the formation of a radical is a prerequisite for electrografting to occur. With these similarities in the formation mechanism it would be interesting to study the effect of reduction or oxidation potentials on film formation of different precursors. Potentially allowing precise control over film thickness that has been demonstrated for diazonium derived layers.

Phenylacetic acid films of varying thicknesses were used as substrates for antibody immobilization and subsequent antigen detection was shown in this work. One potential problem with this type of assay is the inefficiency of the immobilization reaction. Previous stud-

ies have demonstrated that many of the immobilized antibodies are inactive after surface attachment.[13] Additionally, the pre-functionalization of diazonium salts with antibodies has been demonstrated.[14] Using diazonium molecules pre-functionalized with antibodies to deposited film with high reduction potentials could greatly increase the performance of such assays as there would potentially be many more active binding sites. This is assuming that the high potentials would not effect the activity of the antibodies.

Recently, diazonium derived layers have seen growing use in immundiagnostics. A potential interest in immunodiagnostics is the ability to develop a high throughput array that incorporates label-free detection. An immunodiagnostic microarry would reduce current analysis performed by multiple clinical tests onto a single mircoarray, multiple analysis would be performed in a single experiment. Using the pre-functionalization of diazonium molecules many different antibodies could be attached prior to surface modification.[14, 15] The electrochemical grafting could then be performed in an array format using the experimental conditions that would result in the best response for that antibody.

The prevention of non-specific adsorption is critical for all biosensor systems. While the use of diazonium derived layers as low-fouling films in this work did not show the most promising results diazoniums still have the potential to be effective in reducing non-specific interactions due to the highly functionalizable nature of the R-group. Based on the work performed here it's possible that separating the aryl ring from the functional groups could lead to increased performance as a low-fouling film. Present in the literature are examples of diazonium molecules having been pre-functionalized with ethylene glycol.[16] Additionally, ethylene glycol molecules have been functionalized with zwitterionic heads.[17] Incorporation of zwitterionic ethylene glycol onto a diazonium molecule that could then be electrografted to a surface has the potential to be very resistant against non-specific interaction. It would provide some separation between the aryl ring and the exterior of the film to which molecules would be interacting, while the hydrophilic nature of the film should maintain a strong hydration layer around the film.

References

[1] Ceccato, M.; Bousquet, A.; Hinge, M.; Pedersen, S. U.; Daasbjerg, K. *Chemistry of Materials* **2011**, *23*, 1551–1557.

[2] Cao, C.; Sim, S. J. *Biosensors & bioelectronics* **2007**, *22*, 1874–80.

[3] Laforgue, A.; Addou, T.; Bélanger, D. *Langmuir : the ACS journal of surfaces and colloids* **2005**, *21*, 6855–65.

[4] Adenier, A.; Chehimi, M. M.; Gallardo, I.; Pinson, J.; Vilà, N. *Langmuir : the ACS journal of surfaces and colloids* **2004**, *20*, 8243–53.

[5] Aeda, H. M.; Itano, T. K.; Uang, C. Z. H.; Atayama, K. K. **1999**, *15*, 531–536.

[6] Brooksby, P. a.; Downard, A. J.; Yu, S. S. C. *Langmuir : the ACS journal of surfaces and colloids* **2005**, *21*, 11304–11.

[7] Andrieux, C. P.; Gonzalez, F.; Save, J.-m. **2004**, *7863*, 4292–4300.

[8] Andrieux, C. P.; Gallardo, I.; Savaent, J. M.; Su, K. B. *Journal of the American Chemical Society* **1986**, *108*, 638–647.

[9] Wang, D.; Buriak, J. M. *Surface Science* **2005**, *590*, 154–161.

[10] Love, D.; Colichman, E. *Journal of Organic Chemistry* **1962**, *18*, 40–46.

[11] Vase, K. H. j.; Holm, A. H.; Pedersen, S. U.; Daasbjerg, K. *Langmuir : the ACS journal of surfaces and colloids* **2005**, *21*, 8085–9.

[12] Lécayon, G.; Bouizem, Y.; Gressus, C. L. *Chemical physics letters* **1982**, *91*, 506–510.

[13] Chen, S.; Liu, L.; Zhou, J.; Jiang, S. *Langmuir* **2003**, *19*, 2859–2864.

[14] Corgier, B. P.; Bellon, S.; Anger-Leroy, M.; Blum, L. J.; Marquette, C. a. *Langmuir : the ACS journal of surfaces and colloids* **2009**, *25*, 9619–23.

[15] Polsky, R.; Harper, J. C.; Wheeler, D. R.; Dirk, S. M.; Arango, D. C.; Brozik, S. M. *Biosensors & bioelectronics* **2008**, *23*, 757–64.

[16] Gooding, J. *Electroanalysis* **2008**, *20*, 573–582.

[17] Kim, J. H.; Son, J. S.; Park, K. D.; Kim, J. M.; Kim, J. J.; Ahn, K. D.; Han, D. K. *Key Engineering Materials* **2007**, *342-343*, 805–808.